ALMA MATER STUDIORUM

UNIVERSITA DEGLI STUDI DI BOLOGNA

Facolta di Ingegneria

Dottorato di Ricerca in: MECCANICA E SCIENZE AVANZATE DELL'INGEGNERIA

Ciclo XXVI

Settore Concorsual: 09/A3

Settore scientifico disciplinare: ING/IND14

Mechanical behavior of flat and curved laminates interleaved by electrospun nanofibers

Candidato: HAMED SAGHAFI

Coordinatore: Prof. Vincenzo Parenti Castelli

Tutore: Prof. Giangiacomo Minak

Co-Tutore: Prof. Andrea Zucchelli

:

Esame Finale Anno 2014

To MASOOMEH & MAHDI & FATEMEH

Abstract

A major weakness of composite materials is that low-velocity impact, introduced accidentally during manufacture, operation or maintenance of the aircraft, may result in delaminations between the plies. Most studies regarding the effect of low-velocity impact damage reported in the literature have focused on thicker flat plates that are typical of those used for wing structures, but there are a few studies that address the low-velocity impact response of thinner curved composite panels that are typical of fuselage skins. Therefore, the first part of this study is focused on mechanics of curved laminates under impact loading. For this aim, the effect of preloading on impact response of curved composite laminates is considered. By applying the preload, the stress through the thickness and curvature of the laminates increased. The results showed that all impact parameters are varied significantly. For understanding the contribution rate of preloading and pre-stress on the obtained results another test is designed. The outcomes shows that the effect of curvature is more on maximum contact load, maximum displacement, and time duration of impact. The interesting phenomenon is that the preloading can decrease the damaged area when the curvature of the both specimens is the same. Finally the effect of curvature type, concave and convex, is investigated under impact loading. The results proved that the maximum load is more in concave laminates, while the damaged area in convex laminates is more.

In another part of this research, a new composition of nanofibrous mats are developed to improve the efficiency of curved laminates under impact loading. Therefore, at first some fracture tests are conducted to consider the effect of Nylon 6,6, PCL, and their mixture on mode I and mode II fracture toughness. For this goal, nanofibers are electrospun and interleaved between mid-plane of laminate composite to conduct mode I and mode II tests. The results shows that efficiency of Nylon 6,6 is better than PCL in mode II, while the effect of PCL on fracture toughness of mode I is more. By mixing these nanofibers the shortage of the individual nanofibers is compensated and so the Nylon 6,6/PCL nanofibers could increased mode I and II fracture toughness. Then all these nanofibers are used between all layers of composite layers to investigate

their effect on damaged area. The results showed that PCL could decrease the damaged area about 25% and Nylon 6,6 and mixed nanofibers about 50%.

CONTENTS

List of Figures

List of Tables

Chapter 1

Introduction

Composite materials have become more popular over the years. Composites offer many advantages over traditional metallic materials due to their higher stiffness-to-weight and strength-to-weight ratio. The aerospace, automotive, transportation, construction and other industries are applying composite materials for saving the energy, and performance benefits can be obtained using these materials. Composite structures are always exposed to impact during manufacturing, service, and maintenance operations. Impact damage in composites usually results in internal micro damages that are difficult to detect by naked eyes but may cause severe degradation of material properties, such as the compressive strength leading to a reduction in performance of the structure.
The impact resistance of composite laminates has been considered intensively for many years [1-5]. Most of the available literature deals with impact on structures without any pre-stresses. Usually, in addition to impact loading, composite structures may experience pre-stresses produced either by service loads or by the manufacturing/assembly process. When a structure is under tensile load, the effect of internal delamination on the residual strength is small. On the contrary, in compression delamination is the worst destabilizer, since it may become unstable and propagate [6, 7]. The pre-stress can be uniaxial and biaxial tension/compression, pure shear and their combinations, which have been considered by various researchers [8-10]. On the other hand, most of the studies in the literature have focused on thicker flat plates, but there are few studies that address the low-velocity impact response of thinner curved composite panels that are typical of

aircraft wing and fuselage skin [11-14]. Fig. 1 illustrates some parts of the aircraft wing and fuselage exposed to various threats of foreign object damage like birds, hail, runway debris or tire rubber impact. All these parts are curved laminates that can present different response to impact loading under various situations: 1- curvature value 2- preloading 3- curvature type (concave or convex). In the first part of this study, the effect of all these situations on the impact response of curved composite laminates is considered.

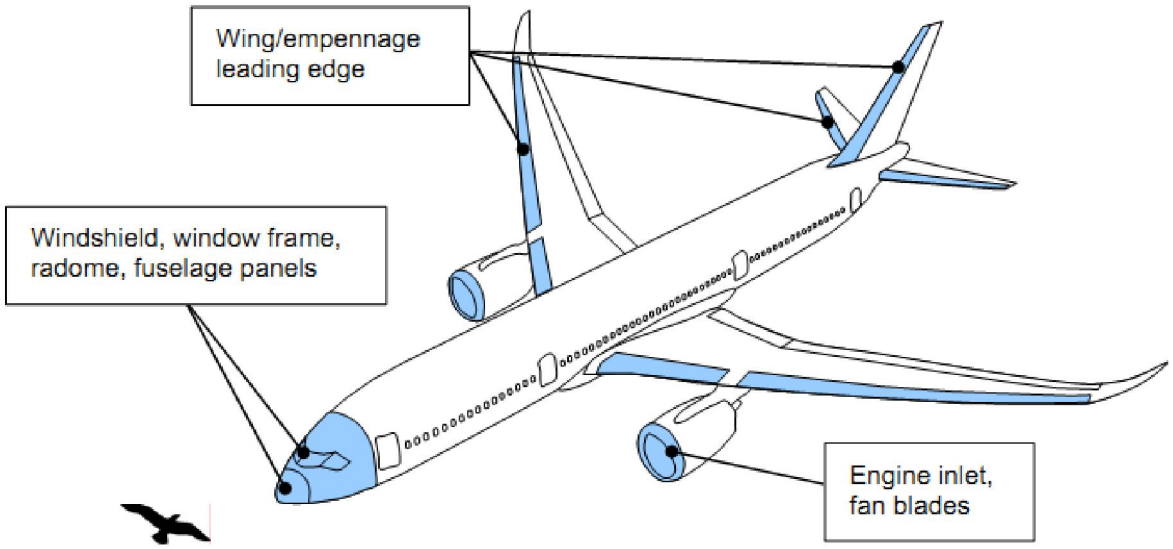

Fig. 1.1. Illustration of aircraft components exposed to the risk of bird strike [15].

When a foreign object impacts on a laminate, several damage modes can occur in composite laminates: matrix cracks, fiber/matrix interface debonding, fiber fracture, and delaminations (Fig. 2). Dominant damage mode depends on the impact parameters of the impactor and the material properties of the composites [16].

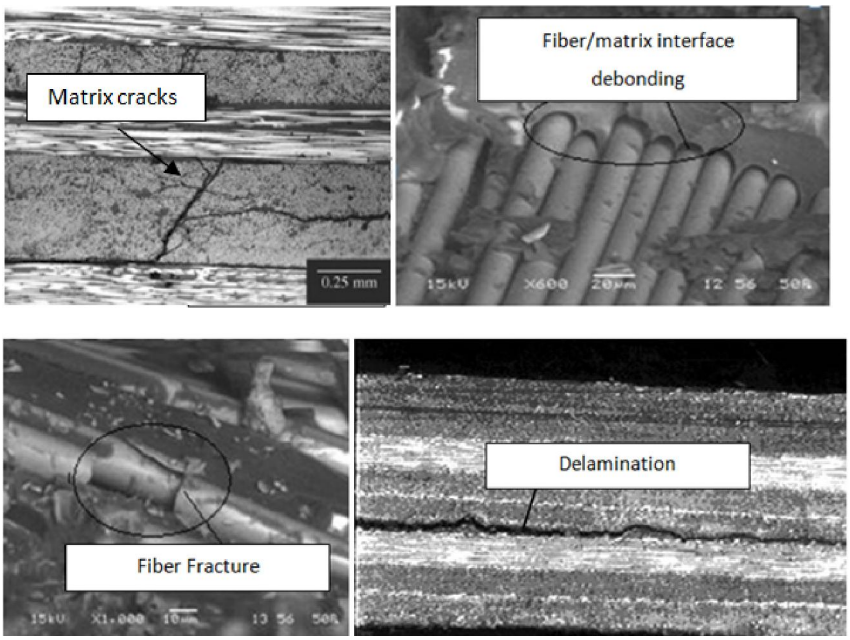

Fig. 1.2. Failure modes of composite laminates under impact loading [17,18]

epoxy is used as the matrix in most of composite laminates, but its inherent brittleness is the main reason for delamination which is one the most important failure mode in composite laminates. So far many attempts have been conducted for resolving this problem that finally lead to development of novel resin systems involving the use of thermoplastics as toughening agents [19-23]. The toughening material can be used as a discrete layer of a secondary material in the form of film, fiber, or particle between composite layers [24-26]. Since the distribution of fibers is easier than particles and also its efficiency is more than films [27-28], many researches have been focused on these materials. Li et al. [27] and Magniez et al. [28] compared the influence of polymeric nanofibers and films on fracture toughness of composite laminates. In the first study, polyvinylidene fluoride (PVDF) nanofiber and film were prepared and interleaved between composite layers for toughening carbon/epoxy laminates. They showed that mode II fracture toughness increase 57% using nanofibers while applying PVDF in form of film decreased this parameter significantly. In the second research, Polysulfone (PSF) used and like the first study they proved nanofibers effect on mode I fracture toughness is more in comparison with PSF film. The results of these two topics are illustrated in Fig. 3. HMW and LMH mentioned in Fig.1-A means

high and low molecular weight, respectively. Because of the nanofiber advantages in toughening of composite laminates, in this study a wide research has been done for decreasing the failure in curved laminates and increasing its performance while it is under the service loading.

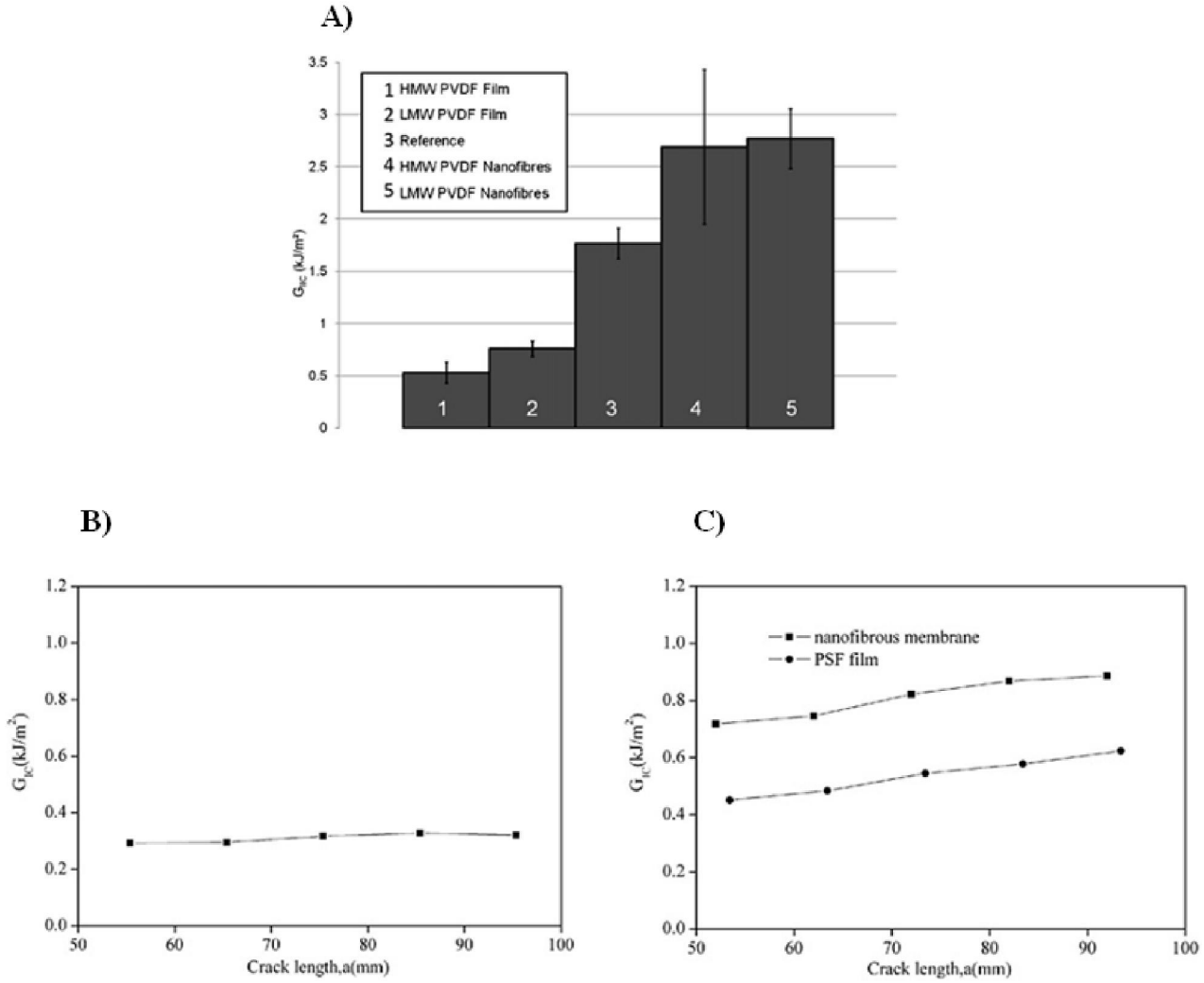

Fig. 1.3. A) The effect of PVDF film and nanofibers on mode II fracture toughness [27].

The comparison of mode I fracture toughness of: **B)** reference laminate **C)** modified laminate with PSF film and nanofibers [28]

In chapter 2, first a wide literature review is presented about what has been presented regarding the effect of curvature and preloading on the impact response of composite laminates. Then three different tests designed for considering the mechanics of curved laminates under impact loading. In

the first one, the effect of preloading on the impact parameters is considered. In this situation, by applying the load the, curvature and the stress in the laminates are changed. For understanding the contribution rate of stress and the curvature on the results of the last test, the second test is designed. Finally for considering the effect of curvature type, concave or convex, the third test is conducted. In chapter 3, electrospinning method for producing nanofibers is introduced with which a composite nanofiber provided for increasing mode I and mode II fracture toughness. For finding its efficiency in toughening epoxy-based laminates some mode I and mode II fracture tests conducted using double cantilever beam (DCB) and the End Notched Flexure (ENF) specimens. In chapter 4, this new composite nanofibers are used for investigating its influence on impact response of curved laminate.

Chapter 2:

Mechanics of Curved Laminates

2.1. Introduction

In this chapter some parameters that affect on impact response of curved composite laminates are considered: 1- curvature effect 2- pre-stress effect 3- curvature type (concave or convex). Before describing experimental method and final result, a review regarding what have been followed by other researcher is presented in this section:

2.1.1. Effect of pre-stress

composite material structures exposed to impact loading are likely to be under a static load prior to impact. Therefore, evaluation the behaviour of preloaded composite under impact is an important topic. Arranging a setup for providing pre-stress conditions is very complicated and so some limited experimental works in this field are available in literature and most studies are numerically.

The impact resistance of pre-tension, pre-compression and unloaded quasi-isotropic graphite/epoxy laminated samples have been studied in [29] with an instrumented drop-weight testing machine. The pre-load stress level was selected to be 20% of the ultimate compressive strength of the material. Pre-tension increased the maximum force, while pre-compression decreased it. However, the damage area exhibited a rather different trend. The damage was minimal for the unloaded samples. The damage area was larger for the pre-compressed samples and the major axis of the damage zone ellipse was aligned with the pre-compression direction. In this case, specimen was damaged and bent into large deflection, i.e. the specimen would be under post-buckling. Therefore, the damage size of precompression specimen was enlarged because of the delamination buckling. Finally, the damage was largest for the pre-tension samples, where the major axis of the damage zone ellipse was perpendicular to the pre-tension direction. Robb et al. [30]

published the most complete paper in this field, which encompasses a wide range of pre-loading (uniaxial and biaxial tension/compression, pre-strain of 0 to 6000με). They conducted drop tower studies on pre-loaded E-glass/polyester laminates. It was found that there is no significant damage growth in GRP samples up to the pre-strain level of ±2000με. They also found that the most damage, least contact force, and least contact duration were caused in a biaxially loaded tension/compression state. Whittingham et al. [31] conducted low velocity impact tests on carbon/epoxy laminates. The following pre-stresses were introduced to specimens: 1) uniaxial tension (1000 and 1500με) 2) bi-axial tension-tension (500/500 and 1000/1000με) 3) bi-axial tension-compression (500/-500με, 1000/-1000με, and 1500/-1500με). The uniaxial-loaded samples were impacted with an impact energy of 6 J and others with energies of 6 and 10 J. Their results showed that there is no significant difference in impact resistances for the unstressed and pre-stressed cases. Therefore there is a good agreement between these results with what presented by Robb et.al [30]. Because in both of these studies they showed that in strain less than 2000με the effect of preloading is not noticeable.

Mitrevski et al. [32] investigated the influence of impactor shape on the biaxially (tension) pre-stressed impact of E glass/polyester laminates. Biaxial tension values applied in this study were 500 and 1000με and impact tests were conducted in 4 and 6J. As the contact surface of the impactor shifts from flat to hemispherical to ogival to conical (Fig. 2.1), the maximum deflection and absorbed energy increased. For the amount of pre-tension applied in this test, no considerable effect on damaged area were observed. Minak et al. [33] investigated carbon/epoxy cylinders which were pre-stressed in torsion prior to low velocity impact tests (7J). They reported that that the delamination initiation is not affected by the torsional preload. On the other hand, as evidenced by the variation in the contact duration and the tube maximum deflection, delamination propagation is highly affected by the torsional load.

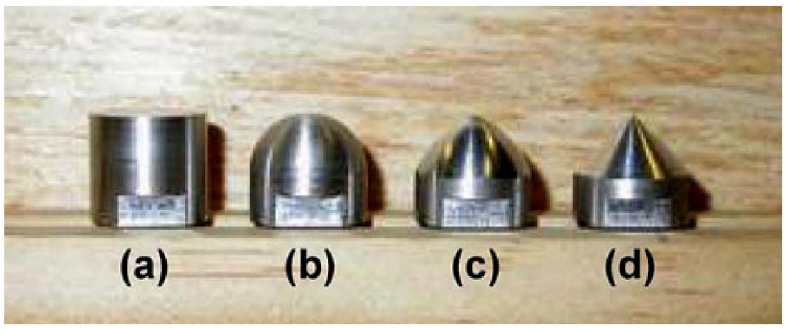

Fig .2.1. Impactor shapes; (a) flat, (b) hemispherical, (c) ogival and (d) conical, all 12 mm in diameter [32]

Many finite element analyses (FEA) have been conducted on the impact response on pre-stressed laminates. Khalili et al. [34] used ABAQUS software for modelling curved laminate and consider its behaviour under low velocity impact. The main goal of this study was finding a suitable method for obtaining accurate and precise answer from the software. Accurate modelling requires the appropriate selection of element type, solution method, impactor modelling method, meshing pattern and contact modelling. By considering several case studies with various conditions, validity of the existed modelling processes was examined. In each case, by comparing the results of various methods with the related available experimental test results in existing literature, the best procedure was proposed which can serve as benchmark method in low-velocity impact modelling of composite structures. Zheng et al. [35] studied dynamic responses of a pre-stressed laminated composite plate under impact based on the linearized elastoplastic contact law as well as shear deformable plate theory. The effects of pre-stresses (biaxial-tension/tension or compression/comprerssion), velocity and mass of the impactor, plate thickness, and shear strength of the laminate on the contact force and plate central displacement are presented. It was found that initial stress does not have noticeable effect on the contact force history but it has significant effect on the plate central displacement. It was found that Compressive pre-stress tends to increase the displacement and also the impact response is proportional to the impact velocity. The contact force increases with the increasing of the mass of impactor, thickness and shear strength of the laminate. Larger deflection of the plate were also introduced by a heavier mass and thinner plate thickness. Ghelli and Minak [36] studied the effect of membrane pre-loads through FEA. It was shown that tensile pre-load increased the peak stress while the compressive pre-load reduced the peak impact stress. Heimbs et al. [37] considered the preloading effect experimentally and numerically using LS-DYNA software and compared the results. The specimens were subjected to uniaxial compressive preloading until 80% of buckling load. The experimental test series showed an increased deflection for the preloaded composite plates, which lead to a higher extent of material damage compared to the unloaded plates with delaminations as one important energy absorption8 mechanism. Therefore, the total absorbed energy was higher for the preloaded plates.

2.1.2. Effect of curvature

Like the last section, some analytical, numerical, and experimental studies have been followed for investigation the effect of curvature on impact response of composite laminates.

Kistler and Waas [38-40] have conducted one the most experimental studies in this field. They considered the effect of thickness, curvature, and boundary conditions. They showed that as the thickness decreased the curvature effect becomes more important. They also concluded that flat panels responded to impacts with larger peak forces but smaller maximum deflection than the curved panels. The influence of curvature on impact force is stronger when the straight edges of the laminate are prevented from displacing outwards. Kim et al. [41] in a similar study mentioned that as the curvature increased the contact force decreased. In other words, both studies showed that as the curved panels became flat the maximum contact force increased. They also showed that a composite design with the smallest radius of curvature and the most interlaminar surfaces the least amount of damage. As the panel became flat, the impact force increased. Ambur and Starnes [42] considered this effect using a wider range of curvature. They showed that the contact force decreases by increasing the radius of curvature until 76cm and after this critical point increasing the radius leads to increase of contact force. The effect of height in curved laminates and also the boundary conditions on energy absorption was investigated by Schulz and Liu [43]. Experimental results showed that the maximum deflection and the energy absorption increased significantly as the camber height increased while the peak load decreased slightly. It was also found that the boundary condition played an important role in the energy absorption process. They used two kinds of clamps: frame-clamped and bolt-clamped boundary conditions. In the first one, when the specimens were held by a rectangular frame and clamped at four corners by toggle clamps slippage between the specimens and the frame could happen. In order to completely eliminate the slippage, the second clamp was used in which additional holes at each end of the frame were prepared to bolt the specimens. Bolting the specimen increased the visible delamination and fiber breakage and several times the specimen broke into two pieces. Study by Short et al. [44] on post-impact compressive strength of curved composites showed a linear trend of damage area with increasing impact energy (3J, 6J, and 9J) for a flat panel and two different radii: 75 and 125mm. The results indicate that the curvature tends to reduce the impact force; examination for each energy level shows lower impact force as curvature is increased.

Numerical studies about the effect of curvature is very vast and different parameters and methods have been used. Leylek et al [45] used MSC.DAYTRAN software to determine the accuracy and efficiency of a nonlinear explicit FE code and compare the results to published experimental data. The study looked at the impact response as a function of composite panel curvature, composite mesh density, impactor mass, velocity and size, and also various suggestions were made for improving the accuracy and efficiency of FE analysis procedures in composite low energy impact studies. In some experimental studies have been done before by changing the curvature, maximum force increased and in some others decreased. Since in this study a wide range curvature radius was considered, this effect can be investigated better. As illustrated in Fig. 2.2, in very low radius of curvature, a small enhancement in the radius leads to a sharp decline in contact force, but in some regions this increase causes a rise in contact force. So far, there is no studies about the exact reason of this phenomenon. Surely many structural factors affect on this response.

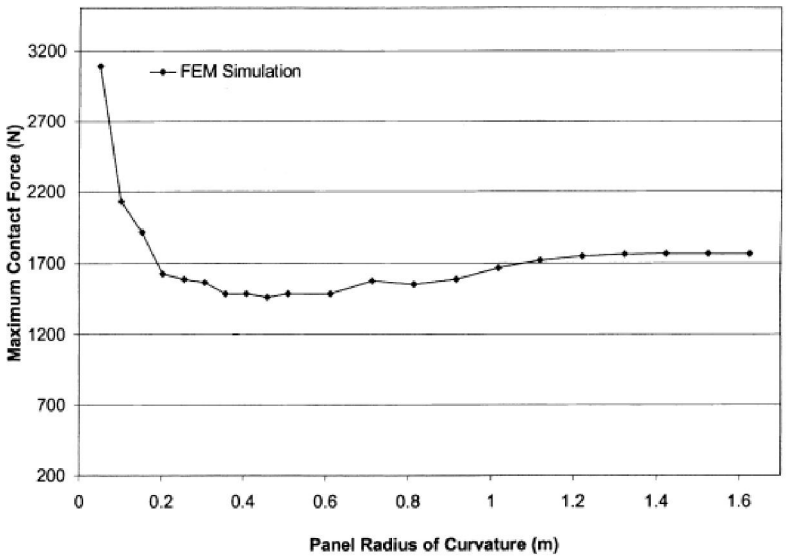

Fig. 2.2. The effect of Radius of curvature on maximum contact force [45]

In another study, Yokoyama et al. [46] developed a damage model formulation based on a methodology that combines stress based, continuum damage mechanics (CDM) and fracture mechanics approaches within a unified procedure by using a smeared cracking formulation. The damage model was implemented as a user-defined material model in ABAQUS FE code within shell elements. They considered the effect of curvature, thickness, and internal pressure on impact response of curved laminate. The results showed that damage

extent under impact loading decreases when combined with internal pressure effects. The results also indicated that larger the plate curvature higher is the amount of dissipated energy during the impact loading. Moreover, the amount of dissipated energy decreases as the plate thickness increases. A finite element code to model dynamic behavior and subsequent damage of a composite cylinder subject to impact loading is successfully implemented by Krishnamurthy et al. [47]. Many parameters considered in this research but what distinguishes this study to others is determining the effect initial hoop stress in a composite cylinder on its impact response. Their test outcomes showed that increased hoop stress enhances the strength and stiffness. The initial hoop stress influence on damage area of each composite layers also was investigated. Ganapathy and Rao [48] considered two kinds of curvature: cylindrical and spherical shell panels. The damage in a spherical shell panel is more than a cylindrical shell panel of same dimensions, since the former is stiffer than the latter.

There are many other studies in this field that the difference between them is: 1- the methodology of determining failure criterion 2- effective parameters such as thickness, curvature, impact energy, boundary conditions and etc [49-55]. Since in what presented here is enough for understanding the effect of curvature, the other studies are not considered.

2.1.3. Effect of curvature type (concave or convex)

Regarding the effect of curvature type on mechanical behaviour of composite laminate under low velocity impact only one conference paper can be found in literature [56]. This study was followed by Vaidya and his group members on E-glass/Vinyl ester composite laminates. Fig. 2.3 is the schematic picture of the test method. The tests conducted on these parameters: 1- Impact energy: 13.5J 2- Two different radii of curvature (200mm and 265mm). The concave curved panels absorbed more energy and load compared to flat and convex curved samples. There is no analysing on damage in this paper and surely a deep consideration needs in this topic. There is another research in this field [57], but the situation is different with what is considering here. Zhang et al. investigated the composite laminates under low velocity impact while the specimen was under post-buckling position (in different modes).

There are some studies in this field under high velocity impact [58,59], but since in this thesis the main study is focused on low velocity impact, more consideration is waived in this section.

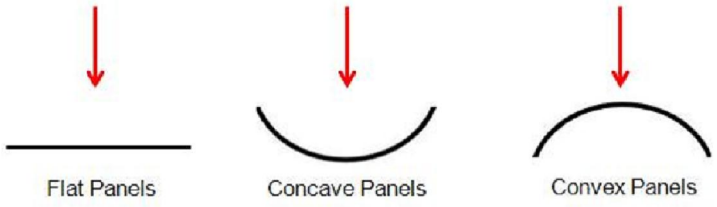

Fig. 2.3. Illustration of impact condition on flat and curved panels. For the curved panel, the impact was imparted on the concave and convex sides respectively [56].

In the following sections some experimental studies will be conducted regarding all topics introduced in this part: 1- The effect of preloading in convex curved laminates 2- the effect of curvature type, convex or concave 3- the effect of preloading on concave laminates under impact loading.

2.2. Experimental program

2.2.1. The effect of preloading on impact response of convex curved laminates

2.2.1.1. Material and specimens:

Unidirectional glass/epoxy prepreg (Ref. 1017) supplied by G. Angeloni Srl was used in this research; its mechanical properties are shown in Table 1. All these parameters was evaluated experimentally except G_{12} which was estimated according to literature [60-62]. Thirty six composite specimens with 168 mm length, 100 mm width, 3.1±0.1mm thickness, and 20 mm height as illustrated in Fig. 2.4 were manufactured in an autoclave by stacking 10 unidirectional plies with sequence of $[0/90/0/90/0]_S$.

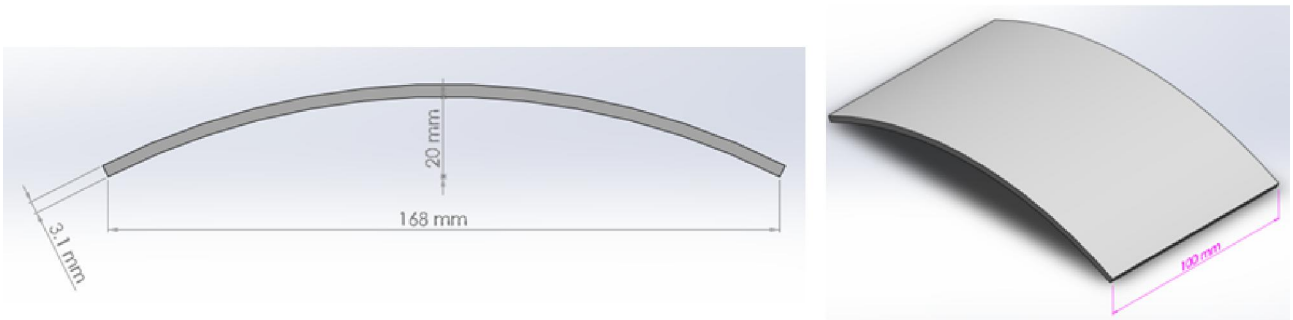

Fig. 2.4. Schematic picture of curved laminate with dimensions

Table 2.1. Mechanical Properties of Glass/epoxy lamina.

E_1 (Gpa)	E_2 (Gpa)	G_{12} (Gpa)	V_{12}	
44	11	4.5	0.28	
X_t (MPa)	**X_c (MPa)**	**Y_t (MPa)**	**Y_c (MPa)**	**S (MPa)**
1000	500	80	130	60

2.2.1.2. Test setup

Three different drop heights of 0.5, 1, and 2m, corresponding to a nominal potential energy of 6, 12, and 24 J, and two different pre-strains of 3000 and 5000 με, were chosen to consider the effect of preloading in different impact energies and boundary conditions. Three specimens were used for each combination of parameters. The tests were conducted in a custom built drop-weight machine equipped with a laser device (to measure the initial velocity) and a piezoelectric load cell attached to the impactor. The signals of both load cell and laser were acquired at 100 kHz sampling frequency without any filtering except the intrinsic one due to the measurement chain. The hemispherical head of the load cell had a diameter of 12.7 mm and the total mass of the impactor was 1.22 Kg. The curved laminates were positioned under this drop tower and preloaded by means of a special fixture designed and fabricated to meet the goals of this research (Fig. 2.5).

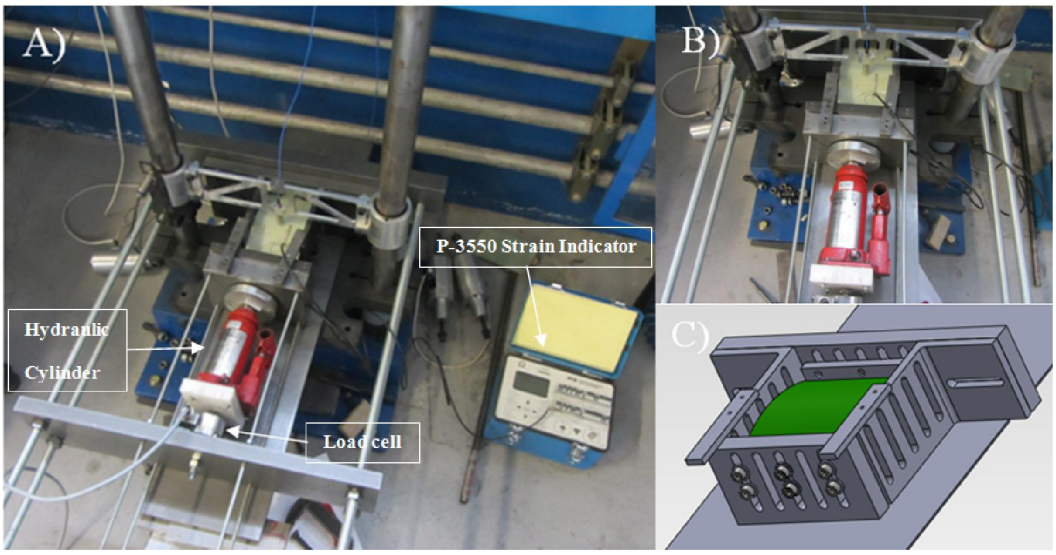

Fig. 2.5. A) Drop weight machine **B)** The fixture used for conducting load **C)** A schematic drawing of fixture

In order to apply the preload two parallel steel plates were used with the load cell placed between one of them and the hydraulic cylinder. A strain gauge was installed on each specimen, but the load cell was used for obtaining more precise results. The impact tests were conducted for two different boundary conditions (Fig. 2.6):

1- The straight edges fixed in *x* and *y* directions and the curved edges free (indicated with "S" in the figures)

2- The same boundary conditions for the straight edges but the curved edges fixed only in *y* direction, by using special supports (indicated with "F" in the figures). The nuts illustrated in Fig. 2.6-B were located in the side rails shown in Fig. 2.5-C and fastened with screws.

Velocity $V(t)$ and central displacement $U(t)$ of the impactor were obtained by calculating the first and second numerical integration of force $F(t)$, respectively, as given in Eqs. (2.1) and (2.2),

$$V(t) = V_i + \int_0^t a(t)dt = V_i - \frac{1}{m}\int_0^t F(t)dt \tag{2.1}$$

$$U(t) = U_0 + \int_0^t V(t)dt \tag{2.2}$$

where V_i is initial velocity before contact obtained from the laser device and U_0 is the initial displacement which is supposed to be zero (as initial condition in t=0). $a(t)$ and m are acceleration and mass, respectively. Absorbed energy E_a can be calculated from the following equation,

$$E_a(t) = \frac{m\,(V^2(t) - V_i^2)}{2} \tag{2.3}$$

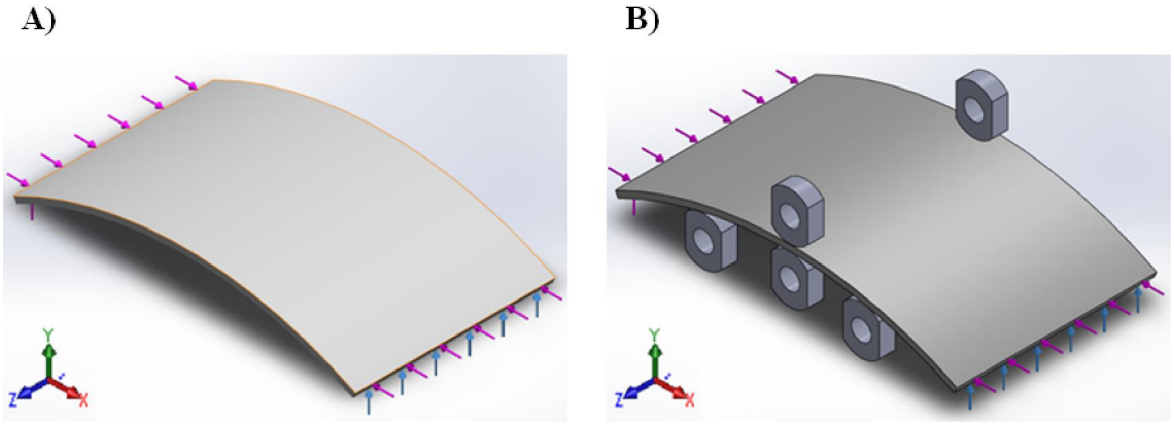

Fig. 2.6. The boundary conditions applied on: A) the specimen labeled with "S"
B) the specimen labeled with "F"

2.2.1.3. Results and discussion

Twelve different combinations were considered to find the effect of preloading on the impact response of curved laminates. The impact force-displacement curves are illustrated in Fig. 2.7 Each situation has a specific code in this figure which is defined as follows: (The type of boundary condition: “S” or “F”-The amount of pre-strain 0, 3000, or 5000-The amount of impact energy: 6, 12, or 24J).

When pressure is applied on curved laminates the curvature and the stiffness increase [38]. On the other hand, also by using the “F” boundary condition the stiffness of laminates increased. Comparing the curves in Fig. 2.7 and considering the relation of maximum force to maximum displacement for both these conditions in comparison with reference specimens (without preload and with the “S” boundary condition), the effect of preloading (by 5000με) on stiffness of laminate is much more than the “F” boundary condition. When these two effects combine, F-5000-6 or 12J, the maximum contact force and minimum deflection were obtained, and on the contrary, for S-0-6 and 12J this behavior is completely the opposite.

The delamination threshold force can be obtained from the force–time history and is described as the force level at which a sudden force drop happens due to material damage [63]. Fig. 2.8 shows the force-time history of curved laminates under 12J impact energy and “S” boundary condition. The position of delamination threshold force on curves is determined by a black oval. As shown, in all curves the delamination starts almost at the same time, but at different values of force. In Fig. 2.8, in the region marked by the red oval, some small force drops or oscillations can be appreciated. Such a behavior of force-time diagram can be associated with the introduction of transverse matrix crack or localized indentation of the specimen as described by Schoeppner and Abrate [64] .It is interesting to note that by increasing the preloading, the impact force required to onset the delamination and matrix cracks increases as well.

In the following section, the effects of preloading and boundary conditions on all impact parameters, i.e maximum contact force (F_{max}), displacement (U_{max}), absorbed energy (E), damaged area (A), and time-duration of impact (t_F) are considered.

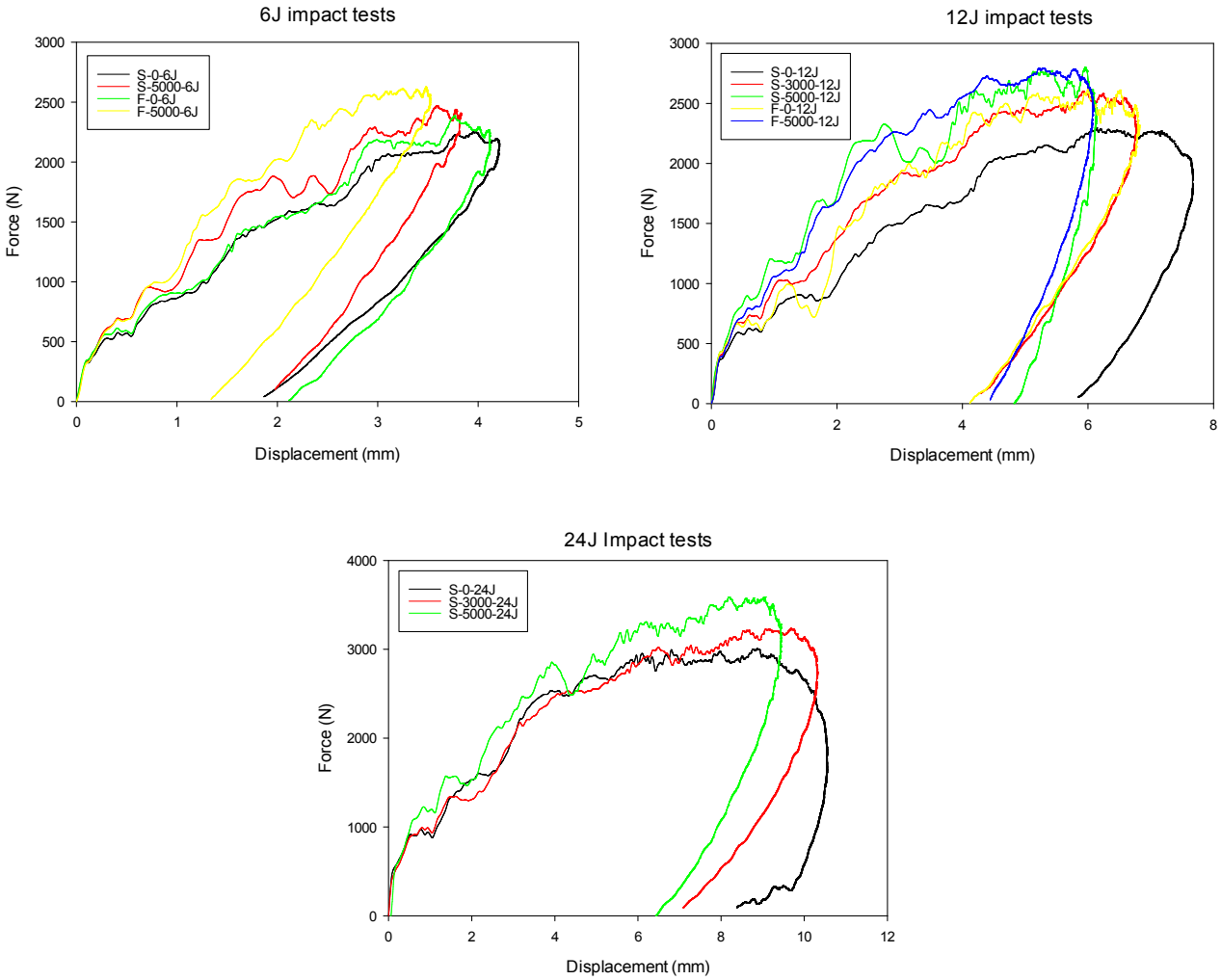

Fig. 2.7. Force versus impactor displacement for all laminates

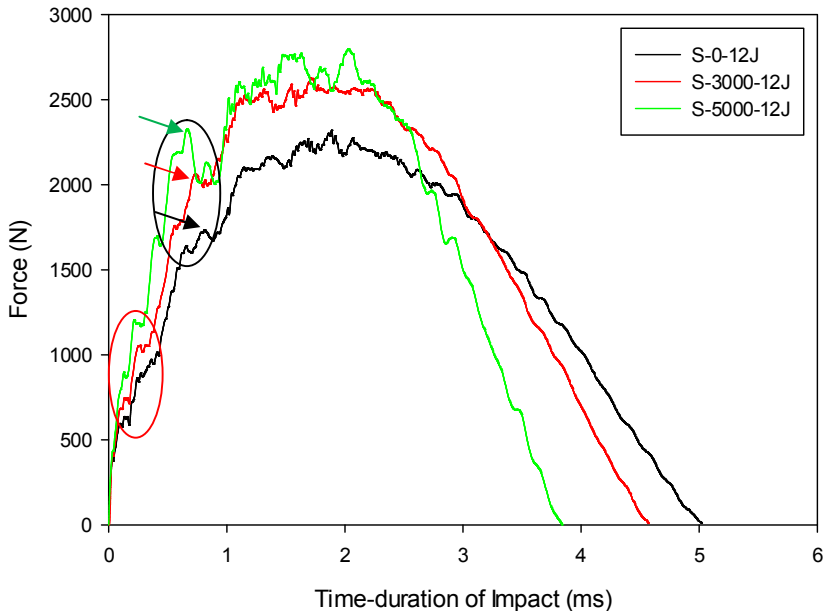

Fig. 2.8. The force history during impact loading under energy of 12J and "S" boundary condition

a) Effect on maximum contact force:

The effect of different combinations on maximum contact force is shown in Fig. 2.9. By increasing the preloading to 3000 and 5000με, the maximum force increased. This phenomenon is related to two different factors: changing the curvature and tension stress in the upper part of the specimen. Using these results, it is not possible to determine what percentage of this increment is due to the effect of curvature and how much to the effect of tension preloading. However, in the next step of this study, this will be considered.

Comparing the outcomes with different impact energies shows that in higher impact energies, the difference between the maximum load of 5000με and 0με is much higher. For example, this difference for 6J-energies is about 290N (9.7% increase), while for 12J it is 480N (20.8% increase) (for the "S" boundary condition) (Table 1-A).

By applying the "F" boundary condition, the maximum load is enhanced because of the decrease in compliance. However, it is interesting to note that when this boundary condition was utilized, the effect of preloading decreased. This means that the difference between the maximum force of F-0-12J and F-5000-12J (7.3% increase) is less than the difference between S-0-12J and S-5000-12J (20.8% increase) (Table 2-B).

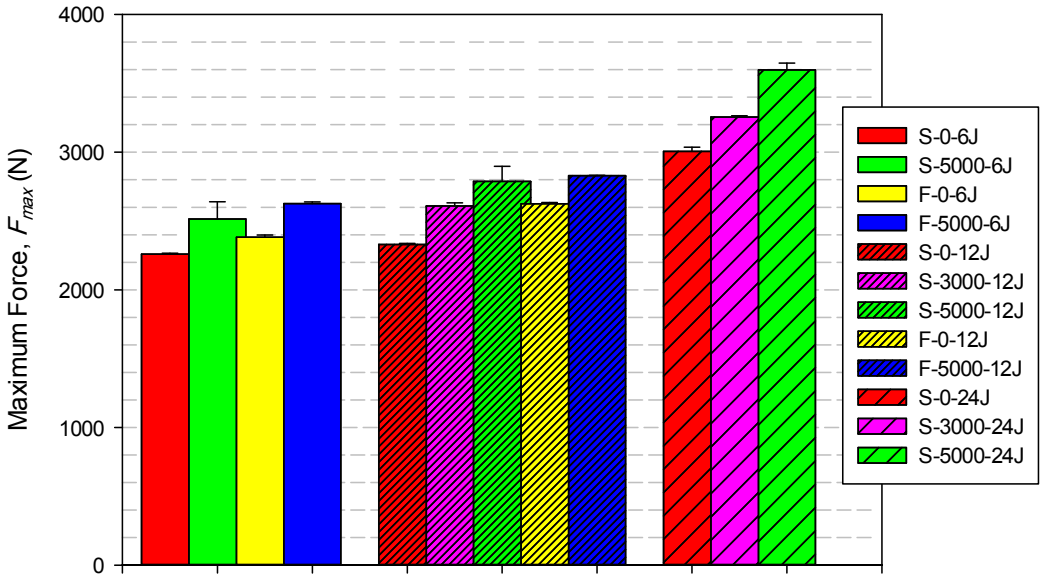

Fig. 2.9. Maximum force of impact tests for all situation

Table 2.2. The effect of A) Pre-load B) Boundary conditions on Maximum force

(A)	S-0-6J	S-5000-6J	S-0-12J	S-5000-12J
Maximum Force (N)	2250	2470	2300	2780
Variation (%)	0	9.7	0	20.8

(B)	S-0-12J	S-5000-12J	F-0-12J	F-5000-12J
Maximum Force (N)	2300	2780	2600	2790
Variation (%)	0	20.8	0	7.3

b) Effect on maximum deflection and time-duration of impact:

The displacement history calculated by Eqs. (1) and (2) includes the specimen deflection and any indentation or penetration. The time duration of impacts and maximum displacements are shown in Figs. 2.10 and 2.11. As shown in these figures and comparing their results with Fig. 2.9, it can be see that the trend is completely similar to each other and opposite to the maximum force. In any condition in which there is an increase in force, the displacement decreases. This is because the increase of curvature decreases the compliance of laminates, thereby resulting in lower central displacement and higher impact force.

Table. 3 presents the preload and boundary condition effect on time-duration of impact and maximum displacement under impact of 6 and 12J. Mostly in all situations, except one, both factors lead to decrease in t_F and U_{max}, but preload influence is significantly more. For instance, Pre-strain of 5000με and "F" boundary condition reduced t_F 12% and 5.9% in comparison with reference laminates, respectively. According to this table, increase of the impact energy from 6 to 12J caused 17.5% and 82% enhancement in t_F and U_{max}, respectively.

Table 2.3. The effect of Preload and boundary conditions on time-duration of impact and maximum displacement (6 and 12J)

	S-0-6J	S-5000-6J	F-0-6J	S-0-12J	S-0-12J	F-0-12J
Time-duration of impact (ms)	4.22	3.71	3.97	4.96	4.22	4.65
Variation (%)	0	-12%	-5.9%	0	-14.9%	-6.25
Maximum Displacement (mm)	4.2	3.82	4.41	7.65	6.12	6.8
Variation (%)	0	-9%	+5%	0	-20%	-11%

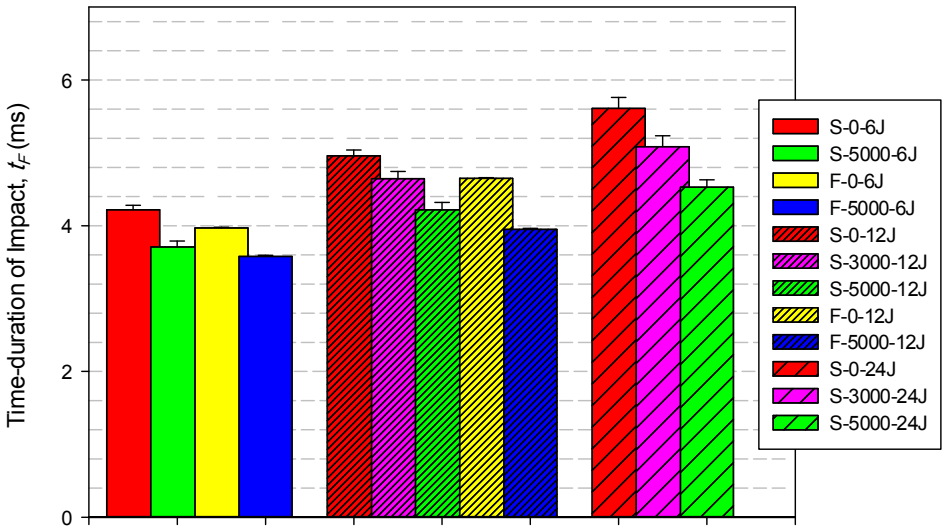

Fig. 2.10. Time-duration of impact tests for all situations

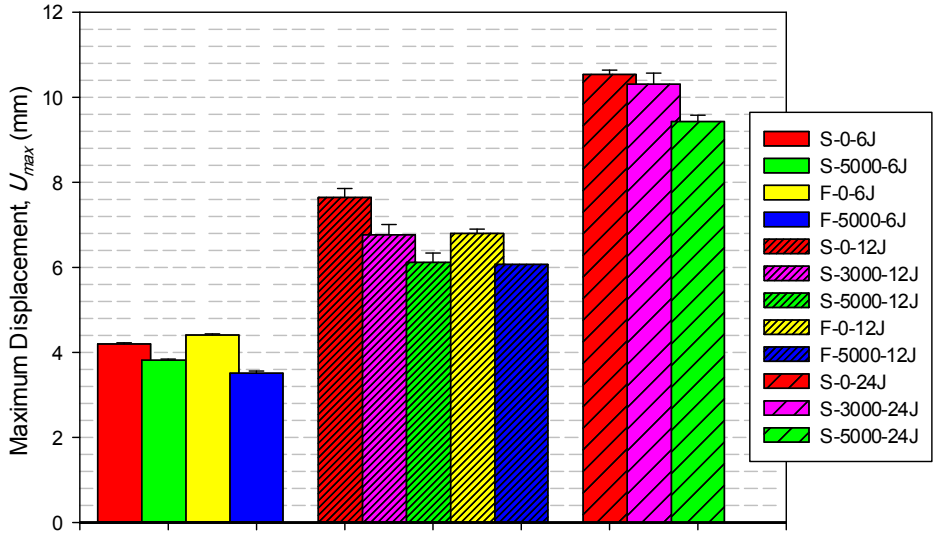

Fig. 2.11. Maximum Displacement of impact tests for all situations

c)Effect on damaged area:

The size of the damaged area is illustrated in Fig. 2.12. To find the exact results of this parameter, the following steps were performed: 1-Near the damaged area, a 1cm-line was drawn 2-Placing a strong light source behind each specimen, some photos were taken. 3- The pictures were imported to AutoCAD software to calculate the area. 4-The 1cm-line was used for scaling all dimensions in the software.

Generally, by raising impact energy, preloading, and applying the "F" boundary condition the damage area increased. The trend of their effects is exactly the same with what mentioned in the last section. Comparing red (reference laminates), green (preloaded laminates), and yellow (supported laminates by "F" boundary condition) columns (6 and 12J) in Fig. 2.12 demonstrates that preloading can cause more damage area for composite laminates.

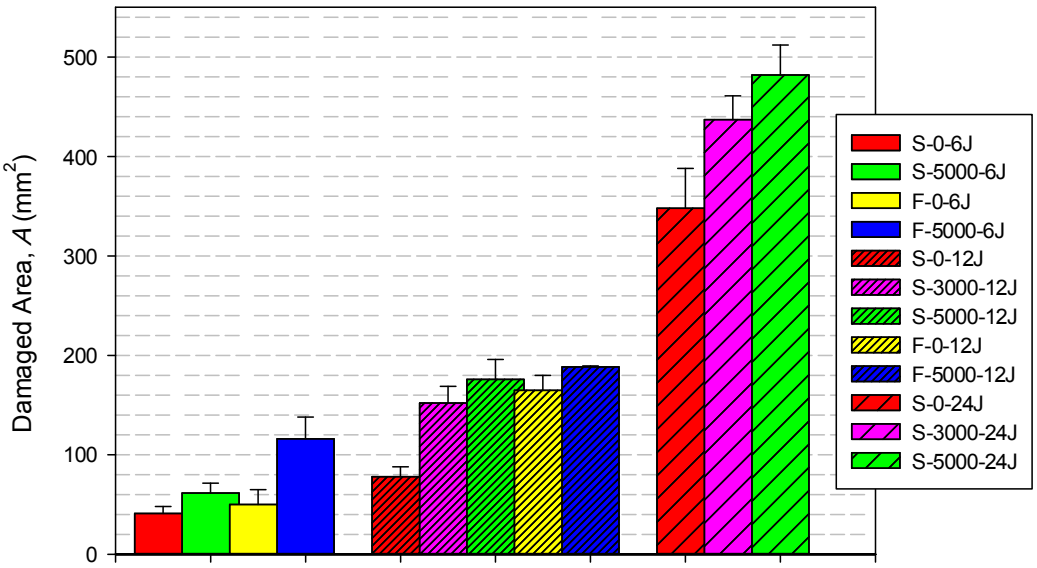

Fig. 2.12. Maximum Displacement of impact tests for all situations

Table 2.4. The effect of preloading value on damaged area (*A*)under 12 and 24J

	Reference (Red column)	**Preloading of 3000με (Violet column)**	**Preloading of 5000με (Green column)**
Panel radius of curvature (*R*) (mm)	190	148	126
Variation(%)	0	-22.1%	-33.7%
Damaged area, *A* (6J) (mm^2)	78	152	176
Variation(%)	0	94.8%	125.6%
Damaged area, *A* (12J) (mm^2)	348	437	482
Variation(%)	0	25.5%	38%

The effect of preloading value on damaged area is presented in Table 4. As shown, the most portion of damage area was caused by 3000με. While this amount of preloading enhanced *A* to 94.8%, 5000με

increased it to 125.6% which is only 30.8% more (for 6J impact energy). From this situation, a very important result can be obtained. By increasing the preload from 0 to 3000με, the radius of curvature (*R*) reduced 22.1%, i.e. curvature increased. Continuing to increase preload up to 5000με, i.e. 66.7% increase, lead to decrease *R* to 33.7% which is only 11.6% less than last situation. Therefore it can be concluded that curvature affects more than preloading on damaged area. This story is the same for 12J-energy impact tests as shown in the table.

When a foreign object impacts on a composite laminate, the following damage modes can occur in the laminate: delamination, splitting, matrix and fiber cracking. Depending on different situations and parameters such as the impact energy, the shape of the laminate, boundary conditions, etc., different damage modes can occur. In order to have a more precise idea, some images from the front and back surfaces of the damaged samples (front surface is impacted) are provided in Figs. 2.12 and 2.13, respectively. As seen, due to the conditions of the impact tests, only delamination, splitting, and matrix cracking can be observed, delamination and matrix cracking being the dominant mode. From the view of the back surface (Fig. 2.13) in all impacted specimens, delamination and matrix crack modes exist, but splitting cannot be observed in non-loaded 6J-tests. One very interesting phenomenon that occurred is that when the preloading increased in the laminates, the level of matrix cracking decreased. This means the maximum matrix cracks can be found in non-preloaded specimens. The existence of compression stress in the lowest layer of the laminate, during impact loading, restricted the propagation of cracks in the matrix. The reason of this phenomenon can be described as follows: preloading causes tensile and compressive stresses on the top and bottom surfaces respectively, while impact loading leads to compression on the top and tension on the bottom. Therefore during impact the stresses caused by these two loads have opposite sign. For matrix cracking the dominant criterion is the maximum tensile stress. When the specimen is under pre-loading, the tensile stress caused by impact loading is less than the situation of without preload. So, by increasing the preload the amount of matrix cracks decreases.

It is also worth mentioning that in lower impact energies, 6 and 12J, the shape of the damaged area is approximately ellipsoid, but in higher impact energy, 24J, it is rhombic like.

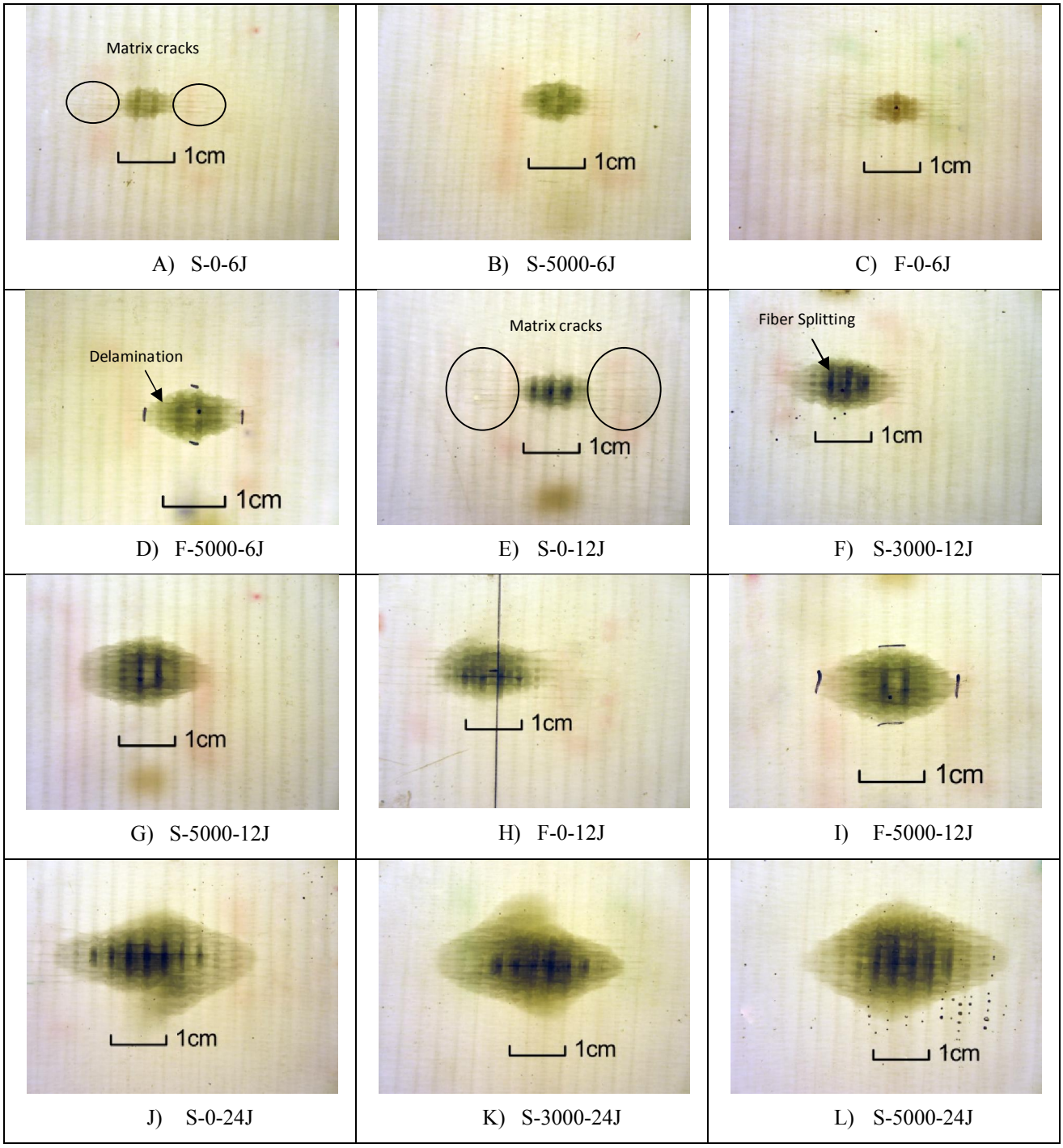

Fig. 2.13. The image of damaged area in back surface

For the front surface (Fig. 2.14), not all specimens are shown because for the 6J-impact tests, the specimens had almost the same shape and mode of failure (delamination) and only the level of the area slightly increased or decreased. Therefore Fig. 2.14-A is illustrated as representative of the others. In higher impact energies, 12 and 24J, all damage modes of delamination, fiber splitting, and matrix cracks are clearly visible. Unlike the back surface, when the specimen is under preloading, the matrix cracks are more on the front

surface. This proves that tension stress in the upper surface and compression stress in the lower one increased and decreased, respectively, matrix cracks in laminate composites. Another point is that the direction of matrix cracks are mostly in the same direction with preloading, while the direction of splitting is orthogonal to it.

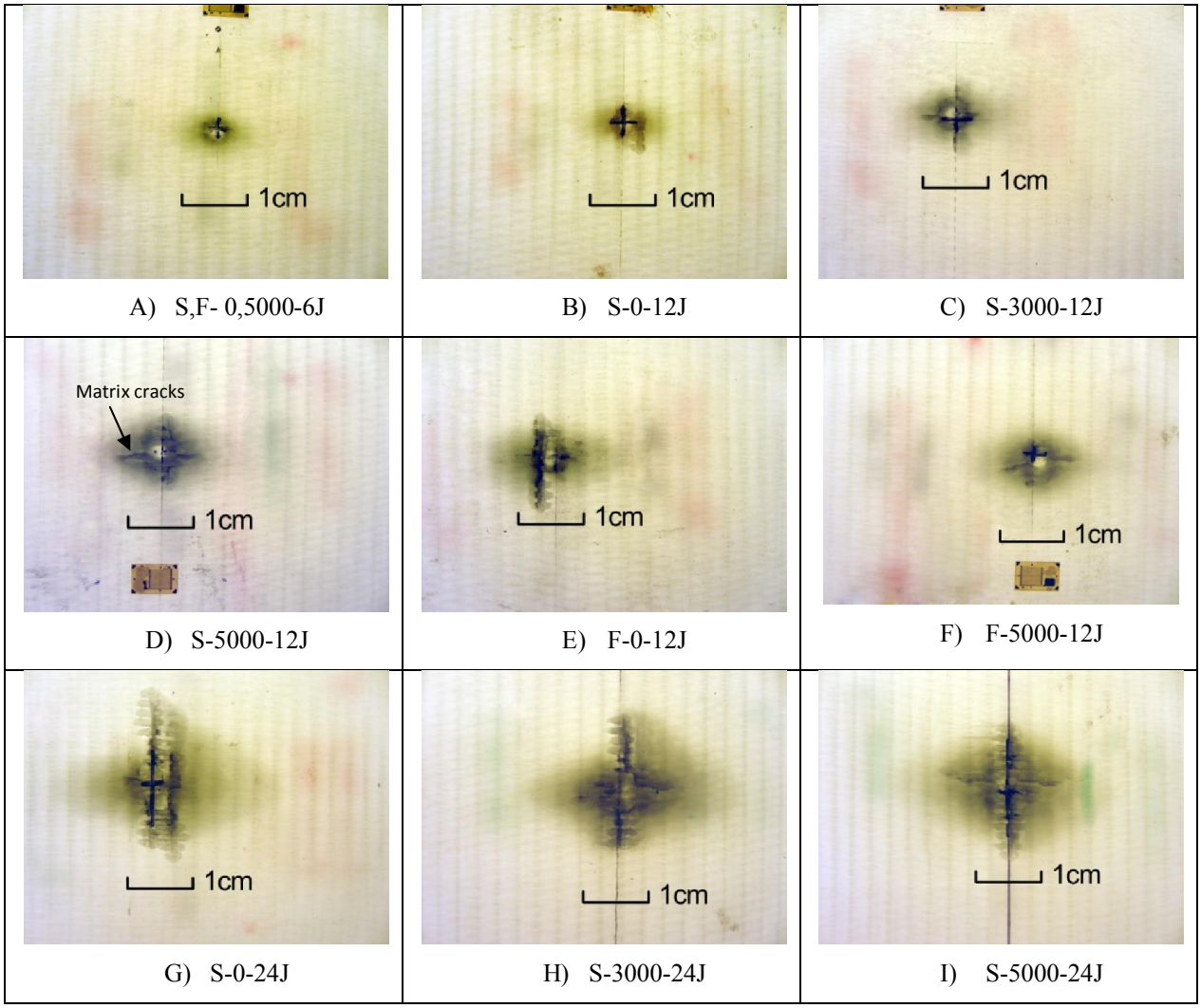

Fig. 2.14. The image of damaged area in front surface

d) Effect on Absorbed Energy:

In this section the effect of preloading on total energy absorbed during impact (E_{at}) is considered. This parameter was calculated by replacing the rebound velocity of impactor at end of the test in Eq. (3). As shown in Fig. 15, there is a decreasing trend in absorbed energy by raising the preloading (regardless of some experimental errors). By comparing this figure with Fig. 2.12, an uncommon behavior attracts attention. It is demonstrated that by increasing the preload, the damaged area increased and absorbed energy

decreased, while flat laminates mostly do not show this phenomenon in different situations [65, 66]. This behavior has been considered before in several papers [30,67, 68]. Robb et al. [30] shows experimentally that by exposing flat E-Glass/polyester laminates under 6000με-biaxial tension, the damage area and absorbed energy are 1.18 more and 0.93 less, respectively, in comparison with unstressed laminates. Sun and Chattopadhyay [67] analytically considered the dynamic response of anisotropic laminated plates under initial stress subject to impact. In their study, also the initial stress was biaxial tension. Contact force and dynamic response are obtained by solving a nonlinear integral equation. They showed that less energy is absorbed if the plate is under pre-stress. The reason for this behavior is more intelligible in numerical studies conducted by Krishnamurthy et al. [68]. They considered the impact response of cylindrical shell panels (curved laminate) and cylindrical shells (full cylindrical laminate) under different situations: mass and velocity of impactor, radius of curvature. In a part of this research, the effect of curvature on the absorbed energy of cylindrical shells was considered. Two parameters of E_s and E_d represent the total energy absorbed by the structure during impact and the energy used for causing indentation/damage. As shown in Fig. 2.16-A [68], the maximum load belongs to R (the radius of the cylinder) =0.05m and so the specimen is in the stiffest position. But according to Fig. 2.16-B [68], the total absorbed energy, E_s, during impact loading is the minimum. On the other hand, the maximum E_d used for damage and indentation is for the position of R=0.05. These curves prove that while total absorbed energy, Es, decreased, damage and indentation can rise. It is also clear that the energy used for indentation/damage is a minor fraction of the energy transferred to the shell, and most of E_s is obviously used in deforming the shell. It should be mentioned that the curves in Fig. 13-A are for different combinations for comparison with curves in Fig. 2.16-B. They are illustrated only for considering the effect of curvature.

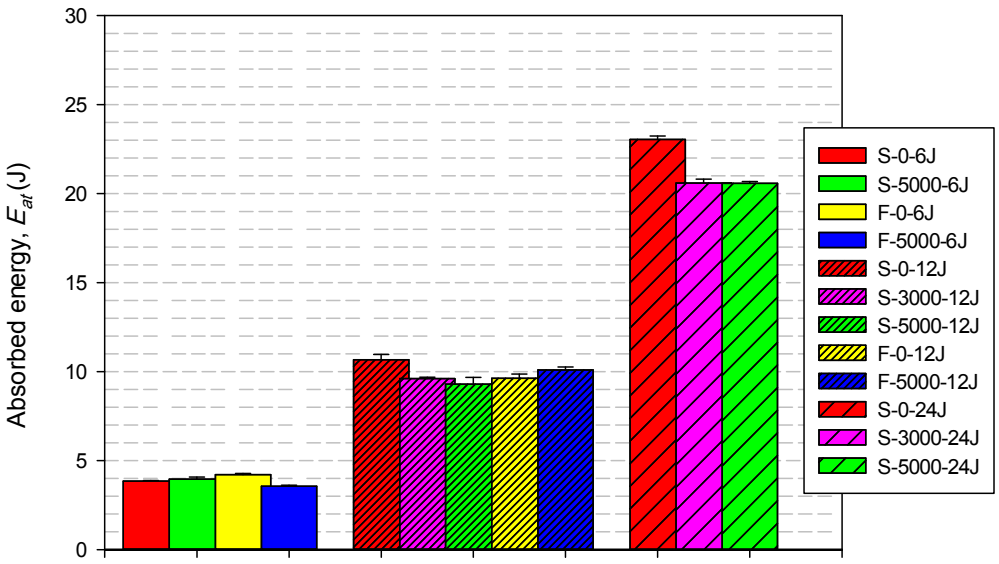

Fig. 2.15. Absorbed energy of impact tests for all situations

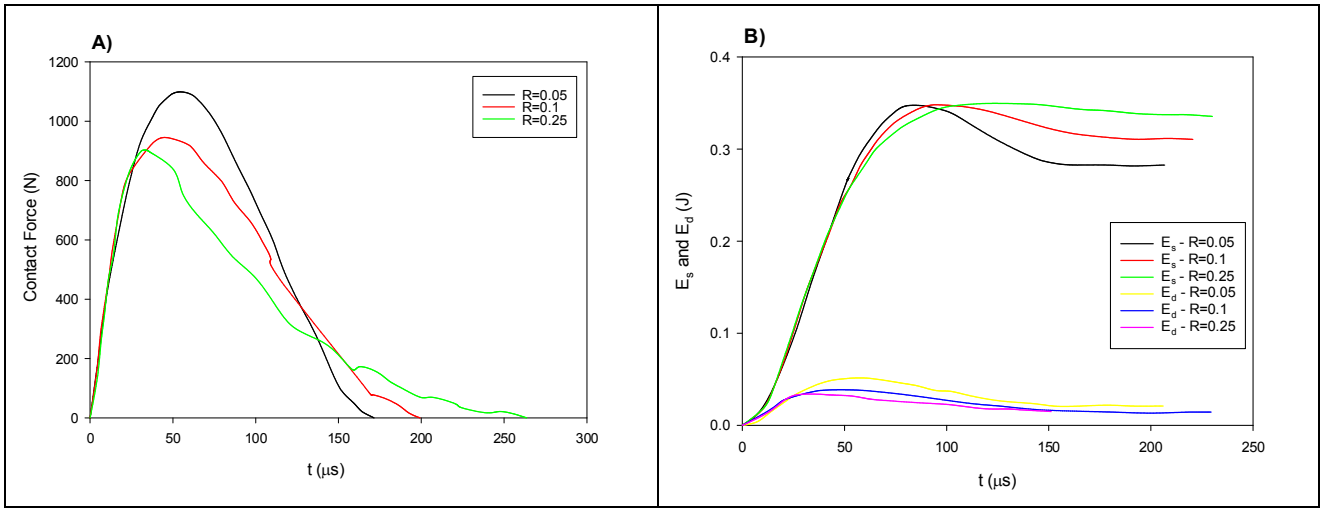

Fig. 2.16. Effect cylinder radius on A) contact force, B) E_s, E_d during impact on a composite cylinder (The curves in (A) and (B) belong to different situation such as various mass and velocity of impactor) [68]

2.2.2. Determining the contribution rate of pre-stress and curvature on impact response of preloaded curved laminates

In the last part, it was shown that preloading changed the impact parameters of curved laminates significantly by increasing curvature and tensile and compression stress through the thickness. A very important question regarding this effect is: what is the contribution level of stress and curvature on impact parameters specially

damaged area. For answering this question a new test was conducted in the following method. Three different specimens were provided:

1- Nine specimens which their curvature was the same with the last test and no preloading will be conducted during the impact test (Type A). 2- Nine specimens which their curvature is the same with the same group, but will be under pre loading during the impact test (preloaded Type A). 3- Nine specimens that their curvature is the same with the second group (after their preloading) and no preloading will be conducted during impact test (Type B). It should be mentioned that the curvature of the Type A specimen is about 190mm and the curvature of the two others is about 125mm. Since the curvature of the second and third groups is the same, so the effect of stress on impact parameters can be determined. Fig. 2.17 is shown the configuration of all samples. The material and test setup is the same with the last test and impact tests were conducted under 6, 12, 24, and 36J. The pre-strain is the second group of specimens is 5300με.

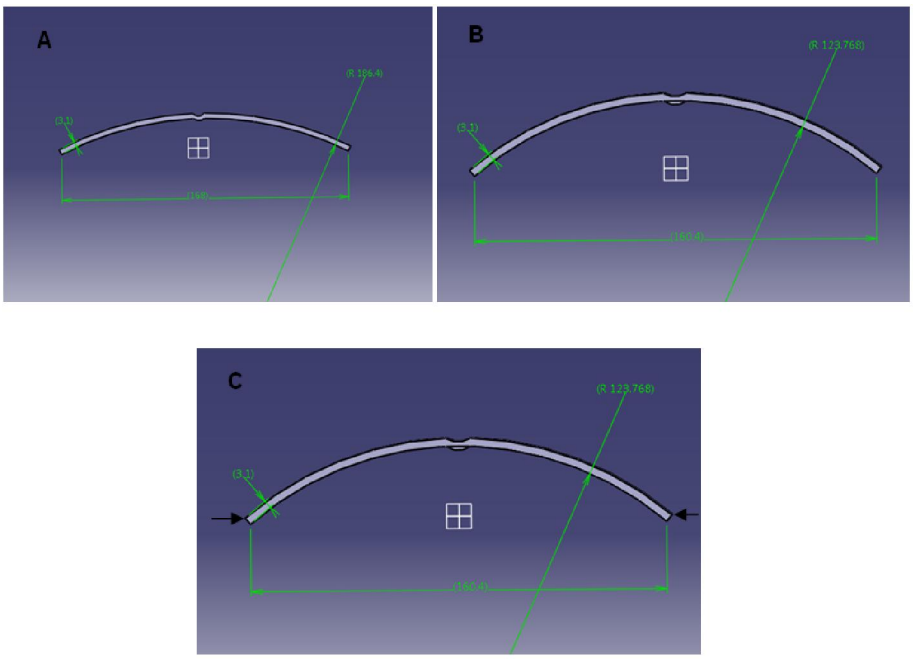

Fig. 2.17. Configuration of the samples for determining the contribution rate of pre-stress and curvature on impact response of preloaded curved laminates: A) Type A B) Type B C) Preloaded Type A.

2.2.2.1. Results and discussion

The Force-Displacement curves obtained from impact tests are shown in Fig. 2.18. As seen the group of "Type B" and "Preloaded Type A" have a very similar behavior, while the group of "Type A" follows a

completely a different trend. Since in the “Type A” specimens the curvature is less and also there is no preloading the stiffness is less, but the other two other groups the stiffness is almost the same which shows the stiffness is more depends on curvature, not pre-stress. For considering more details, the impact parameters: maximum load, maximum displacement, time-duration of impact, and damaged area are presented in Figs. 2.19 and 2. 20.

According to Fig. 2.19 all impact parameters are almost the same for the “Preloaded Type A” and “Type B” specimens that shows pre-stress does not affect on these parameters significantly. On the other hand in the “Type A” specimen in which the curvature is more and there is no pre-stress the impact parameter is completely different. Therefore, the maximum displacement and time-duration of impact is more and maximum force is less in comparison with two other configuration. It is related to this fact that when the curvature is less the stiffness decreased and so under the impact loading less force can be transferred to the specimen.

The effect of the pre-stress and curvature on damaged area is shown in Fig. 2.20. The effect of curvature and pre-stress on the damaged are is completely visible from this figure. By applying preload the curvature and pre-stress increased in the laminate (Preloaded Type A) and so damaged area increased. For understanding the contribution level of pre-stress and curvature in this situation “Type B” specimens were provided that its curvature is the same with “Pre-loaded Type A”, but does not have pre stress. As shown in the Fig. 2.20 the damaged area in “Type B” specimen is much more than “preloaded Type A” that means preloading could decrease the damage in the laminate. This result is very important in designing of composite components. When in a specific structure, a curved laminate composite should be used, by applying a pre-stress this part will be more safe.

Table 2.5 presents more details about the effect of curvature and pre-stress on damaged area. Table 2.5-A shows that decreasing the radius of curvature from 190mm (Type A) to 125mm (Type B) increased the damaged area about 100% in various impact energies. On the other hand, by applying pre-stress on the specimens (Preloaded Type A) the damaged area increased from 36% to 62%. Table 2.5-B showed the effect of pre-stress, while the curvature of both samples of “Preloaded Type A” and “Type B” is the same. The results show that the pre-stress, decreased the damaged area from -16% to -32% in different impact energies.

Table 2.5. Damaged area in different configuration under various impact energies.

A	6J			12J			24J			36J		
	Type A	Preloaded Type A	Type B	Type A	Preloaded Type A	Type B	Type A	Preloaded Type A	Type B	Type A	Preloaded Type A	Type B
Damaged Area	27.3	43	57	51	72	107	151	205	244	211	342	473.5
Variation (%)	--	+57.5	+109	--	+41	+110	--	+36	+92	--	+62	+124

B	6J		12J		24J		36J	
	Preloaded Type A	Type B	Preloaded Type A	Type B	Preloaded Type A	Type B	Preloaded Type A	Type B
Damaged Area	43	57	72	107	205	244	342	473.5
Variation (%)	-24.5	--	-32.7	--	-16	--	-27.7	--

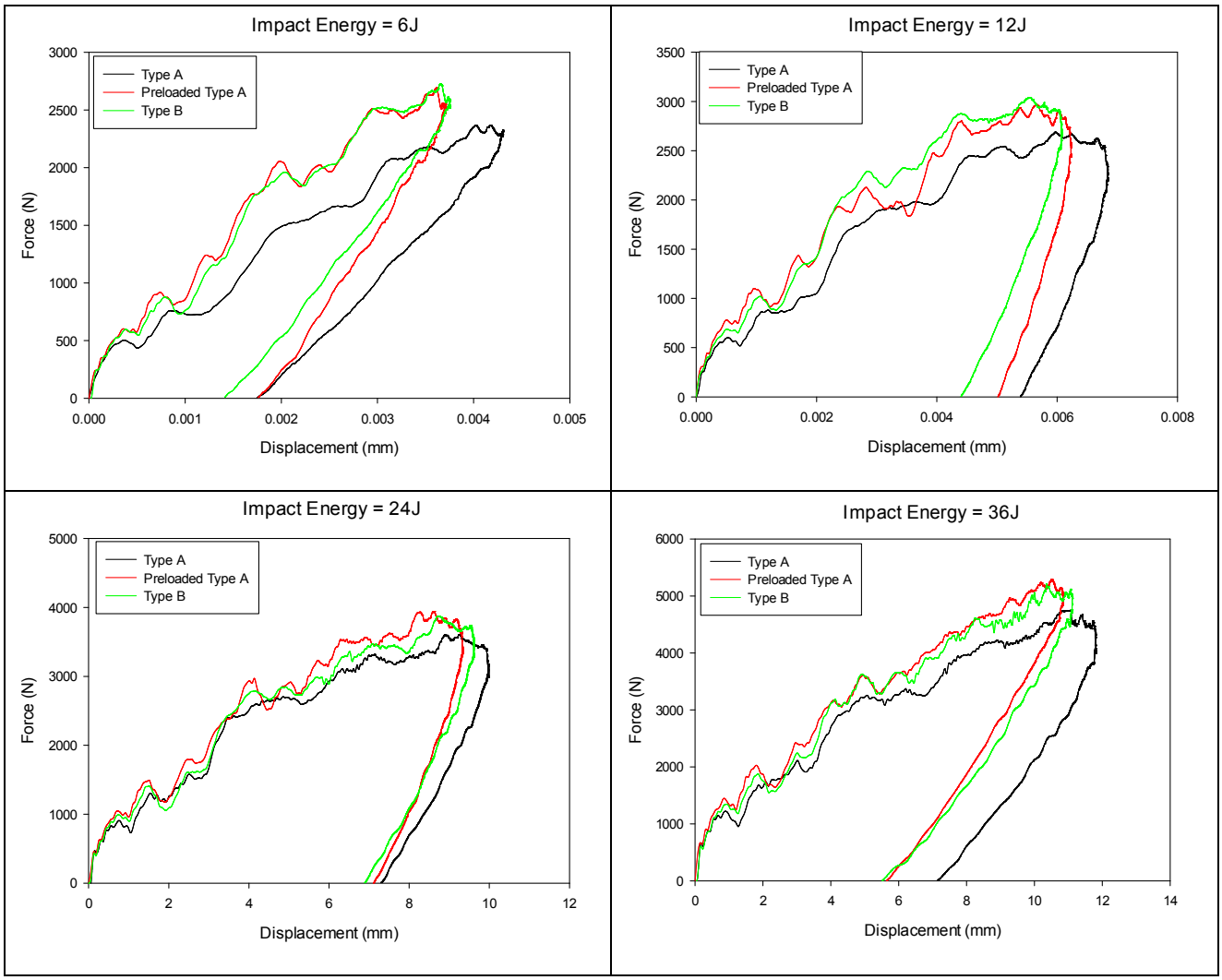

Fig. 2.18. Force versus impactor displacement for impact energies of: 6J, 12J, 24J, and 36J

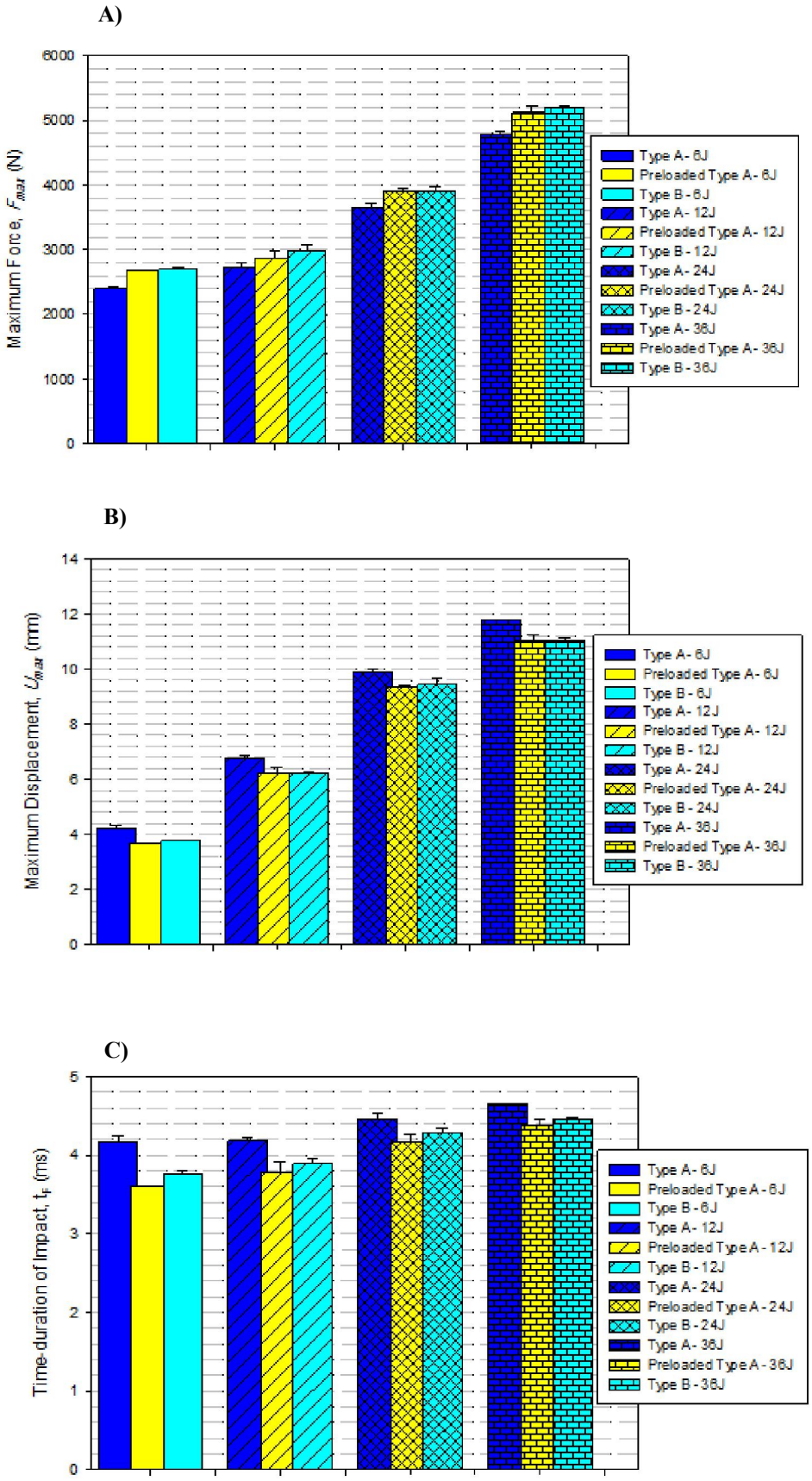

Fig. 2.19. The effect of different configuration on: A) maximum load B) maximum displacement and C) impact duration.

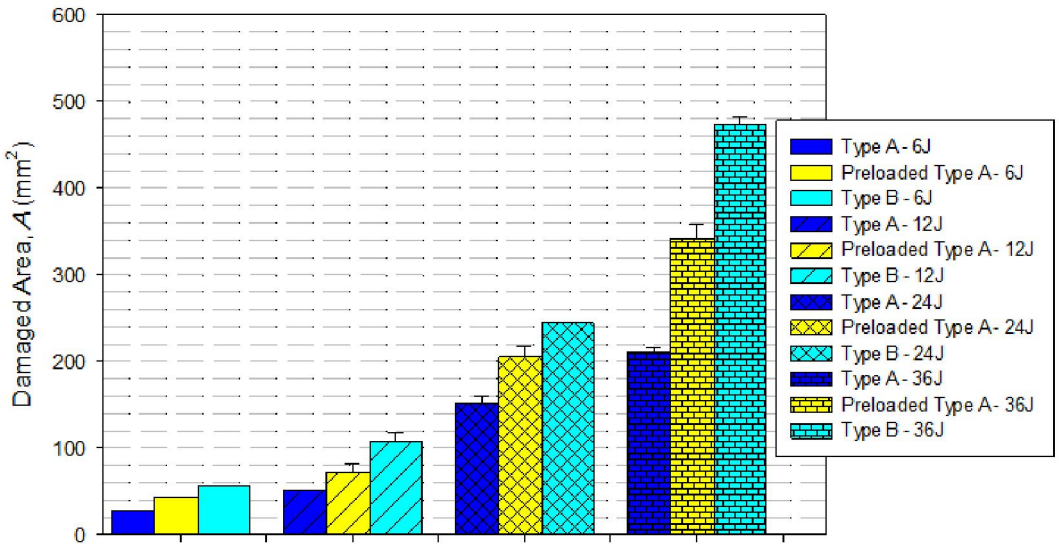

Fig. 2.20. The effect of different configuration on damaged area.

2.2.3. The effect of curvature type, convex or concave

In this section the effect of curvature type, convex or concave, on impact response of composite laminate is considered. For this aim, the impact tests were conducted for each situation under 6,12,24, and 36J.

2.2.3.1. Material, specimens, and test setup

The material and its mechanical properties are the same with what presented in the last part. As seen in Fig. 2.21, another kind of specimen is used for this test. Because in the concave situation, the specimen is under tension stress during impact (membrane effect) so the last specimen could not bear this stress. Fifteen composite specimens with 188 mm length, 100 mm width, 3.3±0.1mm thickness, and 20 mm height as illustrated in Fig. 2.21 were manufactured in an autoclave by stacking 10 unidirectional plies with sequence of $[0/-45/45/90/0]_S$. The test setup is again the same with the last test with only one difference in which 3 holes were made to each straight support to fasten the specimen to the fixture by screws. For each situation, 2 or 3 tests were conducted. If the results of the first two tests were near to each other, the 3 one waived.

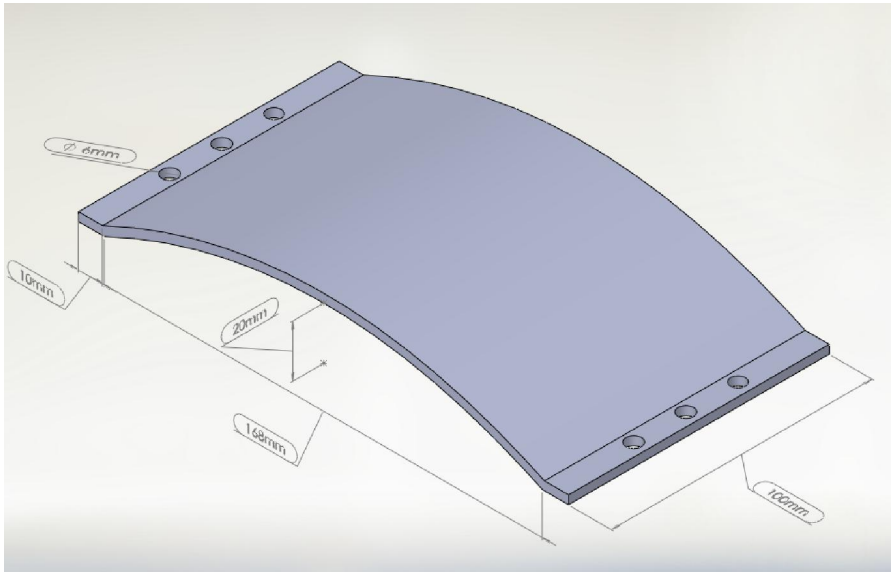

Fig. 2.21. Configuration of the specimen for conducting impact tests on the convex and concave surfaces

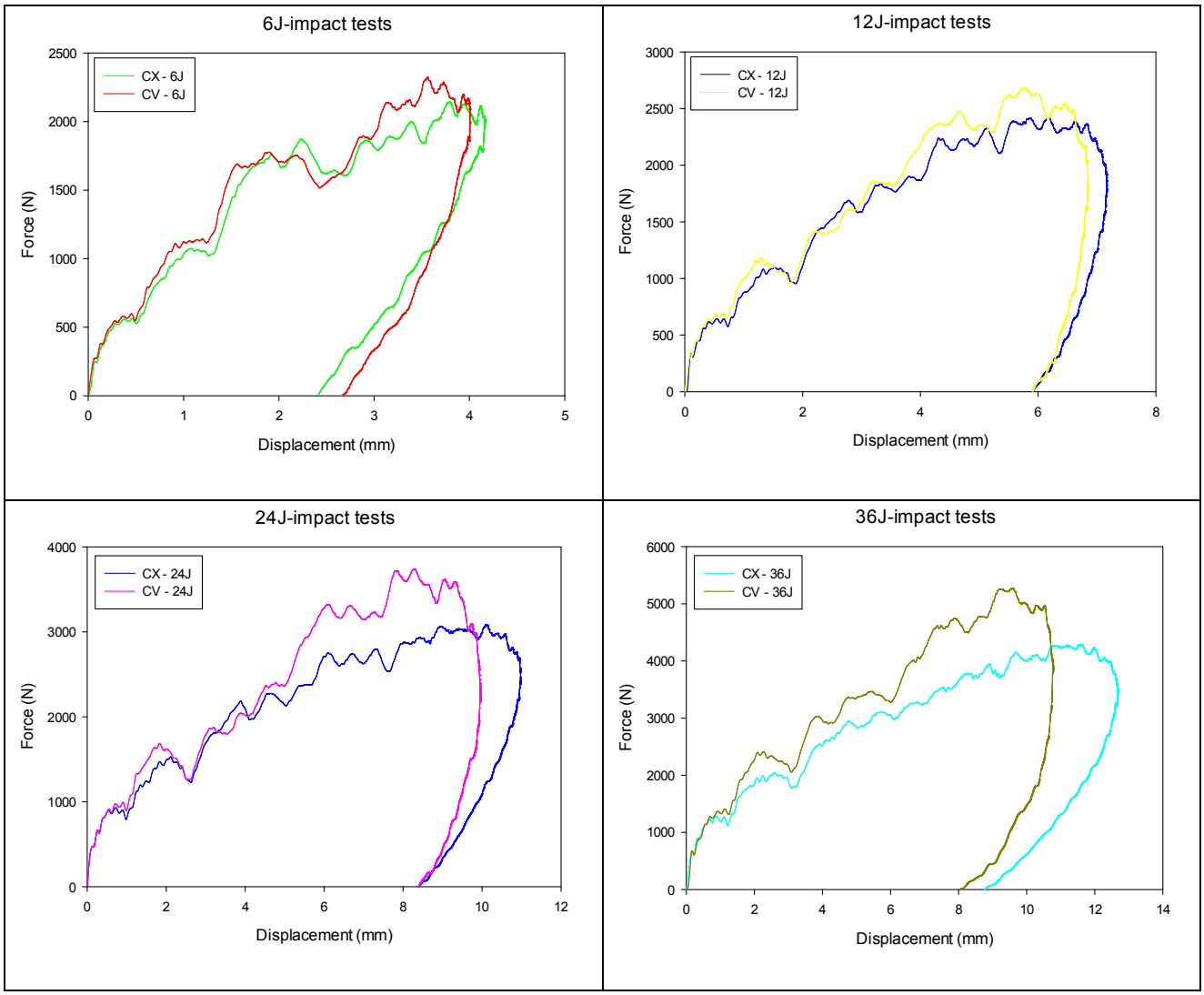

Fig. 2.22. Force versus impactor displacement for impact energies of: 6J, 12J, 24J, and 36J

2.2.3.2. Results and discussion

Fig. 18 shows the Force-Displacement curves in which "CX" and "CV" represent convex and concave configurations. As completely visible, in concave configuration the maximum force is more and maximum displacement is less than convex samples, so the stiffness of concave laminates are more than convex ones. Table 2.6. presents more details about the effect of specimen shape and impact energy on stiffness. As shown, increasing the impact energy causes more difference between the stiffness of concave and convex shapes under impact. For example, in impact energy of 6J the stiffness increased 12.7% by changing the configuration from CX to CV, whereas under 36J it increased 44.4%. This phenomenon can be relate to membrane effect that concave laminates are under tension stress during the impact while convex ones are under compression.

Table 2.6. The variation of stiffness in different configuration (concave or convex) and impact energies.

	6J		**12J**		**24J**		**36J**	
	CX	CV	CX	CV	CX	CV	CX	CV
Maximum Load	2130	2314	2429	2687	3056	3730	4276	5253
Maximum Displacement	4.156	4.005	7.163	6.834	10.96	9.94	12.66	10.77
Stiffness	512.5	577.8	339.1	393.2	278.8	375.25	337.8	487.7
Variation (%)		+12.7		+16		+34.6		+44.4

Like the last section the effect of curvature type on impact parameters, maximum force, maximum displacement, impact duration, damage area, and absorbed energy, is presented. As seen in Fig. 2.23, by changing the curvature from convex to concave the maximum load increased, and maximum displacement and load duration decreased. In all pictures shown in this figure by increasing the impact energy, the effect of changing curvature in more visible. As mentioned before, the difference is because of the membrane effect in which convex specimens are under compression stress during impact and concave ones under tension. When the specimen is under tension the specimen is more stiff, therefore the maximum load is more and the displacement and time duration are less.

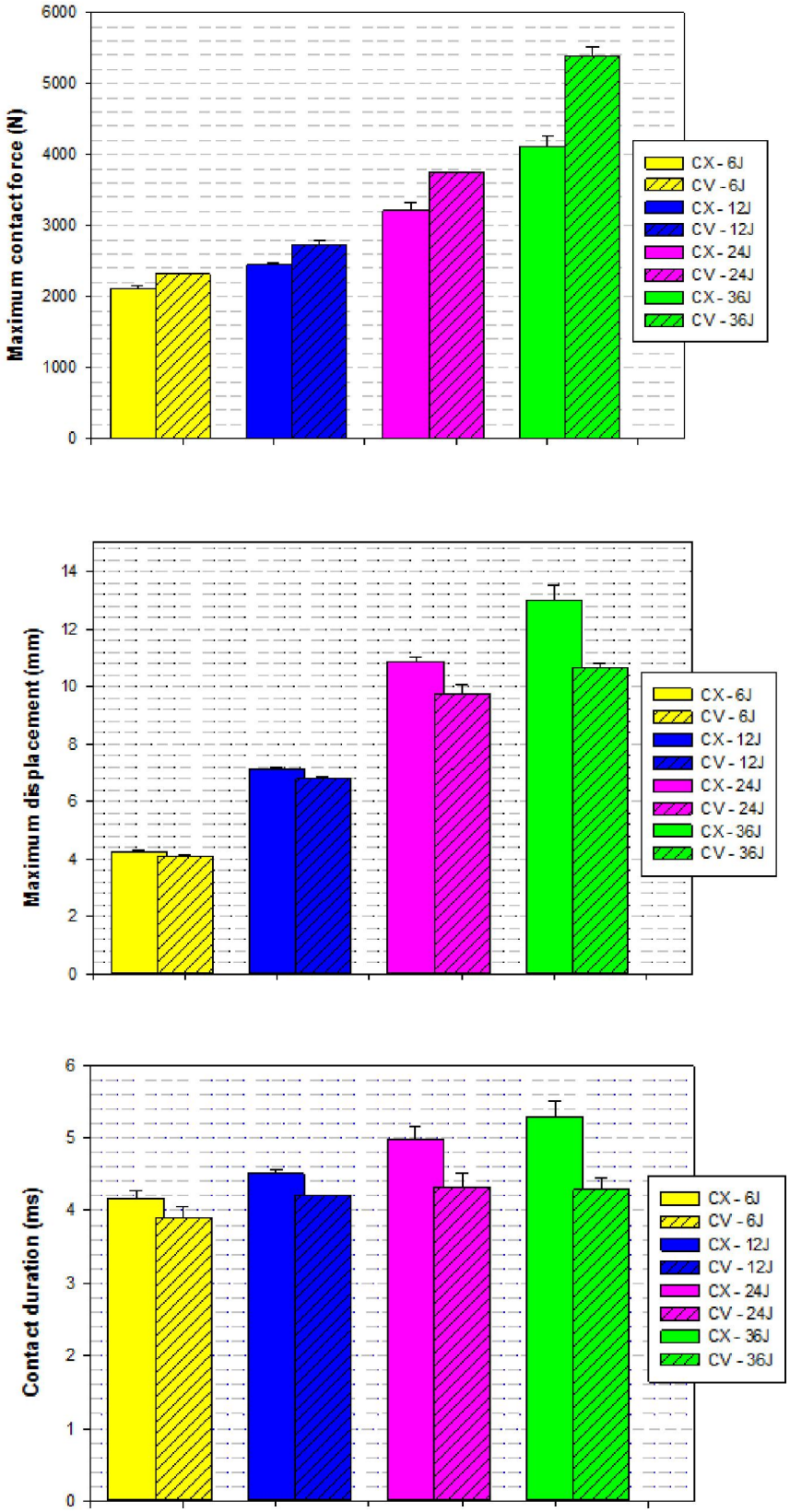

Fig. 2.23. The effect of curvature type on maximum load (N), maximum displacement (mm) and impact duration (ms)

The damaged areas under different impact energies cin concave and convex laminates are shown in Fig. 2.24. As seen, the amount of damage is more in convex configuration. This increased damage extent for convex shells is attributed to compressive membrane stresses that have been shown to promote delamination growth through sub-laminate buckling. In impact energies of 24 and 36J this effect can be seen better.

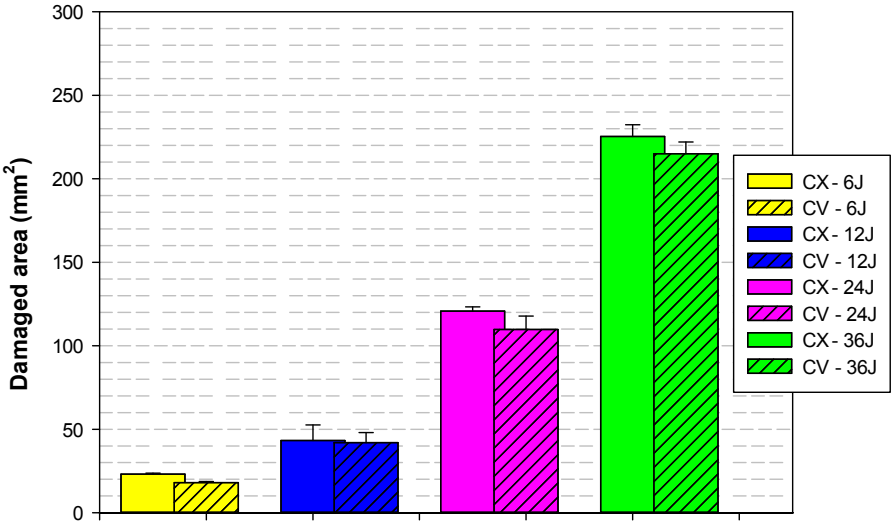

Fig 2.24. The effect of curvature shape on the amount of damaged area

Chapter 3:

Toughening Composite Laminates using nanofibers

3.1. Introduction

Delamination is one of the major failure mode in composite laminates which is a discontinuity between adjacent plies and can be viewed as an interface crack between two anisotropic materials. Susceptibility to delamination is an intrinsic and severe problem of laminates that can ultimately undergo structural failure. Delamination can be caused by many factors such as interlaminar stresses, stress concentration at free edges, joints, matrix cracks, out-of-plane loading, physical discontinuities or mismatch in mechanical properties between adjacent layers [69]. The interest of the research community on this problem is highly connected to industry since many companies are facing this problem, which is particularly critical for aerospace and aeronautical applications. So far researchers have developed many techniques to face the delamination problem such as matrix toughening [70], stitching polymeric filaments [71], optimum stacking sequence [72], through-the-thickness reinforcement [73], Z-pins [74], and fiber braiding [75].

Hojo et. al [70] investigated mode I delamination fatigue crack growth behaviour of carbon/epoxy laminates with two kinds of interlayer/interleaf. One was with heterogeneous interlayer with fine polyamide particles, T800H/3900-2, and the other was with interleaf of new types of thermoplastic resin, ionomer, UT500/111/ionomer. The first one, T800H/3900 -2, indicated the transition of the crack path from the toughened inter layer region (Stage I) to the untoughened inter layer/base lamina interface (Stage II). The crack growth resistance for toughened Stage I was 3.0 times higher than the reference laminates. Though the growth resistance decreased in Stage II, it was still 1.6 times higher than that of the reference laminates. This transition occurred for much shorter increment of the crack length than that under static loading. The

laminates with a new thermo plastic resin (ionomer) interleaf, UT 500/111/ionomer, keep higher crack growth resistance without respect to the increment of the crack length under fatigue loading. The threshold value was 3.3–3.5 times higher than the base laminates. This increase was similar to that of the propagation values of the static fracture toughness. Though the crack path was at the interleaf/base lamina interface, the resin of this region consists of ionomer and epoxy resin, forming toughened interphase. Thus, the crack path was still within the toughened region without respect to the crack length. Fig. 3.1 illustrates the crack propagation in these two laminates.

Another method introduced by Yang et. al [71] studied into a new type of stitched fiber/polymer laminate that combines high interlaminar toughness with self-healing repair of delamination damage by stitching Poly(ethylene-co-methacrylicacid) (EMAA) filaments into carbon fiber/epoxy laminate. They manufactured a three-dimensional self-healing fiber system that also provides high fracture toughness. Double cantilever beam (DCB) tests revealed that the stitched EMAA fibers increased the mode I interlaminar fracture toughness of the laminate about 120%. The 3D stitched network was effective in delivering self-healing EMAA material extracted from the stitches into the damaged region, and it resulted in high recovery in the delamination fracture toughness (around 150% compared to the reference material). This novel self-healing stitching method provides high toughness which resists to delamination growth while also have the functionality to repeatedly repair multiple layers of damage in epoxy matrix laminates.

Finding an optimum stacking sequence was considered by Fuoss and his colleagues [72]. They developed a finite element model to analyze the internal stress state in the laminate and predict delamination damage under impact loading. The effect of three parameters on damage resistance of laminates was considered: interface angle, ply orientation relative to a fixed angle and ply grouping. According to outcomes, they proposed several guidelines to design with laminates, such as avoiding ply grouping and stacking adjacent plies in similar orientation, particularly at interface angles below 45.

Howard et. al [73] proposed a navel method for increasing the capacity of laminate composite under different loading using through-the-thickness 3D reinforcements. They investigated the bonding effect of U-shaped caps to the edge of a laminate analytically and experimentally. In the analytical section a generalized plane strain finite element is used to predict reduction of interlaminar normal stresses when a U-shaped cap is applied. Three-dimensional composite material failure criteria are used in a progressive laminate failure

analysis to predict failure loads of laminates with different edge cap designs. In an experimental program, symmetric 11-layer graphite-epoxy laminates with a one-layer cap of Kevlar-epoxy cloth are shown to be 130% to 140% stronger than uncapped laminates under static tensile and tension-tension fatigue loading. The predicted failure load calculated with the finite element results is 10% lower than the actual failure load. For both capped and uncapped laminates, actual failure loads are lower than those predicted using classical lamination theory stresses and a 2-D failure criterion.

Another method of through-the-thickness reinforcement was presented by Partridge [74] in which Z-Fiber® pins inserted in laminate composite (Fig. 3.2). For determining the effectiveness of this method, delamination tests samples were prepared from unidirectional continuous carbon fiber/epoxy prepreg (IMS/924), made into 3 mm thick unidirectional laminates with and without a block of Z-pins in the crack path. Fracture testing was carried out under Mode I and Mode II loading conditions.

Three-dimensional braided carbon fiber epoxy resin composites (Fig 3.3) are significant structural materials in the fields of astronauts and aeronautics. The effect of the process and test parameters on the mechanical properties was studied by Tang et al [75]. The results indicate that the mechanical properties can be significantly affected by the parameters of braiding: by decreasing the braided angle, the elastic moduli and the ultimate tensile strength showed an obvious increase.

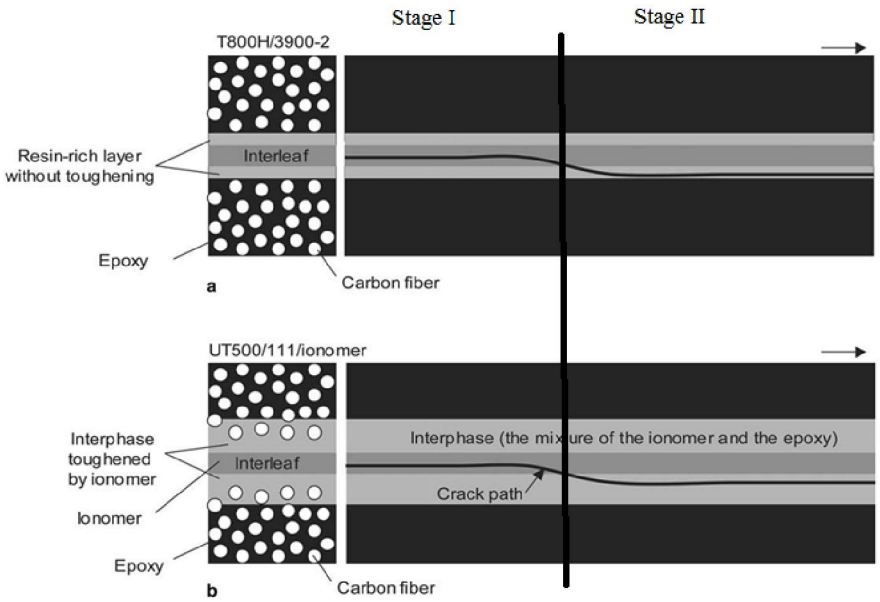

Fig. 3.1. Schematic models of crack paths under mode I loading: (a) interlayer-toughened laminates, (b) ionomer-interleaved laminates [70]

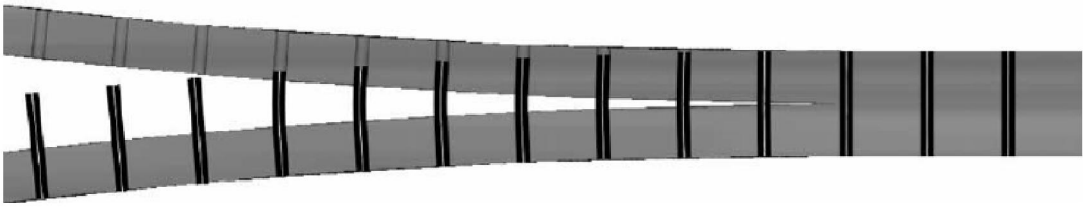

Fig. 3.2. Steady-state crack propagation of Z-pinned laminates [74].

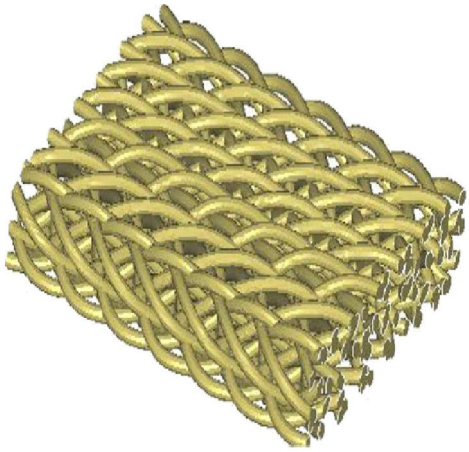

Fig. 3.3. Schematic structure of 3-D braided laminate [76]

In this research, the concentration is on the first topic regarding the toughening of epoxy as a matrix in the composite laminates. For toughening epoxy, the modifier can be in three forms: film, particles, and nanofibers. Nanofibers exhibit interesting characteristics such as very high surface area to volume ratio, flexibility in surface functionalities, higher porosity and smaller pores, and excellent mechanical performance such as stiffness and tensile strength, compared to micro-fibers of the same material. As mentioned before among these forms using nanofibers are easier and much more effectiveness.

Usage of electrospun nanofibers as a interlayer between composite layers was proposed firstly as a patent by Dzenis and Reneker [77]. They proposed to interleave a laminate with polymeric nanofibrous non-woven mat fabricated trough the electrospinning process. They demonstrated that a fiber reinforced composite laminate with polymeric electrospun nanofibrous mats placed at one or more ply interfaces is characterized by an improved delamination resistance.

In the following sections these topics are presented: 1- Electrospinning method for producing nanofibers 2- The application of nanofibers in toughening composite laminates 3- presenting a case study using two different kinds of nanofibers to increase the mode I and mode II fracture toughness.

3.2. Electrospinning:

Electrospinning is a fascinating and easy technique for producing fibrous mats from different kinds of synthetic and natural polymers. The structure and morphology of such fibers can be controlled from a few micrometers to a few nanometers and highly aligned fibrous (Fig 3.4-A) or randomly oriented (Fig 3.4-B) matrices can be fabricated.

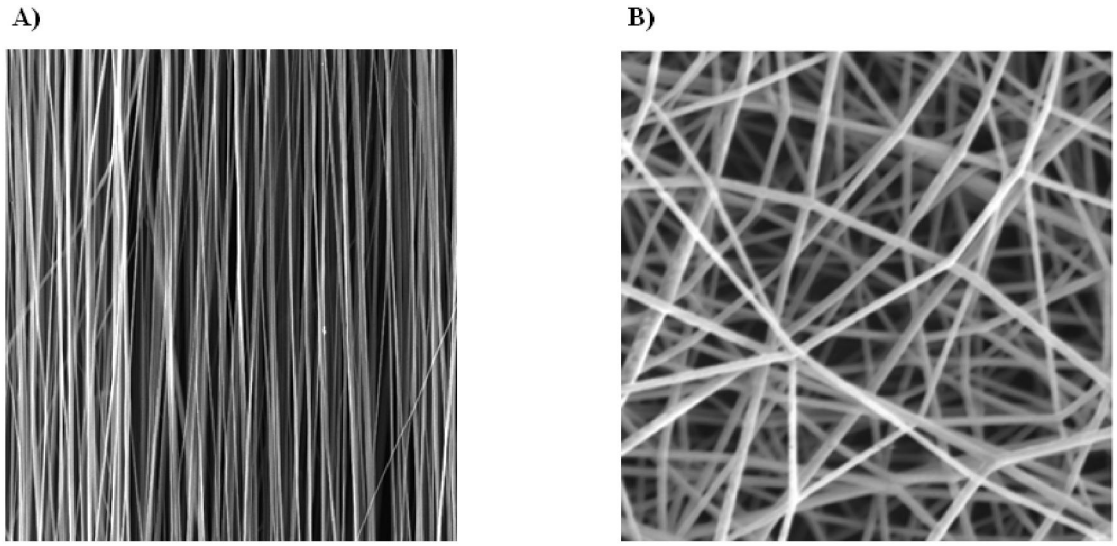

Fig. 3.4. Different kinds of nanofibers: A) Aligned nanofibers B) Random nanofibers

Electrospinning had been known as electrostatic spinning and until 1933 only a few papers published regarding its application in producing of thin fibers [78–80]. Formhals presented his first invention in 1934 about the process and the machine for producing filaments using electric charges [81]. Since before him the method of producing artificial threads using electric field had been applied, his patent did not attract the other researchers' attention. His spinning device contained a movable collector on which the threads were gathered in a stretched state. The machine could produce parallel threads onto the collector such that they could be unwound continuously. One the most disadvantages of the process suggested by Formhals was that the final product of the fibers was wet because of the short distance between the collector and spinning zone.

For resolving this problem he change this distance by revising his machine. In this way, the drying time increased and so the final electrospun fibers ware completely dry [82]. After Formhals studies, so many other researches have been on this topic, but the term of "electrospinning", derived from "electrostatic spinning", has been used relatively recently (in around 1994), but as mentioned before its origin can be traced back to more than 60 years ago.

As seen in Fig. 3.5, an electrospinning system consists of three major components: a high voltage power, a capillary tube with a small-diameter needle, and a grounded collecting plate (usually a metal screen, plate, or rotating mandrel). The process utilizes a high voltage source to inject charge of a certain polarity into the polymer solution which is then accelerated towards a collector of opposite polarity. Most of the polymers are dissolved in some solvents before electrospinning to form the polymer solution. This fluid is then introduced into the capillary tube for the electrospinning process. The polymeric solution held by its surface tension at the end of a capillary tube is subjected to an electric field which induces an electric charge on the liquid surface. When the electric field reaches a critical value, the repulsive forces overcome the surface tension ones. Eventually, a charged jet of the solution is ejected from the tip of the Taylor cone and an unstable and rapid whipping of the jet occurs in the space between the capillary tip and collector. This motion leads to the evaporation of the solvent, leaving the polymer behind. There are many parameters that influence the electrospinning process and so the final morphology of the fibers: 1- the type of the solvent and polymer 2- Solution concentration 3- Voltage value 4- Distance between needle tip and the collector 5- the rate of the solution 5- environmental conditions 6- Motion and shape of collector 7- needle diameter. The effect of some of these factors are considered in the following paragraphs.

The concentrations of polymer solution play an important role in the fiber formation during the electrospinning process because it is strongly related to the viscosity of the solution. Morphology of nanofibers are dependent on solution viscosity [83]. When the concentration is very low, polymeric micro or nano-particles can be obtained that is electrospray instead of electrospinning [84]. Increase of the polymer concentration, therefore, can decrease the numbers and sizes of beads, and eliminate beads completely in some cases. Fig. 3.6 is shown the effect of increasing concentration on the morphology of the electrospinning final product.

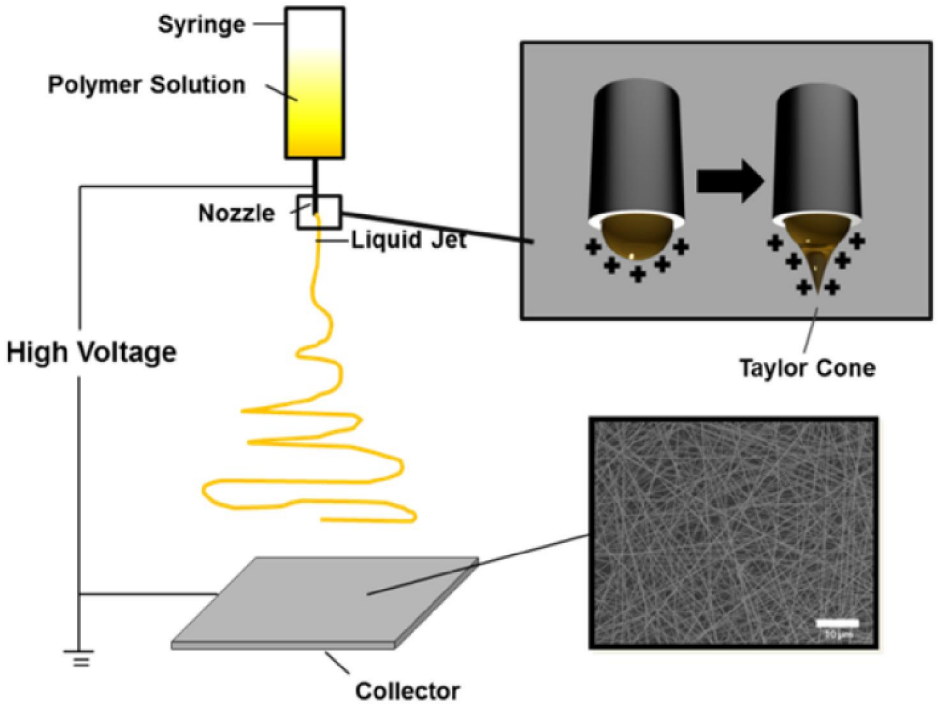

Fig. 3.5. Schematic diagram of set up of electrospinning apparatus

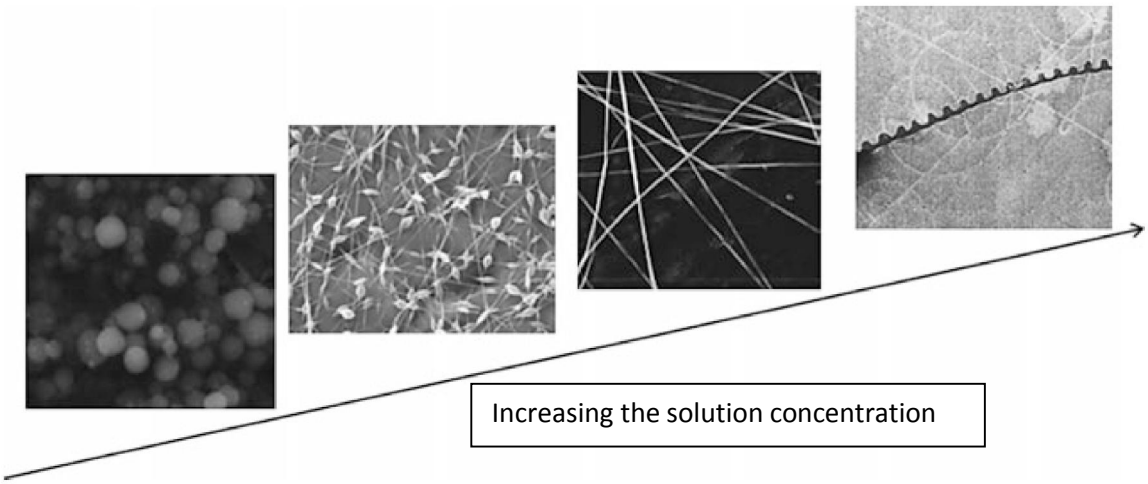

Fig. 3.6. SEM images of the evolution of the products with different concentrations from low to high during the electrospinning [85,86]

In electrospinning process, applied voltage is one the most important factors among others. Only the applied voltage higher than the threshold voltage, charged jets ejected from Taylor Cone, can occur. Regarding the

effect of the voltage on the diameter of electrospun fibers some different and opposite reports have been published. For instance, Reneker and Chun [87] have shown that voltage does not affect significantly on the diameter of electrospun polyethylene oxide (PEO) nanofibers. There are also some evidences that higher voltages facilitated the formation of large diameter fiber like Zhang et al. study on poly (vinyl alcohol) (PVA)/water [88]. Several researches suggested that higher voltages can increase the electrostatic repulsive force on the charged jet that leads to decreasing nanofiber diameter. Yuan et al. [89] investigated the effect voltage on morphologies and fiber alignment with polysulfone (PSF)/DMAC/acetone as model. Applying 10, 15, and 20 kV of voltage leads to 344, 331, and 323nm of nanofiber diameter. In addition, some studies also proved that higher voltage offers the higher possibility of beads formation [90,91].

The flow rate of the polymer solution is another important process parameter. Generally, it is suggested that the flow rate is better to be low until the solution has enough time for polarization. If the flow rate is very high, bead fibers with thick diameter will form rather than the smooth fiber with thin diameter. Yuan et al. [89] investigated the effect of the flow rate on the morphologies of the PSF fibers from 20% PSF/DMAC solution at 10 kV. In their study, bead fibers with thicker diameters can be obtained as the flow rate is 0.66 ml/h, while with flow rate of 0.4 the final mat is completely smooth and thinner.

The distance between the collector and the tip of the syringe can also affect the fiber diameter and its morphologies. When this distance is short, the time is not enough for the fibers to be solidified and inversely if the distance is very long, the fibers consists of many beads. Therefore, for finding a quality of nanofibers an optimum distance should be found. As shown by Yuan et al [89] increasing the distance, a thinner fibers can be obtained (It means after finding the optimum distance, increasing a little of this parameter the fiber can be thinner, but it should not be so much because will make beads in the fibers).

Environmental parameters such as temperature and humidity also affect the process of electrospinning and morphology of nanofibers. Mituppatham et al. [92] considered this effect using polyaide-6 and their showed that increasing the temperature caused thinner nanofiber. Regarding the effect of humidity: Generally lower humidity dry and solution and enhance the evaporation rate during electrospinning. On the contrary, higher humidity leads to thicker nanofiber. Because in this situation the charges is less and so stretching force become weaker. It should be mentioned that changing environmental parameters can vary the

electrospinning process. For example, if a smooth nanofiber can be produced by 15kV of voltage, changing the humidity forced the process to change the voltage for obtaining the same quality of the nanofiber.

3.3. Nanofiber applications

When the diameters of polymer fiber materials change from micrometers like 10–100 μm to submicrons or nanometers, several amazing advantages such as large surface area to volume ratio, flexibility in surface functionalities, and mechanical performance (e.g. stiffness and tensile strength) compared with any other known form of the material can be obtained. These outstanding properties make the electrospun nanofibers to be suitable choice for many important applications. As seen in Fig. 3.7, nanofibers are applicable in many fields, but mostly they have been used in health and medicine sector.

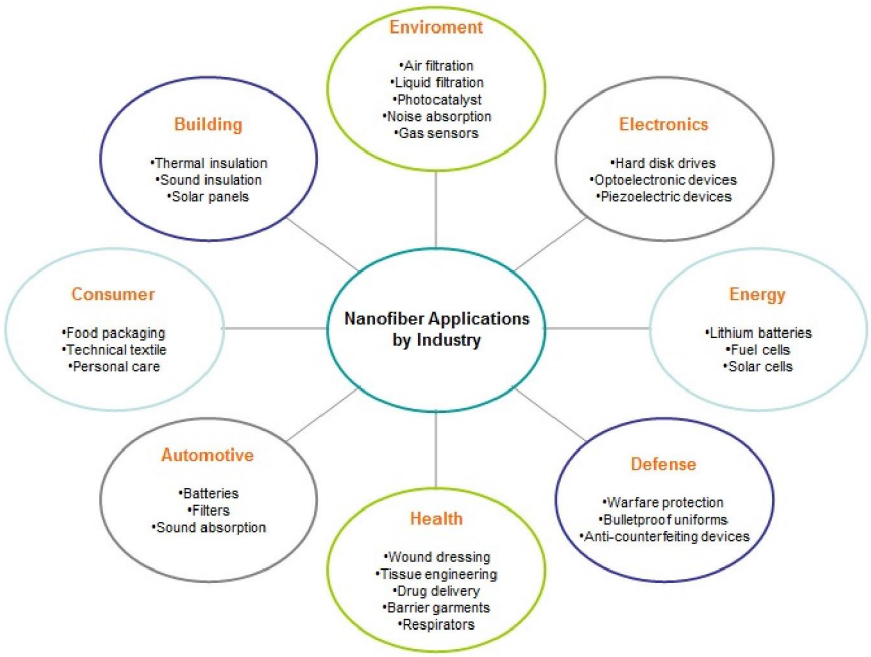

Fig. 3.7. The application of nanofibers in different fields

Since this study deals with integration of polymeric electrospun nanofibers into epoxy-based composite materials to improve delamination resistance and fracture toughness of interfaces, in the next section a review of the works already published on this topic is presented.

3.3.1. Application of nanofibers in composite materials

Dzenis et al. [93] firstly patented the use of nanofibers to reinforce carbon fiber composite laminate. In their patent authors showed that a reinforced laminate with electrospun nanofibrous mats placed at one or more ply interfaces can improve delamination resistance (Fig. 3.8). Indeed, composite laminates incorporating nanofibrous reinforcements are expected to have an improved interlaminar fracture toughness, strength, and delamination resistance towards static, fatigue, and impact loadings. In particular, the nanofibrous reinforcement can be useful in suppressing and arresting delamination from any source, including matrix cracks, free edges, notches or holes, ply drops, bonded joints, bolted joints, out-of-plane loading, and etc.

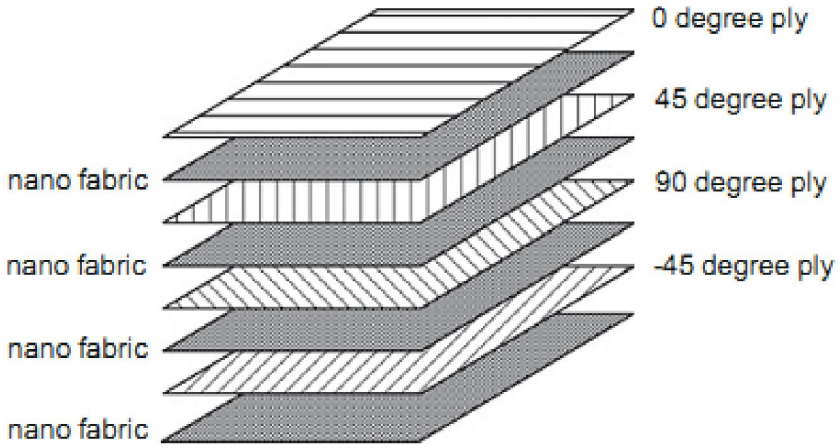

Fig. 3.8. A schematic picture of interleaved composite laminate [94]

Before introducing nanofibers as an interlayer for strengthening composite laminates, different methods have been used such as using polymeric films and particles. Therefore, usage thermoplastic for toughening epoxy-based laminated was known from many years ago, but as mentioned before the efficiency of nanofibers is much more than other shapes of interleaving.

Table 3.1. Summary of some studies regarding the effect of film, particles, and chopped fibers on the fracture response of interleaved laminates

Reference No.	Laminate type	Interleaved film, particle or fiber	Maximum curing temprature	Dimension of interleaved material	Improvement of mode I fracture toughness	Improvement of mode II fracture toughness
[95]	Carbon/Epoxy (1K plain woven)	Polysulfone (Particles)	190	50 to 150μm and 150 to 250μm	220%	-----
[96]	1K carbon fabric/epoxy	Polysulfone (film)	190 (2 hours)	5,10,15,20%	20%: 2.7times	-----
[97]	Carbon/Epoxy (Unidirectional)	Ethylene-based ionomer (film)	140 (1.5 hour)	12, 25, 100 and 200 μm	3, 4.8, 6.5, 11 times more	-----
[98]	Satin weaved carbon fiber fabric	chopped Kevlar fibres and epoxy resin AY 105	120 (4 hours)	150 μm of epoxy resin AY 105 and 0.5, 1, 1.5 mg/cm^3 of Kevlar	-----	1.5 to 2 times
[99]	Plain weave carbon fibre fabric	Chopped phenoxy fibres (48 mm of diameter)	180 (2 hours)	5% and 10% (with regard to the total matrix content)	2 and 10 times	-----
[70]	Unidirectional Carbon/epoxy	1- fine polyamide particle 2- UT500/111/ionomer	----	1-30μm 2-25 nd 100μm	1-1.6 to 3 times 2-3.4 times	-----

Some of the studies regarding the effect of interleaves in the form of particles, films, and thick fibers on fracture response of composite laminates are listed in Table 3-1. Yun et al. [95] interleaved Polysulfone (PSF) particles between plain woven carbon/epoxy laminates. Two groups of particles were used in this test: 50 to 150μm and 150 to 250μm and also various concentrations: 5,10,15, and 20 wt% of the matrix. Since glass transition temperature of polysulfone is between 180 to 190 ^{o}C, the specimens were cured in 190 ^{o}C. It is shown that by phase separation which happened during curing process PSF could increase the fracture toughness. In next sections more information is presented about this mechanism. It is sown that two different size of the particles showed similar increasing pattern up to 10 wt % of PSF and from 10 to 20 wt %, the fracture toughness of the large size PSF particles was higher than that of the small size particles. The fracture toughness of 20 wt % the large size particles-modified epoxy composite was 2.2 times higher than that of the unmodified epoxy. Yun et al. [96] in another study instead of particles of PSF used its film. They showed that the concentration of the PSF affected on its morphology after curing: increasing the concentration leads that the morphology changes from sea-island to nodular structure. In another study in this field, Matsuda et al. [97] considered the influence of Ethylene-based ionomer thickness (12, 25, 100, and 200μm) on mode I interlaminar fracture toughness of carbon/epoxy laminates. The fracture toughness increased as increasing the thickness of inserted ionomer film. This enhancement happened sharply by inserting thin ionomer film,

and the additional increase with increasing the ionomer thickness was smaller. According to Fig. 3.9 they also showed that crack path was at the interfaces between the interphase region and the ionomer region for 12 mm- and 25 mm-ionomer-interleaved CFRP, and mainly inside the inter-phase region for 100 mm- and 200 mm-ionomer-inter-leaved CFRP. Unlike many papers that only consider the mode I fracture toughness, Yadav et al. [98] investigated the effect of interleaving in mode II. The five different types of laminates were fabricated: 1- laminates without interleaf (baseline) 2-laminates with interleaf of epoxy resin AY 105 of 0.15 mm thickness 3,4,and 5- laminates with interleaf layer of epoxy AY 105 of 0.150 mm thickness and chopped Kevlar-49 fibers in an amount of 0.5, 1.0 and 1.5 mg/cm^2. Mode II fracture toughness of composite enhanced about two times by interleaving epoxy AY 105 and up to 1.5 times by adding chopped Kevlar reinforcement. Flexural modulus declined up to 12% by interleaving and improved up to 6% by increasing amount of Kevlar. Therefore, although Kevlar decreased the fracture toughness, but on the other hand could compensate the decrease of stiffness. Wong et al. [99] used dissolvable chopped phenoxy fibers, which are added at the interlaminar region in a carbon fiber/epoxy composite. The thermoplastic phenoxy fiber dissolved in the epoxy during curing and a phase separated morphology with phenoxy-rich secondary phase was formed upon curing (like PSF). It was found that the average Mode-I fracture toughness value, increased ten times with only 10 wt.% (with regard to the total matrix content) phenoxy fiber added. Other properties such as Young's modulus, tensile strength and thermal stability were not adversely affected.

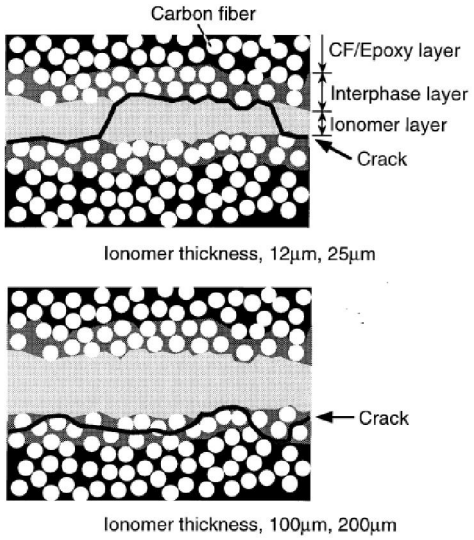

Fig. 3.9. Schematic figures of the crack path at transverse section for the ionomer-interleaved CFRP [97].

The effect of interleaving on impact response of composite materials has been also considered [100-103], but much more limited than studies regarding its effect on fracture response. Sohn et al. [100] interleaved different kinds of materials to consider and compare the efficiency of each one on mechanical behavior of composite under impact loading. The interleaving using PEEA film was suitable in decreasing the damaged area while the residual compressive strength was much lower than other interleaved laminates. The good interfacial bond strength of Zylon fiber with the epoxy matrix increases the fiber-bridging effect, and thus contributes to the remarkable improvement in interlaminar fracture resistance. Four different types of Kevlar fiber reinforcements (15 mm in length and 0.8 wt% (uniform and coarse distributions); 15 mm in length with 0.4 wt%; and 5±7 mm in length with 0.4 wt%) were used. The uniformly and coarsely distributed Kevlar fibers did not make much difference. Better impact performances were shown by Kevlar fibers of 5±7 mm and 0.4 wt% than those of 15 mm and 0.8 wt%, perhaps due to the intensive fiber-bridging effect with the increased number of fiber ends. For all these situation the failure mode was considered by SEM. Duarte et al. [101] applied different types of polymers as the interlayer. Olefin film was a good choice for decreasing the damaged area under impact loading, but this was accompanied by a reduction in compression strength, due to a lack of lateral support for the fibers. Their results showed that using a polyetherimide film, it produced reduction in damaged area, and significant improvements in compression after impact strength. A very interesting study about the influence of interleaf sequence has been followed by Yi and An [102]. Fig. 3.10 illustrates different sequences which investigated in this study. PEK-C was used as the toughening agent which its morphology after curing is like PSF and phenoxy mentioned before. As seen in the picture the minimum damaged area is related to the laminate which all its layers interleaved by PEK-C. For evaluation the response of each interleaved laminate under impact, compression after impact (CAI) test also was conducted for each situation which the results are shown in Fig. 3.11. According to these results, from situation “B” to “G” the CAI strength increased. The situation of “H” is like “G”, but the thickness of interleaf is more and in situation “I” which is the weakest one the interleaf was placed in every two plies. From these results, it is found that the interleaf position affect considerably on impact response of composite laminates. Lu et al. [103] applied poly(ethylene-co-acrylic acid) as interlayer in the midplane of unidirectional CFRP laminates. The impact penetration energy of the composite beam increased strongly. They also used a microscope during a static flexure test and found out that a dramatic change of failure

mode can happen from the dominantly compressive fracture of the baseline laminate to the dominantly tensile fracture process upon interleaved laminate. These observations were attributed to the change in stress distribution upon introduction of the interleaf layer.

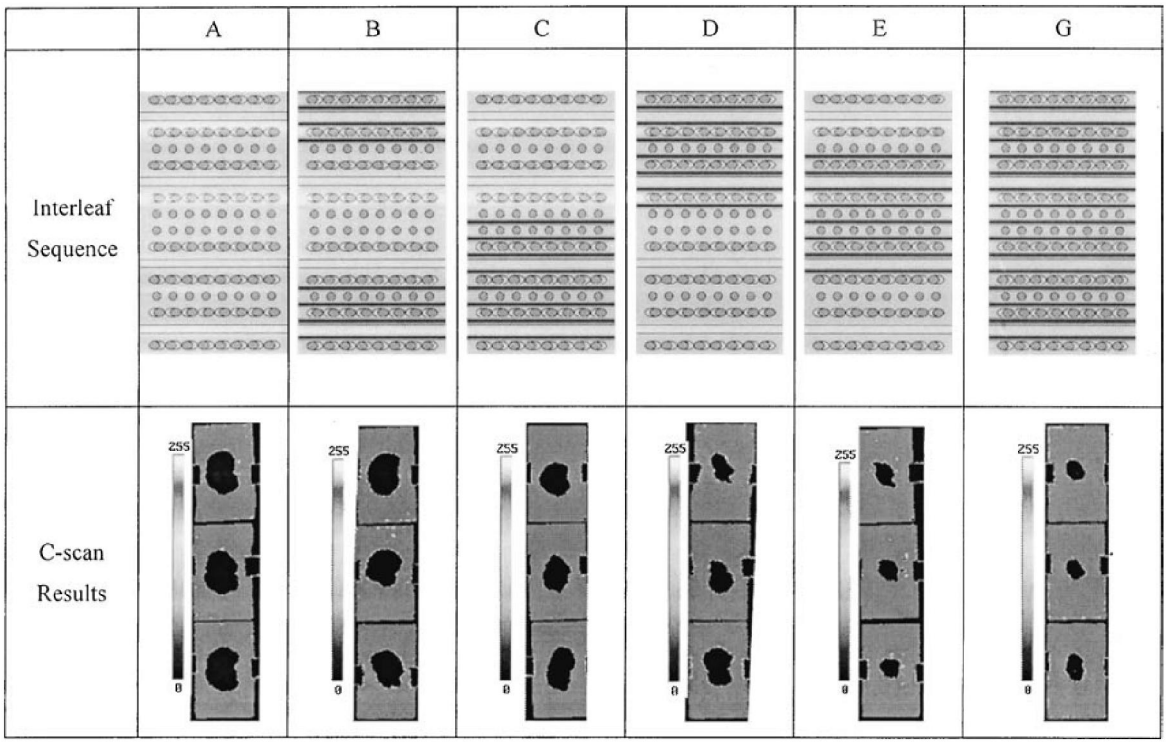

Fig. 3.10. Interleaf sequence of the specimens studied and the C-scan result showing the impact damage [102].

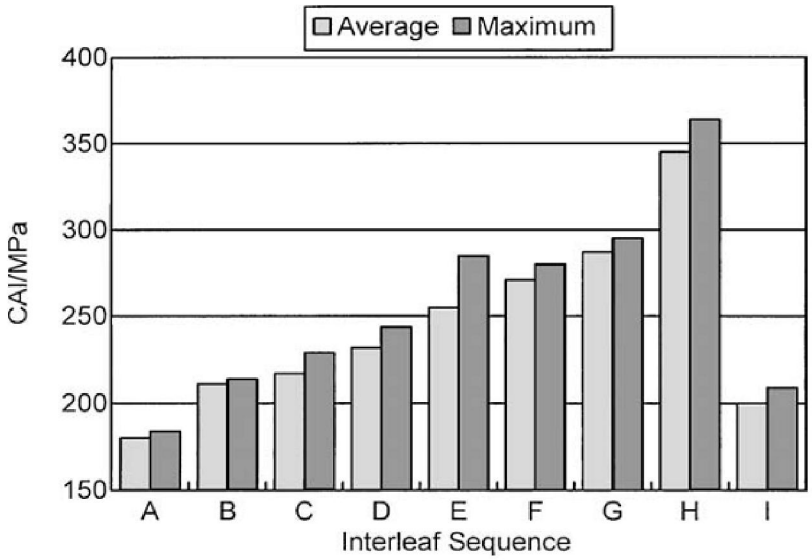

Fig. 3.11. Compression after impact (CAI) of the specimens in dependence on the interleaf sequence [102]

After introducing nanofibers as the interlayer for increasing fracture toughness of polymeric composite laminates many researches have been followed and different kinds of polymers used to consider their effect in this regard. Various polymers have different mechanism and role for toughening the matrix that it will be considered in this section.

Polysulfone (PSF) is one the famous thermoplastics for toughening epoxy. Before its usage in the form of nanofiber, many studies conducted in other forms [104-106]. As shown in Fig. 3.12, during curing process the PSF is separated from epoxy that is like islands in the sea. The increase of toughness is completely related to the separated phase because stress concentrations caused by particles that produce initiating shear bands which form plastic zones and so absorbed more energy during loading [107]. On the other hand, when the crack propagates and reaches the PSF phase, it is deviated and so more energy is required for the propagation. Li et al. [108] used PSF nanofibers and film for toughening CFRP laminates. They performed mode I fracture tests and discovered a strong effect of the interleave: mode I fracture toughness of the nanofibers toughened composite was 869 J/m^2 for 5.0 wt.% PSF nanofibers content, which was 140% and 280% higher than those of PSF films toughened and untoughened composite respectively due to the uniform distribution of PSF spheres (Fig. 3.13).

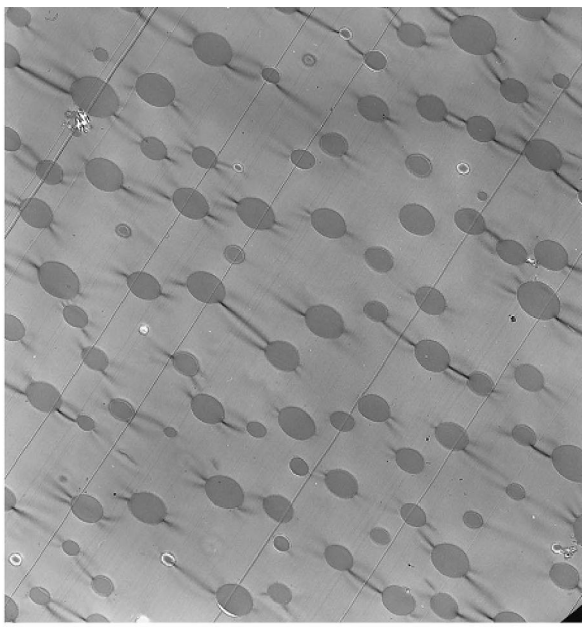

Fig. 3.12. Morphology of epoxy/PSF after curing [106]

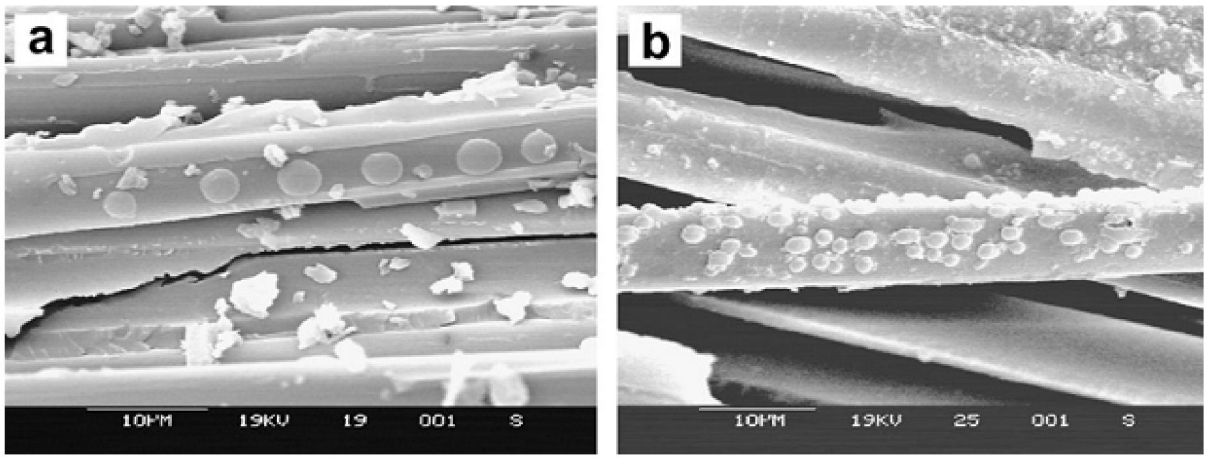

Fig. 3.13. SEM images of composite fracture surface toughened by 3 wt%:

(a) PSF nanofibrous membranes (b) PSF films [108]

Zhang et al. [109] present an interesting discussion about the efforts to obtain optimal process parameter to electrospin Polycaprolactone (PCL), Polyvinylidene uoride (PVDF) and Polyacrylonitrile (PAN) nanofibers. They performed Mode I fracture and DMTA tests to determine the conditions which allow the best mechanical performances. Their findings show an optimal concentration of 15 wt.% of PCL solution for electrospinning to produce composites with enhanced mode I interlaminar fracture toughness, stable crack growth and maintained flexural strength and modulus. The morphology of PCL is like PSF and during the curing process make a separation phase (Fig. 3.14).

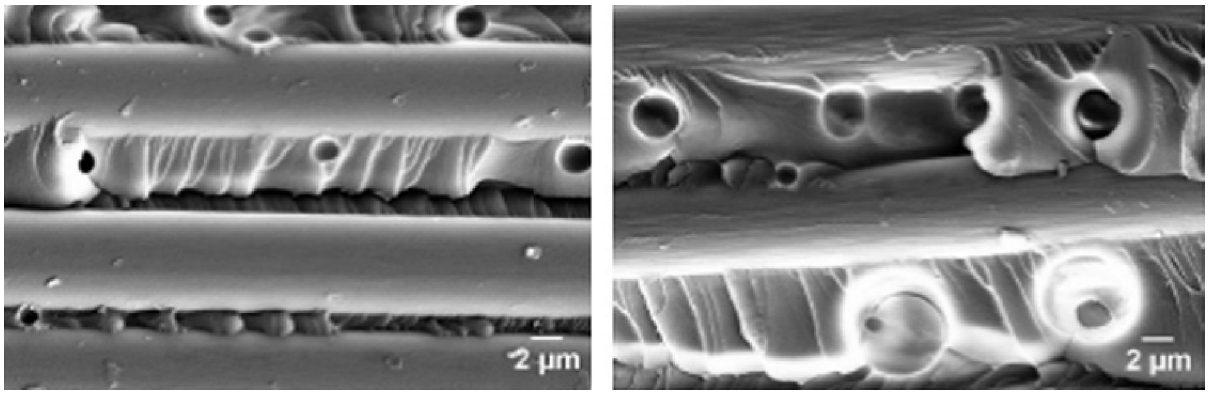

Fig. 3.14. SEM micrographs of delamination fracture surfaces after mode I fracture tests for specimens toughened by PCL nanofibers [109]

Another polymer which attract the attention of many researchers for enhancing the fracture toughness is Nylon 6,6. Palazzetti et al. in various studies [110-112] considered the effect of Nylon 6,6 on fracture and impact response of plain CFRP. Wide range of parameters such as the nanofibers diameter, the thickness of mats, the alignment of nanofibers in the mat was considered. In their first study [110] they used two different modified specimen: 1- two nanofibrous mats interleaved in the two sides of laminate (down and up) and 2- three layers of laminates interleaved in the downer side (Fig. 3.15). All the specimens were subjected to static and dynamic tests to assess their stiffness, harmonic frequencies and damping. The experiments were repeated before and after low velocity impacts in order to investigate the effect of nanofibers to static and dynamic properties when the laminates were impacted. Their results showed that the stiffness of modified laminates is 10% less, but the damping ratio is 160% more. Impact tests on nano-modified specimens also reveal an 8% lower peak force (for the lowest energy impact) and 14.3% less energy absorbed compared to the virgin ones. In another study [111], they considered the influence of Nylon 6,6 nanofibers on mode I and II fracture of Gr/epoxy laminates. Results showed that electrospun nanofibrous mat is able to increase by 23.2% the mechanical energy absorbing capability and by about 5% the mode I fracture toughness. Fracture mode II tests revealed that the nanofibrous mats contribute to improve the maximum stress before the material crisis (6.5% of increment) and a measurable increment of (8.1%) the maximum mechanical energy that can be absorbed by the material during the crack propagation was registered. The acoustic emission (AE) technique was also used to monitor both mode I and mode II tests. The AE information highlight that the nanofibrous mats mitigate the interlaminar matrix failure on both the fracture modes. In the third study [112] they used different geometrical features of electrospun nanofibers: nanofiber orientation, nanolayer thickness, and nanofiber diameter to consider their effect on fracture toughness. In mode I tests, increasing the thickness of mat and diameter of nanofibers leads to decreasing fracture toughness and the efficiency of random nanofibers were more than aligned one. In mode II tests, thickness of the mat did not affect on fracture toughness and aligned nanofibers were more suitable. Mode II tests also revealed that smaller nanofibers give to the specimen an improved absorbing energy capability, while bigger diameters can improve the maxi-mum tension that the specimens can carry on, with respect the virgin configuration. They also conducted a numerical research in this regard and compare its outcome with experimental results [113].

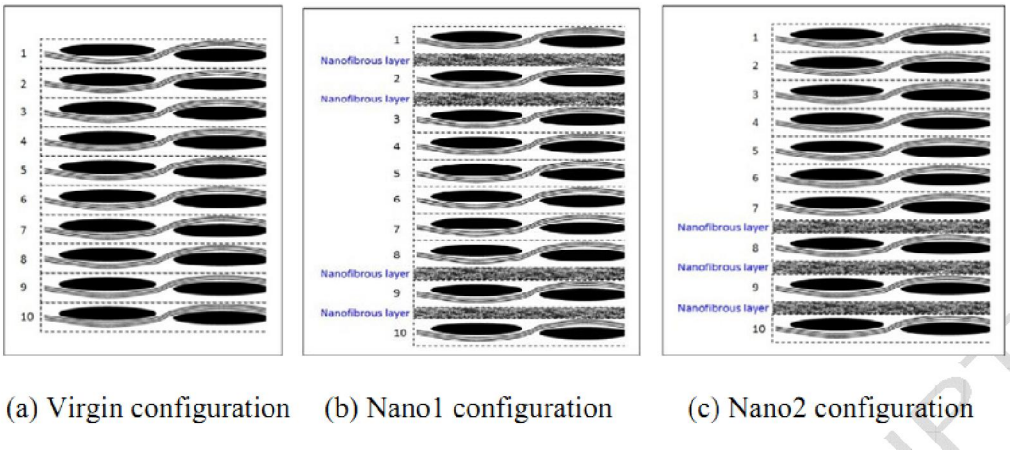

Fig. 3.15. Different types of interleaving for considering their response under impact loading [110]

Akangah et al. [114] interleaved carbon/epoxy laminates using Nylon 6,6 and conducted some impact tests in very low impact energies, 0.46 to 1.8J. The results showed that polymer nanofabric interleaving increased the threshold impact force by about 60%, reduced the rate of impact damage growth rate to one-half with impact height and reduced impact damage growth rate from 0.115 to 0.105 mm^2/N with impact force.

Another interesting polymer is the polyetherketone-cardo (PEK-C), used also to electrospun nanofibers directly deposited on carbon fabric. Zhang [115] investigated the influence of nanofiber diameter and interlayer thickness on the Mode I delamination fracture toughness, flexure property and thermal mechanical properties of a CFRP interleaved with nanofibers. They have achieved considerably enhanced interlaminar fracture toughness. Finer nanofibers result in more stable crack propagation and better mechanical performance under flexure loading. Composites modified by finer nanofibers maintained the glass transition temperature (T_g) of the cured resin and increasing nanofiber interlayer thickness improving the fracture toughness while compromising the flexure performance.

So far the method of electrospinning for producing nanofibers described and its application on toughening of composite laminates is reviewed. According to the literature each nanofibers has a specific benefit and each one is more effective either in mode I or mode II fracture (or perhaps is suitable for both modes but is not very effectiveness). In next parts, for the first time the combination of nanofibers is used for improving the efficiency of polymeric laminates. For this aim, PCL and Nylon 6,6 are applied since according to the literature both of them are a good choice for toughening epoxy.

3.4. Materials and Specimen fabrication

3.4.1. Materials

Unidirectional glass/epoxy prepreg (Ref. 1017) supplied by G. Angeloni Srl is used as composite material. Nylon 6,6 Zytel E53 NC010 provided from DuPont in the form of pellets and PCL purchased from Sigma-Aldrich (Table 3.2) were used to electrospun nanofibers. Formic acid, Acetic acid, and Chloroform provided from Sigma Aldrich were used as solvents.

Table 3.2. PCL and Nylon 6,6 properties

Property	PCL	Property	Nylon 6,6
Form	Pellets	**Form**	Pellets (3mm)
Density (g/mL at 25 ^{o}C)	1.145	**Density (g/mL at 25 ^{o}C)**	1.14
Melt Temperature (^{o}C)	60	**Melt Temperature (^{o}C)**	263
Number average molar mass (M_n)	70000-90000	**Glass Transition Temperature (T_g) (^{o}C)**	50

3.4.2. Electrospinning process and nanofiber producing

The steps of producing nanofibers using electrospinning is shown in Fig. 3.16. Polymeric solutions used for the electrospinning process were made dissolving the 14% wt of Nylon 6,6 in a solvent made 50:50 v/v by Formic Acid and Chloroform [111]; PCL solution was made by dissolving in Formic Acid/Acetic Acid solvent (60:40 v/v) in a polymer concentration of 15% w/v [116]. Schueren et al. [116] showed that the viscosity of PCL solution changes with time, but remains stable within the first 3 hours after dissolving PCL. Therefore after this specific time the electrospinning parameters such as voltage, distance from needle to collector and rate will be varied for obtaining a steady state condition.

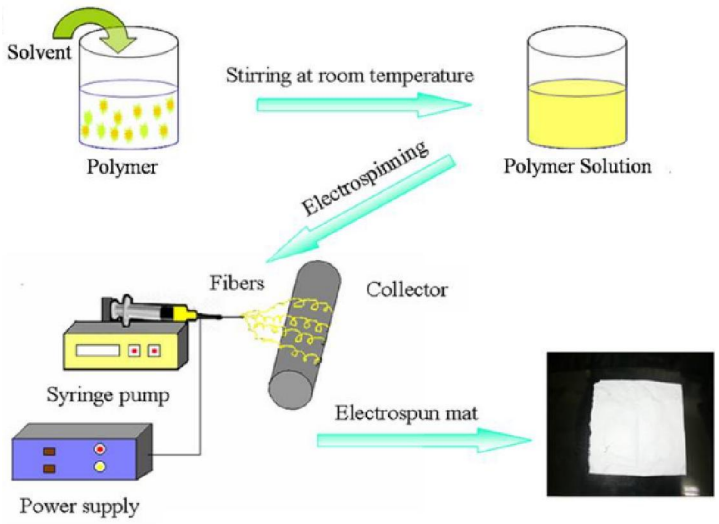

Fig. 3.16. The steps of producing nanofibers using electrospinning method

The solutions were then transferred to an in-house electrospinning apparatus for producing nanofibers. Fig. 3.17 the electrospinning machine manufactured by Spinbow company. This semi-automatic machine equipped with two chambers that each one consists 4 needles. The chambers moved vertically and the Aluminium collector horizontally. The machine also has some brushes that every 3 min cleaned the tip of needles. As seen the picture the red pump is used for transferring the solution from the syringes to the chambers using tubes.

Electrospinning process was optimized and carried out as presented in Table 3.3. Three different nanofiber mats were produced: 1- PCL nanofibers 2- Nylon 6,6 nanofibers 3- Nylon 6,6/PCL (mixed) nanofibers. It is important to electrospun the same nanofiber content for all the mats. Therefore, since the concentration of both solutions and density of Nylon 6,6 and PCL (Table. 3.2) are almost the same, an equal amount of solution was electrospun. For this goal 2.4 ml of PCL and 2.4 ml of Nylon 6,6 were used for individual mats and for mixed one 1.2 ml of PCL and 1.2 ml of Nylon 6,6 were utilized as follow: 0.4 ml of PCL, 0.6 ml of Nylon, 0.4 ml of PCL, 0.6 ml of Nylon, 0.4 ml of PCL. The final thickness of PCL, Nylon 6,6 and mixed mats were 27, 31, and 30 μm, respectively. The SEM images of electrospun nanofibers are presented in Fig. 3.18. The nanofibers were electrospun with random directions, and formed heterogeneous crossing junctions in mat. The nanofiber diameters of PCL and Nylon 6,6 were about 550 nm and 250 nm, respectively. Fiber diameter distribution was determined by measuring 200 fibers per sample, with an image acquisition software (EDAX Genesis).

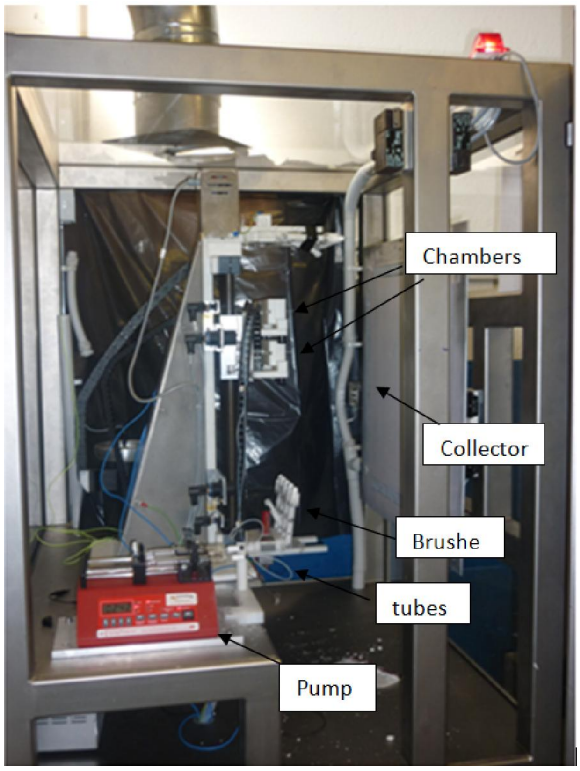

Fig. 3.17. Electrospinning machine

Table 3.3. Electrospinning parameters for producing PCL and Nylon nanofibers

	PCL	Nylon
Applied Voltage (kV)	16	23
Feed rate (ml/min per nozzle)	0.017	0.005
Needle tip – collector distance (cm)	10	10
Humidity	40%	40%

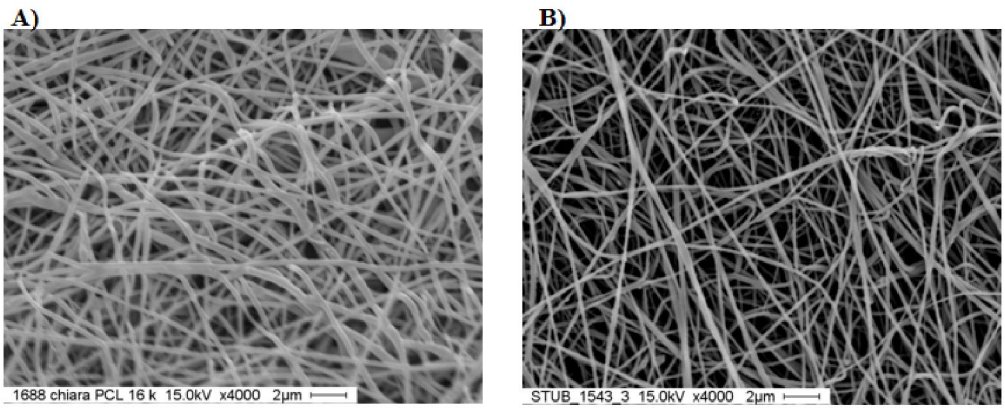

Fig. 3.18. SEM images of: A) PCL nanofibers B) Nylon 6,6 nanofibers

3.4.3. Fabrication of test panels

Double cantilever beam (DCB) (width B = 20 mm, length L = 140 mm, nominal thickness t = 4.2 mm, and initial crack length a = 60mm) and End notched flexure (ENF) specimen (width B = 20 mm, length L = 130 mm, and nominal thickness t = 4.2 mm, and initial crack length a = 40mm) specimens were prepared for tests under mode I and mode II loading, respectively (Fig. 3.19). For manufacturing the specimens, 16 unidirectional layers stacked on each other; the nanofiber mat and a 15µm Teflon sheet (for producing initial crack) were put between the mid-layers before curing process. Test panels were cured by using a vacuum bag in autoclave at 150°C for 1 hour, according to supplier's specifications. Specimens were cut from the laminates using a rotating diamond disk. For DCB tests, aluminium blocks were used to apply the load, as shown in Fig. 3.18-A. For each configuration, 5 specimens were manufactured and tested.

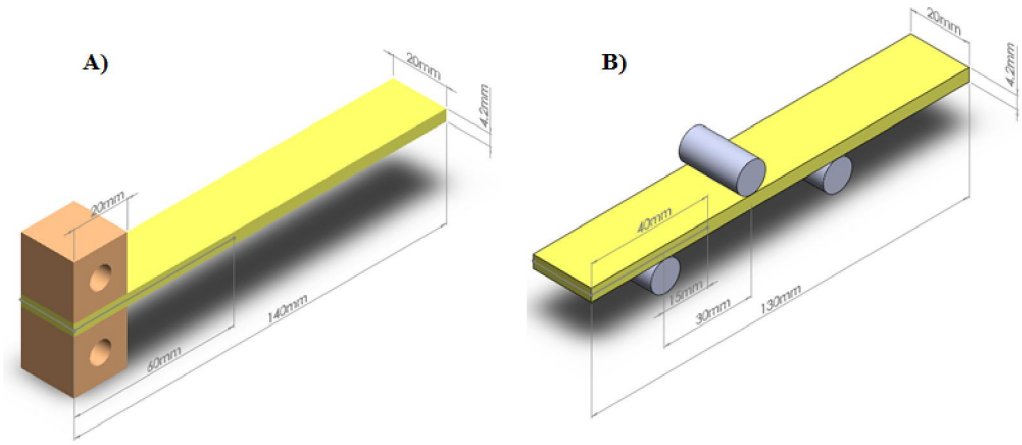

Fig. 3.19. Sample geometry for: A) double cantilever beam (DCB) B) end notch flexure (ENF)

3.5. Experimental Tests

mode I and mode II fracture tests were carried out in a computer-controlled servo-hydraulic universal testing machine Instron 8033 with force capacity of 5 to 250 kN. The cross head speed was controlled at 0.5 and 1.5 mm/min for ENF and DCB tests respectively, and data was recorded 10 times per second. The energy release rate for mode I fracture (G_I) testing is obtained from Modified Beam Theory (MBT) Method in the ASTM standard [117]:

$$G_I = \frac{3P\delta}{2B*(a+|\Delta|)} \cdot \frac{F}{N} \tag{3.1}$$

where P is the load, δ is he displacement, F is a correction factor for large displacements, N is a correction factor for the stiffening caused by the metal blocks and Δ is a correction for crack tip rotation and deflection. Δ is determined from a linear regression analysis of $(C)^{1/3}$ versus a data, while C is the compliance (δ/P). The direct beam theory was used to calculate the energy release rate for mode II fracture (G_{II}) using the following expression [118]:

$$G_{II} = \frac{9a^2P\delta}{2B(2L^3+3a^3)} \quad (3.2)$$

3.6. Results and discussion

In this section the fracture response of reference and nanofiber-modified laminates are presented:

3.6.1. DCB tests

In Fig. 3.20 examples of the force-displacement curves of reference and nanofiber-modified laminates are presented. Each curve can be divided into three different sections: 1- for the beginning up to first load drop (shown on the curves with circle); 2- from the first load drop up to maximum load (initiation stage); 3- from the maximum load up to end of test (propagation stage).

As shown, PCL-modified laminates cause the maximum load in comparison with reference and Nylon 6,6-modified specimens which exhibit almost the same trend during crack propagation stage. Although reference and Nylon 6,6 reinforced laminates present some similarities in mode I fracture behaviour, the crack starts to propagate sooner in reference laminate as shown from the force drop observed at 7 mm displacement. The crack in PCL-reinforced laminates begins to propagate earlier than the laminate with Nylon 6,6/ PCL (mixed) nanofibers. The maximum force of mixed-mat laminate is lower than those laminates with PCL, but after a specific point (black square in the figure), both of them follow the same trend. An interesting phenomenon which can be observed in this figure is that the initiation stage in PCL and reference laminate begins at lower displacement than what happen in Nylon 6,6 and mixed laminates, and therefore it can be concluded that Nylon 6,6 can postpone the starting of the initiation. Also it should be mentioned that all the laminates have the same behaviour in the first stage of loading.

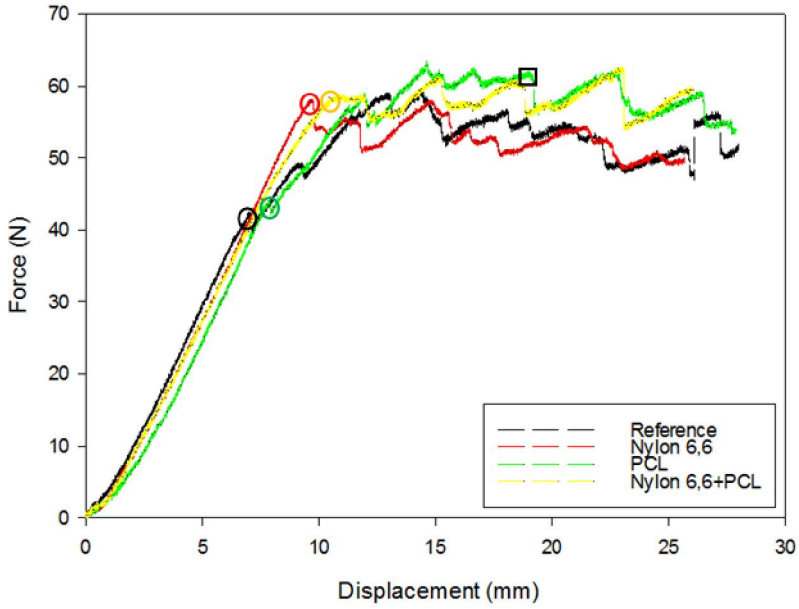

Fig. 3.20. Force-displacement curves of modified and reference laminates (DCB tests)

Fig. 3.21-A and B compare the amounts of G_I in two different stages of initiation and propagation: the effectiveness of Nylon 6,6 and PCL is completely inversed in initiation and propagation sections. It means that G_I is increased 36 and 12 % using Nylon 6,6 and PCL nanofibers respectively during initiation phase, while it is -3 and 17% in propagation stage, respectively. A different behaviour is observed mixing the Nylon 6,6 and PCL nanofibers: specimens addicted with mixed nanofiber increased fracture parameter in both stages: 40% (initiation) and 10% (propagation) with respect pristine specimen. Fig. 3.21-C presents average of G_I during loading, from start of crack propagation up to the end of the test, i.e. the average of initiation and propagation stages. Both Nylon 6,6 and PCL nanofibers present an increased G_I: 4.5% and 25%, respectively. The effectiveness of PCL is much more in mode I loading. It is interesting that the ability of mixed nanofiber to increase toughness of laminate is between individual nanofibers with 21% enhancement.

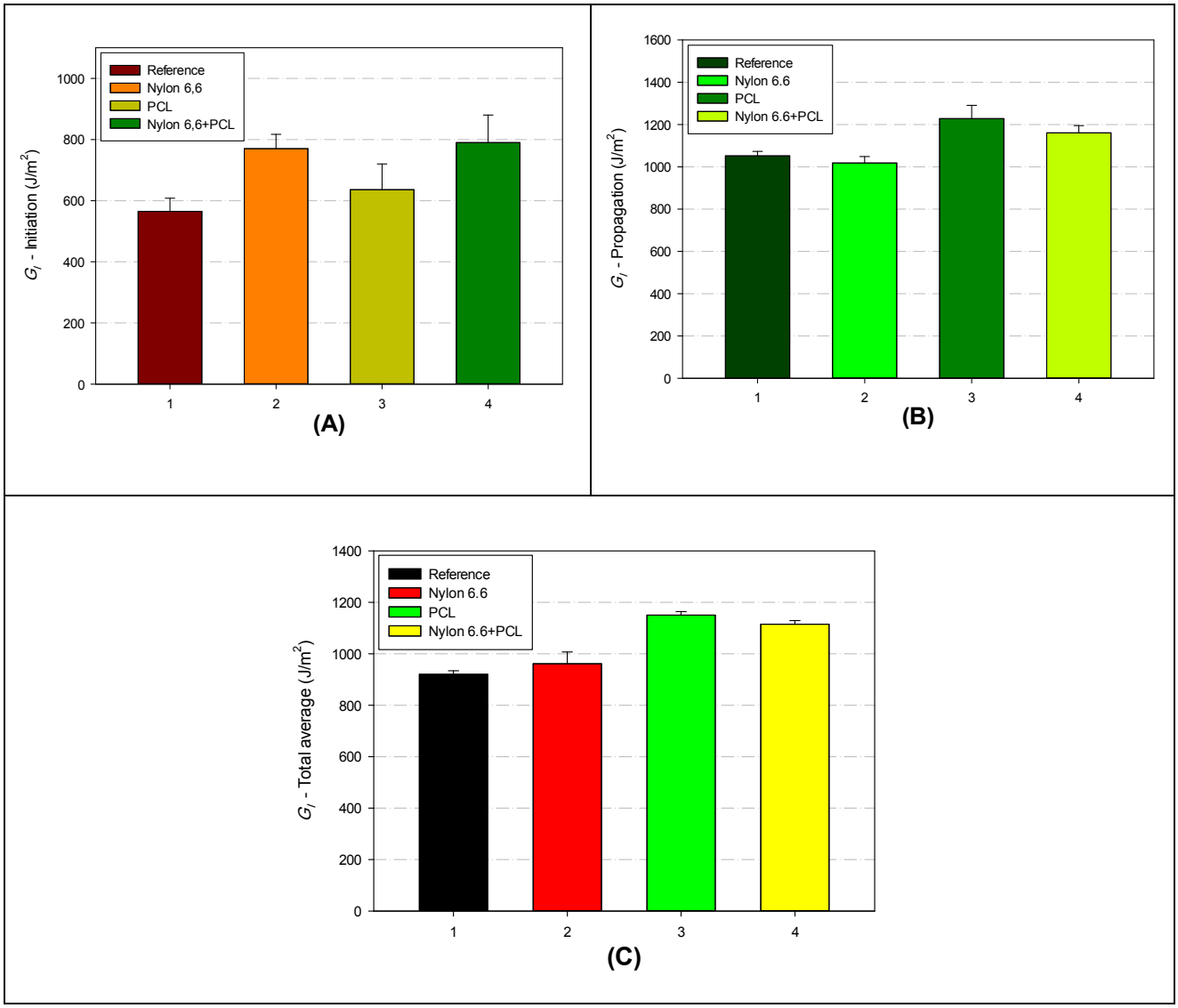

Fig. 3.21. The results of energy release rate for mode I fracture (G_I) for: A) initiation stage B) propagation stage and C) average of G_I during loading

3.6.2. ENF tests

Fig. 3.22 presents the force-displacement curves of mode II fracture tests for reference and modified laminates. It is shown that Nylon 6,6 modified specimens can resist more against crack propagation than reference laminate and their maximum force increased about 30%. Although maximum forces of PCL and Nylon 6,6/PCL-reinforced laminates are almost the same, drop-force position of the second one happened in higher displacement (12% increased). From this figure it can be observed that the curvature slope of all nano-modified and of the reference laminates is almost the same. This experimental evidence is related to the fact that the nanofiber mat is placed in the mid-plane of the laminate and to the fact that mat thickness does

not significantly affect the total thickness of the laminate. Therefore, the linear elastic behaviour of the all types of laminates can be considered the same.

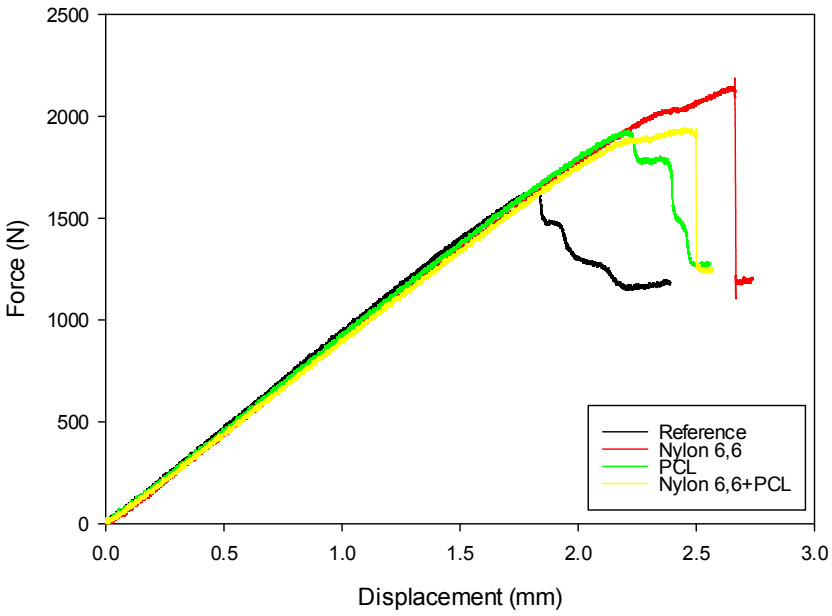

Fig. 3.22. Force-displacement curves of modified and reference laminates (ENF tests)

Fig. 3.23-A shows G_{II} values of nanofiber-reinforced and reference laminates. Unlike mode I tests, the effectiveness of Nylon 6,6 is high with 68% enhancement in G_{II}, but the effect of PCL in mode I and II are almost similar to each other: 25% in mode I and 24% in mode II in comparison with reference laminate. The influence of Nylon 6,6/PCL like mode I results and is between the of PCL and Nylon 6,6 nanofibers.

Generally, by comparing Fig. 3.23-A and Fig. 3.21-C the ability of mixed nanofibers in toughening epoxy is highlighted with 21% in mode I and 56% in mode II, while by using Nylon 6,6 and PCL separately the toughening effect is lower (Table 3.4). A very important point in usage of mixed nanofibers is that one of them should be powerful in mode-I loading and second one in mode-II. For example, the combination of Nylon 6,6 and polyvinylidene fluoride (PVDF) nanofibers is not a good choice. Because the effectiveness of PVDF is appreciated under mode II loading and at the same time it is very weak in mode I [28] and according to this study Nylon 6,6 is also suitable only in mode II, therefore it cannot be expected that their combination can increase G_I and so their combination just increased one mode of loading.

The mechanical energy from the begin of the test to maximum load is illustrated in Fig. 3.23-B. Comparing 3.23-A and B, it is shown that the trend of absorbed energy in this part of loading is similar to G_{II}. It means PCL, Nylon 6,6 and Nylon 6,6/PCL nanofibers can absorb 34, 85 and 68% more than in the case of reference laminates respectively.

Table 3.4. The effect of each kinds of nanofiber mat on G_I and G_{II} (The values are presented in percent in comparison with reference)

	Mode I loading	**Mode II Loading**
Nylon 6,6	4.5%	68%
PCL	25%	24%
Nylon 6,6+PCL	21%	56%

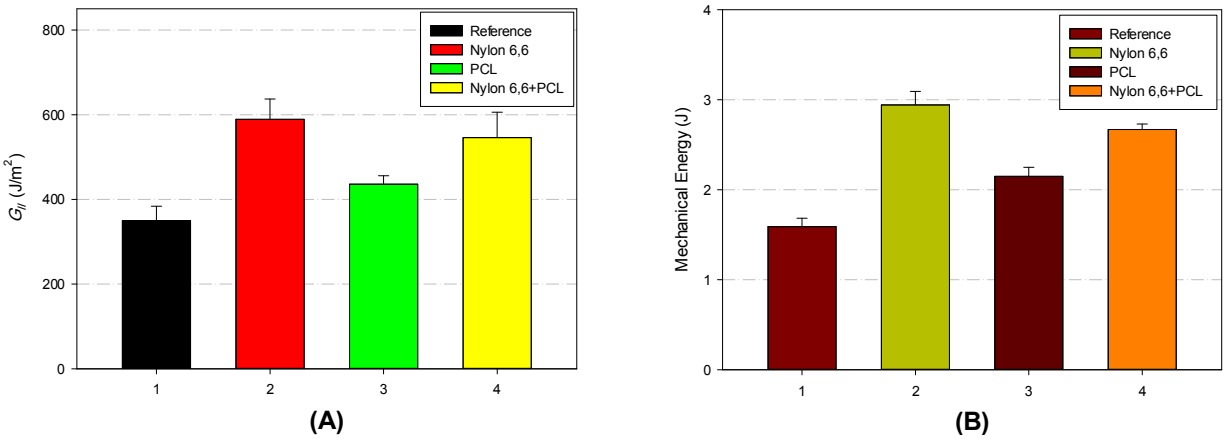

Fig. 3.23. ENF mechanical test results: (A) energy release rate for mode I fracture (G_{II}) for all specimens (B) mechanical energy during loading until maximum load

3.6.3. Morphology of fractured surface

Fracture surfaces of specimens were also examined using a scanning electron microscope (SEM) to provide an insight into the toughening mechanisms. Fig. 3.24-A represents fracture surface of reference laminate under mode I loading where the 'hackle' fracture pattern is clearly visible. Fracture surface of PCL-reinforced laminate is depicted in Fig. 3.24-B and C. The hackle formation was still visible but significantly

less distinguished, even occasionally to a non-hackle fracture pattern (Fig. 3.24-C). Therefore it shows that fracture process in non-modified laminates is completely brittle and PCL nanofibers significantly change it. Generally by blending thermoplastics such as PAN, PVDF, Polysulfone, PCL and etc [108, 103] with epoxy, after the cure, different phenomena can take place. So far many studies have been followed about the morphologies of cured PCL/epoxy blends and details can be found in [119, 120], but totally a heterogeneous morphology was observed in which the spherical particles were uniformly dispersed in the continuous matrix (phase separation). The spherical phase was ascribed to PCL-rich phase while the continuous was attributed to the epoxy matrix (Fig. 3.25). Fig. 3.24-D illustrates the PCL-rich particulate microphases on the fracture surface. The increase of toughness is completely related to the separated phase because stress concentrations caused by particles that produce initiating shear bands which form plastic zones and so absorbed more energy during loading [107]. On the other hand, when the crack propagates and reaches the PCL phase, it is deviated and so more energy is required for the propagation. It is worth mentioning that since PCL is completely melt and blended with matrix, fiber bridging happened during loading from first to end of DCB test.

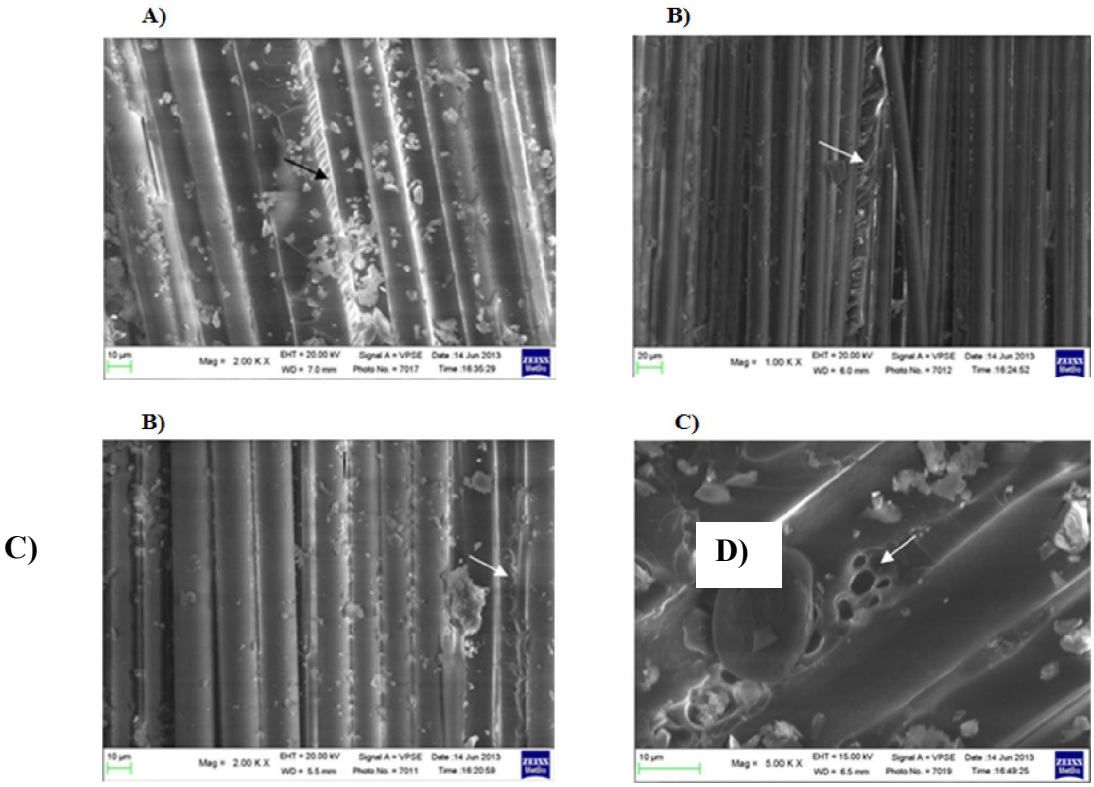

Fig. 3.24. SEM pictures of delamination fracture surface: (A) Reference Laminate (B) PCL-reinforced laminates (C) PCL-reinforced laminates (another position) (D) Phase separation in PCL-reinforced laminates.

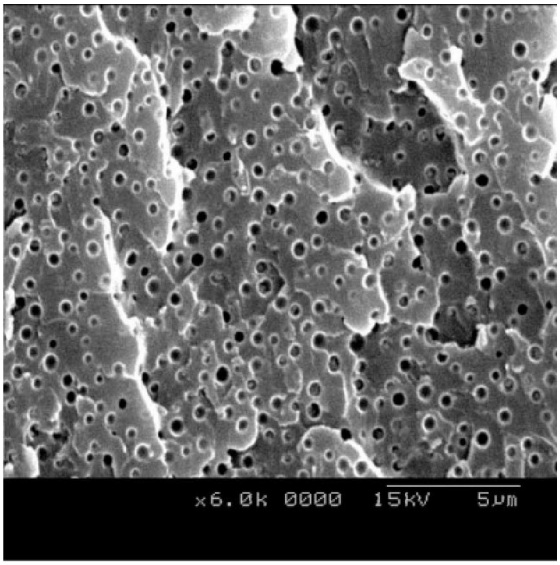

Fig. 3.25. SEM micrographs of epoxy/PCL blends after curing [120].

Fig. 3.26 shows the SEM photographs of fractured surface under mode I condition for Nylon 6,6 and PCL/Nylon 6,6-modified laminate taken near the initial crack. According to Table 3.2 and Fig. 3.26, the curing temperature is lower than melting point of the polymer and higher than the glass transition temperature: it leads to the fact that Nylon 6,6 nanofibers are completely visible (Fig. 3.26-A and B), and have a rubbery characteristics. The latest leads to a plastic deformation and to the behaviour of matrix illustrated in Fig. 3.26-A. It should be noted that in early stage of crack propagation the fracture surface is covered by a white layer of nanofiber, therefore the glass fibres are not visible in the pictures and also in this position no fiber bridging happened. The fracture surface morphology of PCL/Nylon 6,6-modified laminate is shown in Fig. 3.26-C. What observed from fractured surfaces of interfaces interleaved by Nylon 6,6 is also true in the case of fractured surfaces of interfaces nano-modified by Nylon 6,6/PCL. Since Nylon 6,6 covered the fracture surface and PCL were the upper part of mat nanofiber, so it is not possible to consider the effect of PCL in this morphology.

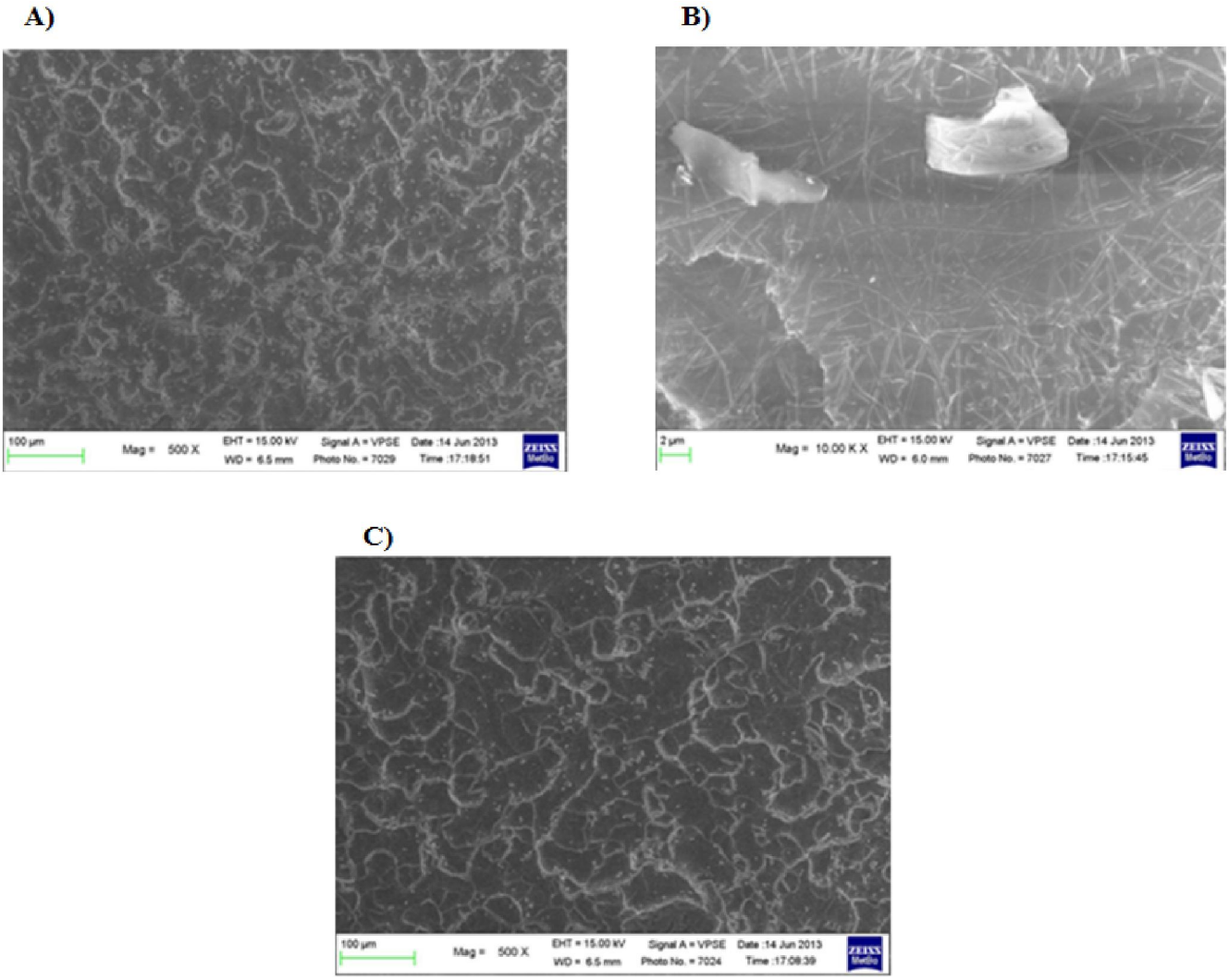

Fig. 3.26. SEM pictures of delamination fracture surface: (A) Nylon 6,6-reinforced laminates (B) Nylon 6,6-reinforced laminates (more magnification) (C) PCL/Nylon 6,6-reinforced laminates (mixed nanofibers).

3.7. Conclusion

Toughening of glass/epoxy laminates was achieved by interleaving mixed PCL/Nylon 6,6 nanofibers. For considering this effect, the ability of individual PCL and Nylon mats for increasing the fracture toughness of laminates compared with mixed one. The results prove that while Nylon 6,6 are only useful for mode II loading and PCL effect is almost the same in mode I and mode II, the mixed nanofibers could use the efficiency of both individual nanofibers in modes I and II. The morphology of fracture surface showed that PCL nanofibers completely melt and act as a second phase in the matrix (phase separation). Nylon 6,6 did not melt, since curing temperature was higher than its glass transition temperature, it showed a rubbery behaviour.

Chapter 4:

Impact Response of Nanofibers-Interleaved Curved Laminates

4.1. Introduction

In chapter 2 the impact response of curved laminate in different situation was considered and in chapter 3 it was shown that nanofibrous mats are a good choice for toughening composite laminates. For this consideration, two different nanofibers, Nylon 6,6 and PCL, and also their mixture were used for investigating their effect on mode I and mode II fracture toughness. It was proved that the efficiency of Nylon 6,6 is better in mode II and PCL effect on fracture toughness is better than Nylon 6,6 in mode I. By mixing these two nanofibers each nanofiber could compensate the shortage of another one.

In this chapter all these nanofibers are used for considering their influence on impact response of interleaved nanofibers. Studies in this field is very limited that mentioned in chapter 3.

4.2. Experimental program

4.2.1. Materials, Electrospinning, specimen fabrication, and test setup

The PCL, Nylon 6,6 and GFRP laminates which are used for this study are the same with what applied for considering the fracture behaviour of interleaved laminate (Chapter 3). For each nanofiber-interleaved laminate 9 specimens were provided which means 27 samples for all modified laminates and 9 specimens as the reference. The nanofibrous mats were interleaved between all layers of composite that its stacking sequence is: $[0/90/0/90/0]_S$.

Since very wide nanofibrous mats were required in this study, a new electrospinning machine was used for producing nanofibers (Fig. 4.1-A). This semi-automatic electrospinning machine consists of four needles (4.1-B) that each one connects to one syringe by a Teflon tube (4.1-C). Unlike the last machine used in the

last chapter, this new machine has a roller which fixed in *x* and *y* direction and the needles move in the longitudinal direction of the roller (Fig 4.1-A). For collecting nanofibers from the roller, a specific paper attached to it before starting electrospinning, so after finishing the process the nanofibrous mat can be removed by the paper (Fig. 4.2). The dimension of nanofibrous mats produced by this machine is 40cm*47cm and its thickness is 40±5μm.

The characteristics of the PCL and Nylon 6,6 is the same with the last test, but since the electrospinning machine was changed the electrospinning parameters varied according to Table 4.1. As seen the only difference between electrospinning parameters of PCL and Nylon 6,6 is the feed rate. For producing individual Nylon 6,6 and PCL nanofibers all four needles were used and for each mat 12ml of solution was used. For producing mixed nanofibrous mat (Nylon 6,6/PCL), both of them electrospun at the same time (in the last study for considering the fracture behaviour mixed nanofibers produced by layers of PCL and Nylon 6,6 – chapter 3). For mixed mat, 6ml of PCL and 6ml of Nylon 6,6 were used and since the feed rate of PCL electrospinning is three times more than Nylon 6,6, so 1 needle used for PCL and three others used for Nylon 6,6.

All samples are curved and its configuration is shown in Fig. 2.6. All these samples interleaved by nanofibers in all layers and then transferred to autoclave for curing in 150^{o}C for 1 hour and under the pressure of 6.4 bar. It should be mentioned the rate of curing from room temperature to 150^{o}C is 2^{o}C/min. Then the sample were cut using a high-speed rotating diamond disc. The average thickness of reference laminate is 3.28mm and nanomodified one is 3.31 which means the effect of nanofiber on the thickness is less than 1 percent.

Test setup is the same with the setup used for considering the effect preloading on impact response of curved laminate (Chapter 2) and the impact tests conducted for four different impact energies: 6, 12, 24, and 36J. For each situation, 2 or 3 tests were conducted. If the results of the first 2 samples were near to each other, the third one waived.

A)

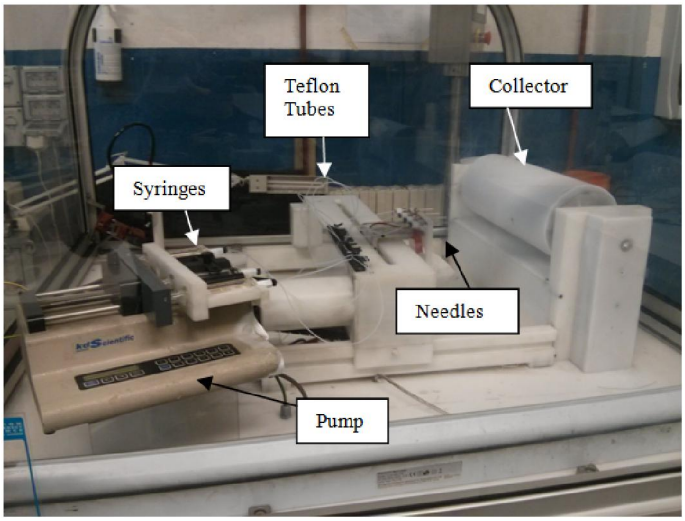

B)

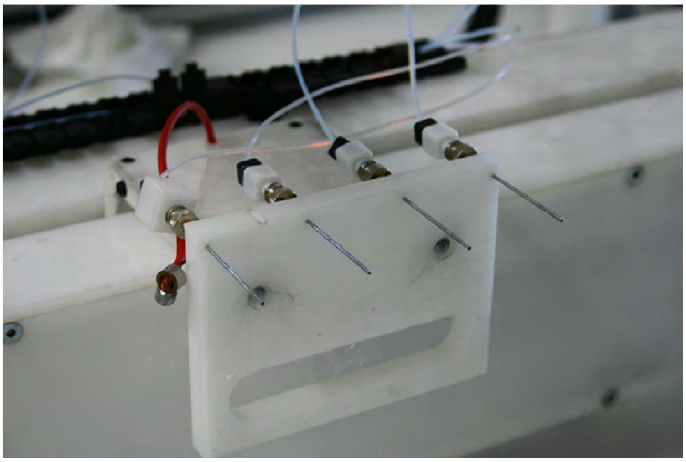

C)

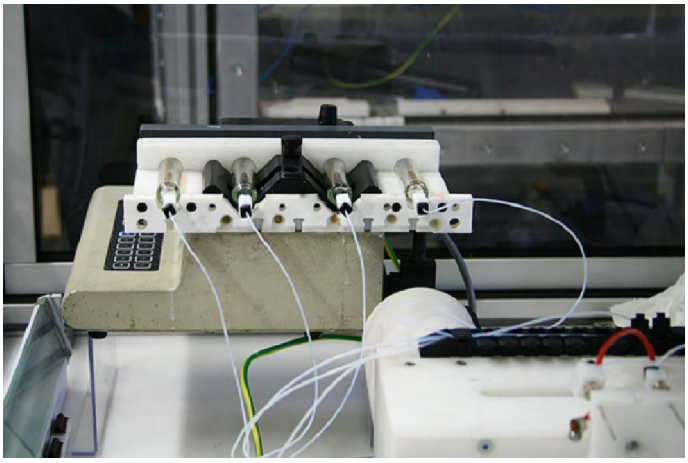

Fig. 4.1. The electrospinning machine

Fig. 4.2. Collecting the nanofibrous mat from the collector

Table 4.1. Electrospinning parameters for producing PCL and Nylon nanofibers in the new electrospinning machine

	PCL	Nylon
Applied Voltage (kV)	23	23
Feed rate (ml/h)	0.9	0.3
Needle tip – collector distance (cm)	15	15
Humidity	40%	40%

4.3. Results and discussion

Fig. 4.3. illustrates the contact force-displacement curves of impact test for reference and nanomodified laminates. At the first glance it is visible that nanomodified does not change significantly these curves. Therefore for more consideration the impact parameters: maximum force, maximum displacement, time-duration of impact, and damaged area are shown in Figs. 4.4 and 4.5. The difference between the reference laminate and nanomodified laminate in all these situation is less than 5% that is in the error range. Generally as the maximum impact force, maximum displacement, and time-duration of impact is a bit more, less, and less, respectively, in nanomodified laminates in comparison with reference laminates that show nanomodified one is a bit more stiff.

The interesting things in this project is the effect of Nylon 6,6 and PCL and their mixture on damaged area. A shown in the Fig. 4.5, PCL and Nylon 6,6 could decrease the damaged area noticeably, but the efficiency of Nylon 6,6 is much more than PCL. For investigating more details the amount of damaged area in each situation is presented in Table 4.2 for the reference and nanomodified laminates. In lower impact energies, 6J and 12J, the effect of PCL on damaged area is low with decreasing 9% and 7%, respectively, and the effect of mixed nanofibers, PCL/Nylon 6,6, is less than pure Nylon 6,6. In higher impact energies, 24J and 36J, the efficiency of Mixed nanofibers is more than Nylon 6,6. For example, mixed nanofibers could decrease damaged area about 60%, while Nylon 6,6 declined it 52%. Generally the influence of Nylon 6,6 and mixed nanofibers is noticeable in all impact energies and their difference is very limited. According to the electrospinning parameters mentioned in the past, each nanofibrous mat for Nylon 6,6 takes 12 hours and mixed one 6 hours. Since the process of the mixed one is much more fast and its efficiency is almost the same and sometimes better, so using the mixed nanofibrous mat is proposed.

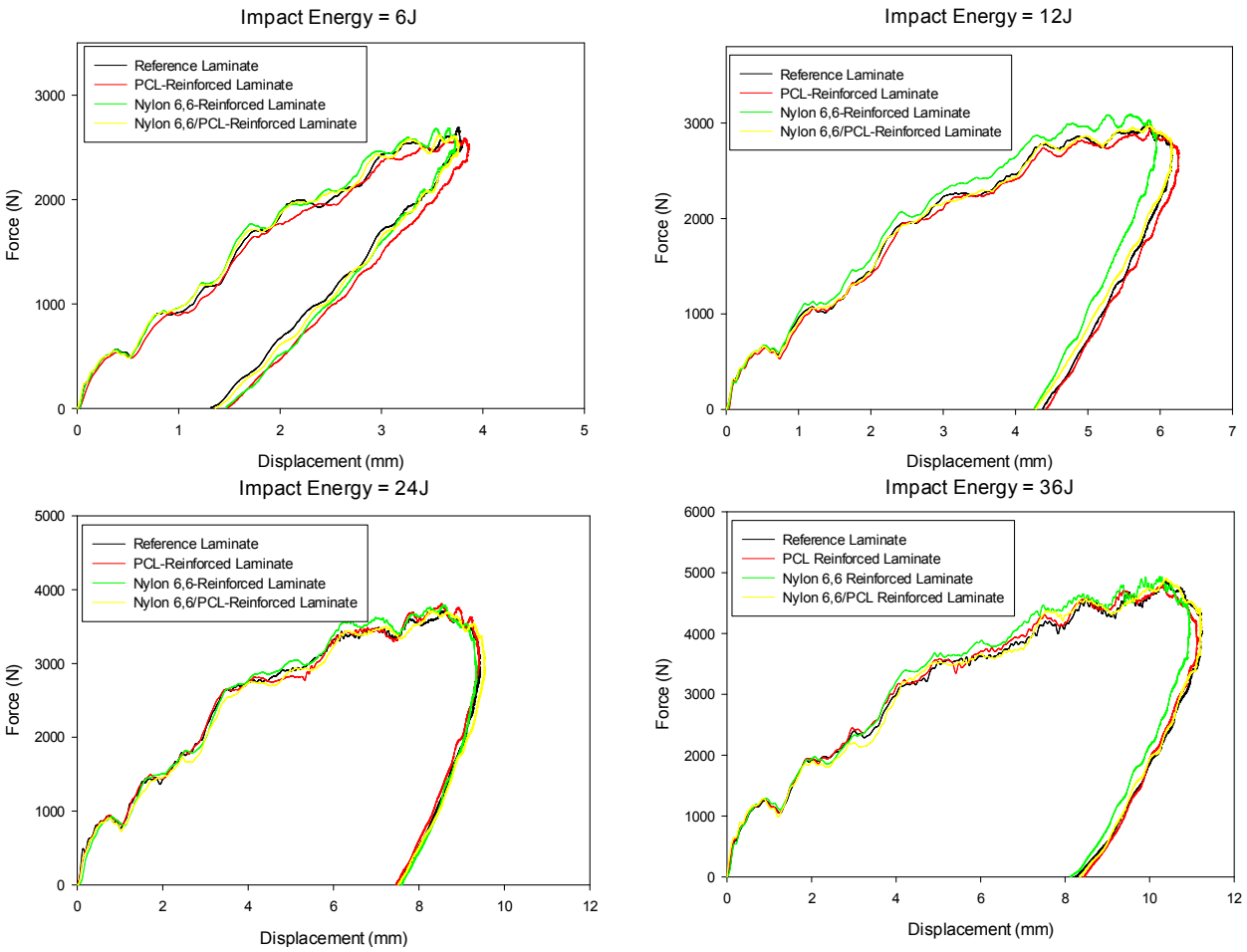

Fig. 4.3. Force versus impactor displacement for the reference and nanomodified laminates under impact energies of: 6J, 12J, 24J, and 36J

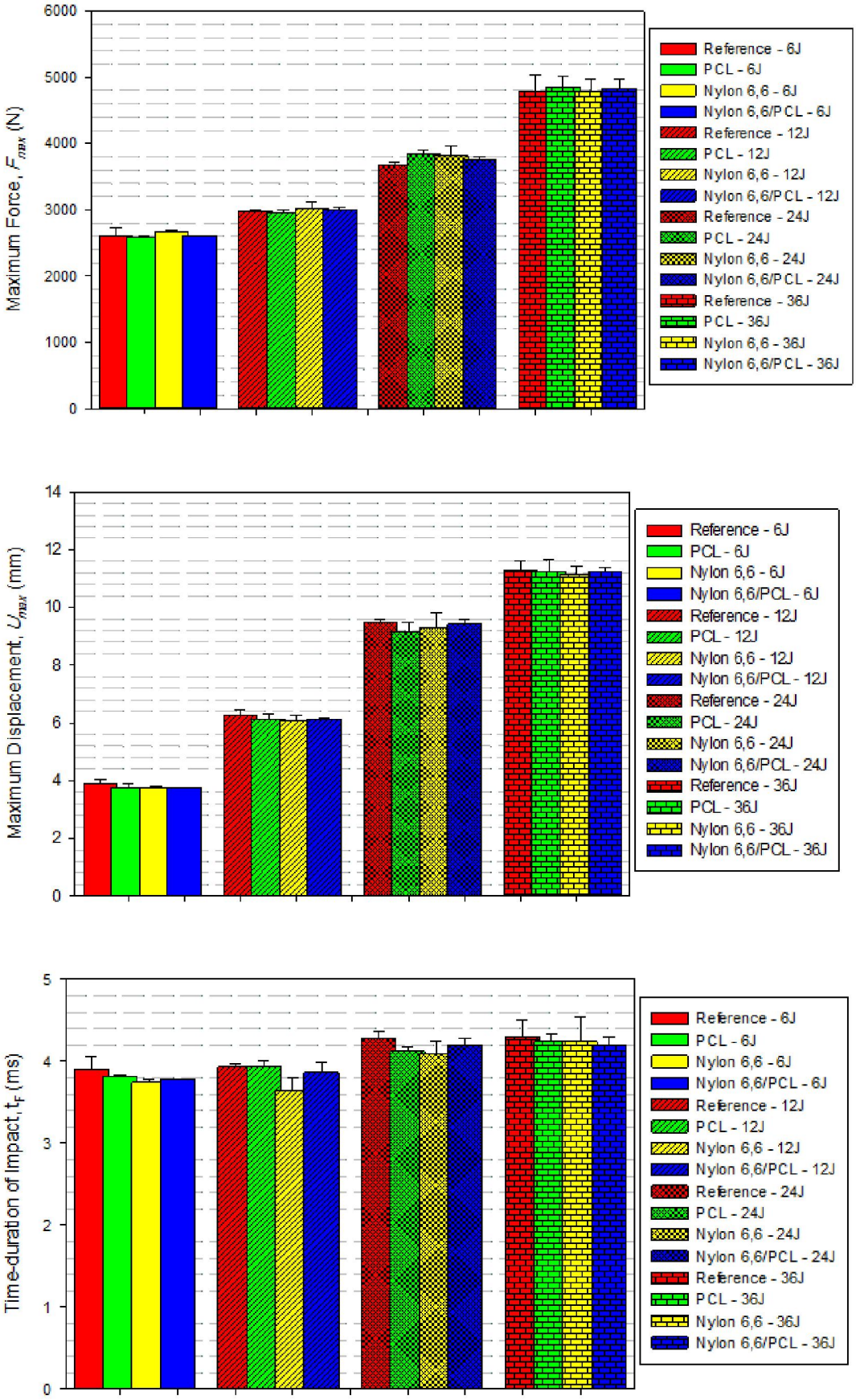

Fig. 4.4. The effect of nanofibrous mat on: A) maximum load B) maximum displacement and C) impact duration of the reference and nanomodified specimens.

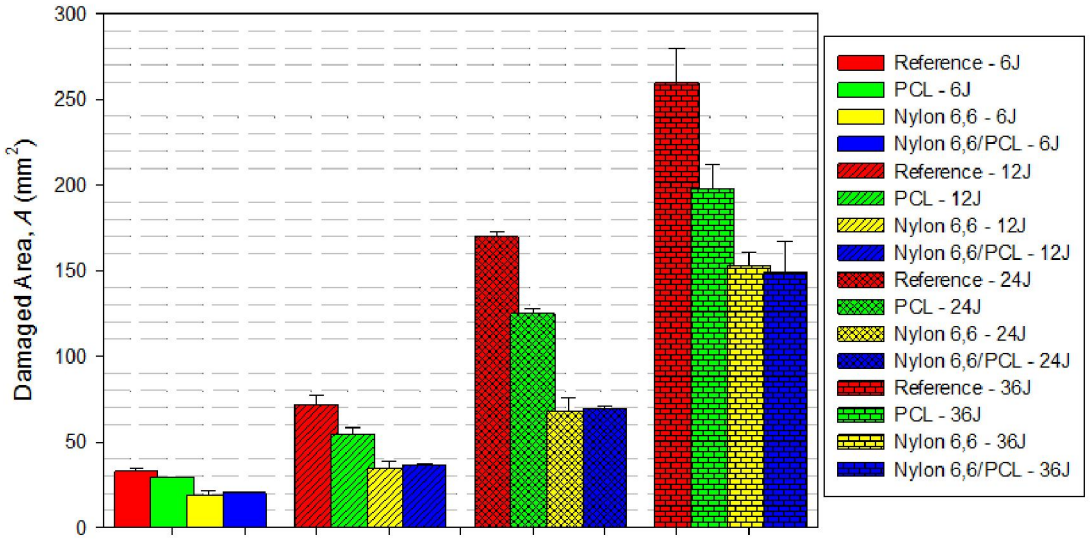

Fig. 4.5. The effect of nanofibrous mat on damaged area of the reference and nanomodified specimens.

Table 4.2. The effect of nanofibrous mat on damaged area under different impact energies.

	6J				12J			
	Ref	PCL	NY	Mix	Ref	PCL	NY	Mix
Damaged Area	32	29	19.22	20.1	58.3	54.4	34.52	36.25
Variation (%)	---	-9.3	-40	-37.1	---	-6.7	-40.8	-37.8

	24J				36J			
	Ref	PCL	NY	Mix	Ref	PCL	NY	Mix
Damaged Area	170	125	81.5	69.22	260	197	152	149
Variation (%)	---	-26.5	-52	-59.3	---	-24.2	-41.5	-42.7

The pictures of damaged area on the back surface of the specimens (non-impacted surface) are also presented in Fig. 4.6 for the reference and modified specimens under 24 and 36J. As seen in the pictures the delamination and matrix cracks are the dominant failure in all samples. By comparing the damaged area in all situation it can be seen that the effect of nanofibers is more on delamination, not on the matrix cracks of the back surface.

Impact Energy = 24J

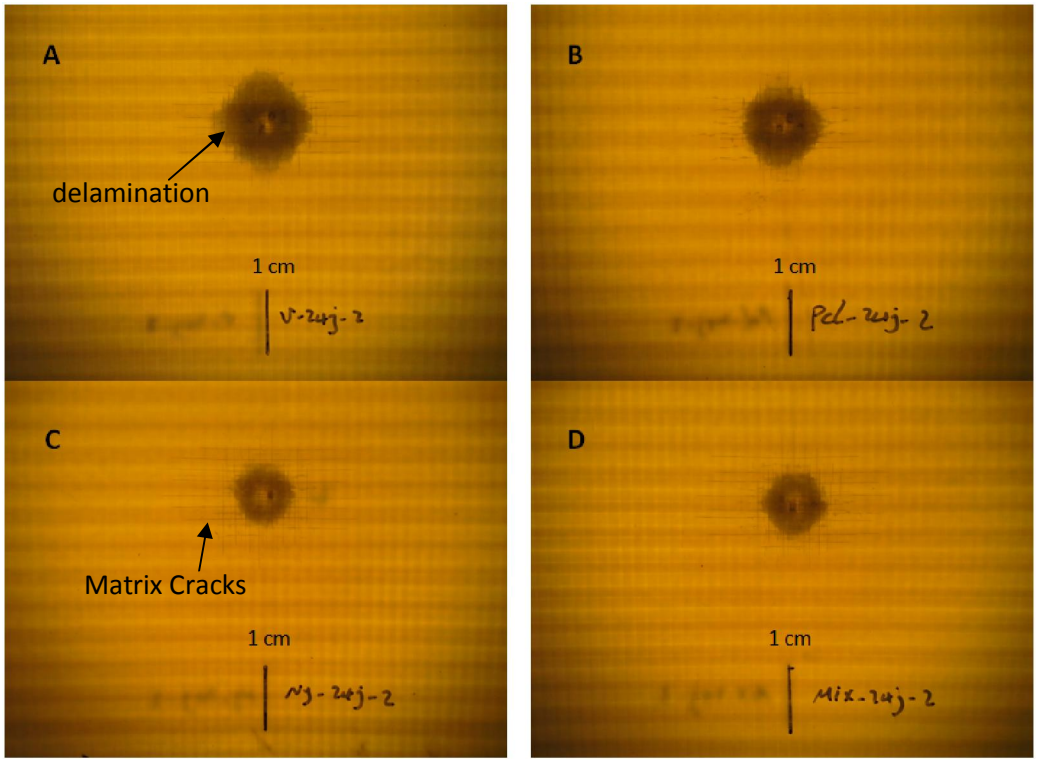

Impact Energy = 36J

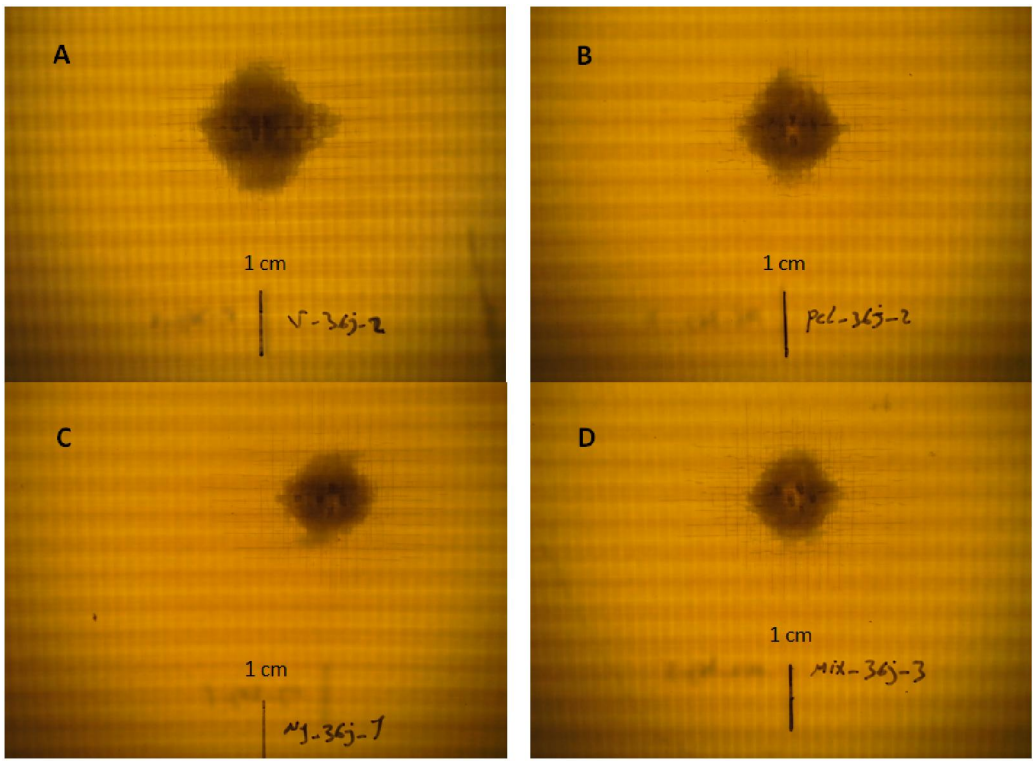

Fig. 4.6. Damaged area of the reference and nanomodified samples under 24J and 36J

4.4. Conclusion

In this chapter the effect of Nylon 6,6, PCL, and their mixture on impact response of composite laminates was considered. The nanofibrous mats were produced by electrospinning method and interleaved between all layers of composite laminates. The results showed that PCL could decrease the damaged area about 25% and Nylon 6,6 and mixed nanofibers about 50%. Since the efficiency of mixed nanofibers is almost the same with Nylon 6,6, but producing of them is much more easier, so applying the mixed nanofibers are suggested.

References:

[1] C. Atas, O. Sayman, An overall view on impact response of woven fabric composite plates, Composite Structures, Volume 82, Issue 3, February 2008, Pages 336-345.

[2] J. López-Puente, R. Zaera, C. Navarro, The effect of low temperatures on the intermediate and high velocity impact response of CFRPs, Composites Part B: Engineering, Volume 33, Issue 8, December 2002, Pages 559-566.

[3] E. Sevkat, B. Liaw, F. Delale, B. Raju, Effect of repeated impacts on the response of plain-woven hybrid composites, Composites Part B: Engineering, Volume 41, Issue 5, July 2010, Pages 403-413.

[4] G. Minak, S. Abrate, D. Ghelli, R. Panciroli, A. Zucchelli, Low-velocity impact on carbon/epoxy tubes subjected to torque – Experimental results, analytical models and FEM analysis, Composite Structures, Volume 92, Issue 3, February 2010, Pages 623-632.

[5] L.J. Deka, S.D. Bartus, U.K. Vaidya, Multi-site impact response of S2-glass/epoxy composite laminates, Composites Science and Technology, Volume 69, Issue 6, May 2009, Pages 725-735.

[6] S. Heimbs, S. Heller, P. Middendorf, F. Hahnel, J. Weibe, Low velocity impact on CFRP plates with compressive preload:Test and modeling, International Journal of Impact Engineering, Volume 36, Issues 10–11, October–November 2009, Pages 1182-1193.

[7] T. Mitrevski, I.H. Marshall, R.S. Thomson, R. Jones, Low-velocity impacts on preloaded GFRP specimens with various impactor shapes, Composite Structures, Volume 76, Issue 3, November 2006, Pages 209-217.

[8] B. Whittingham, I.H. Marshall, T. Mitrevski, R. Jones, The response of composite structures with pre-stress subject to low velocity impact damage, Composite Structures, Volume 66, Issues 1–4, October–December 2004, Pages 685-698.

[9] M.D. Robb, W.S. Arnold, I.H. Marshall, The damage tolerance of GRP laminates under biaxial prestress, Composite Structures, Volume 32, Issues 1–4, 1995, Pages 141-149.

[10] K.M. Mikkor, R.S. Thomson, I. Herszberg, T. Weller, A.P. Mouritz, Finite element modelling of impact on preloaded composite panels, Composite Structures, Volume 75, Issues 1–4, September 2006, Pages 501-513.

[11] K.S. Krishnamurthy, P. Mahajan, R.K. Mittal, Impact response and damage in laminated composite cylindrical shells, Composite Structures, Volume 59, Issue 1, January 2003, Pages 15-36.

[12] S.M.R. Khalili, M. Soroush, A. Davar, O. Rahmani, Finite element modeling of low-velocity impact on laminated composite plates and cylindrical shells, Composite Structures, Volume 93, Issue 5, April 2011, Pages 1363-1375.

[13] L.S. Kistler, A.M. Waas, On the response of curved laminated panels subjected to transverse impact loads, International Journal of Solids and Structures, Volume 36, Issue 9, 1 March 1999, Pages 1311-1327.

[14] P.J. Schulz, D. Liu, Effects of camber height and boundary condition on energy absorption of arched composite laminates, Composites Science and Technology, Volume 69, Issue 6, May 2009, Pages 718-724.

[15] S. Heimbs, Bird Strike Simulations on Composite Aircraft Structures, 2011 SIMULIA Customer Conference.

[16] M. Aktaş, C. Atas, B.M. İçten, R. Karakuzu, An experimental investigation of the impact response of composite laminates, Composite Structures, Volume 87, Issue 4, February 2009, Pages 307-313.

[17] S. Sethi, B.C. Ray, Evaluation of structural integrity and mechanical behavior of advanced FRP composites, International Journal of Structural Integrity, Volume 2 Issue 2, 2011, Pages 214 - 222

[18] J. R. Tarpani, M.T. Milan, D. Spinelli, W.W. Bose, Mechanical performance of carbon-epoxy laminates Part II: quasi-static and fatigue tensile properties, Materials Research, Volume 9, Issue 2, 2006, Pages 121-130.

[19] N.G. Yun, Y. G. Won, S.C. Kim, Toughening of carbon fiber/epoxy composite by inserting polysulfone film to form morphology spectrum, Polymer, Volume 45, Issue 20, 16 September 2004, Pages 6953-6958.

[20] K. Mimura, H. Ito, H. Fujioka, Toughening of epoxy resin modified with in situ polymerized thermoplastic polymers, Polymer, Volume 42, Issue 22, October 2001, Pages 9223-9233.

[21] D.W.Y. Wong, L. Lin, P.T. McGrail, T. Peijs, P.J. Hogg, Improved fracture toughness of carbon fibre/epoxy composite laminates using dissolvable thermoplastic fibers, Composites Part A: Applied Science and Manufacturing, Volume 41, Issue 6, June 2010, Pages 759-767.

[22] P.J. Hogg, Toughening of thermosetting composites with thermoplastic fibers, Materials Science and Engineering: A, Volume 412, Issues 1–2, 5 December 2005, Pages 97-103.

[23] M.M. Davoodi, S.M. Sapuan, D. Ahmad, A. Aidy, A. Khalina, M. Jonoobi, Effect of polybutylene terephthalate (PBT) on impact property improvement of hybrid kenaf/glass epoxy composite, Materials Letters, Volume 67, Issue 1, 15 January 2012, Pages 5-7.

[24] D. Ajit, Kelkar, Ram Mohan, Ronnie Bolick, Sachin Shendokar, Effect of nanoparticles and nanofibers on Mode I fracture toughness of fiber glass reinforced polymeric matrix composites, Materials Science and Engineering: B, Volume 168, Issues 1–3, 15 April 2010, Pages 85-89.

[25] G. Li, P. Li, Y. Yu, X. Jia, S. Zhang, X. Yang, S. Ryu, Novel carbon fiber/epoxy composite toughened by electrospun polysulfone nanofibers, Materials Letters, Volume 62, Issue 3, 15 February 2008, Pages 511-514.

[26] D.W.Y. Wong, L. Lin, P.T. McGrail, T. Peijs, P.J. Hogg, Improved fracture toughness of carbon fiber/epoxy composite laminates using dissolvable thermoplastic fibers, Composites Part A: Applied Science and Manufacturing, Volume 41, Issue 6, June 2010, Pages 759-767.

[27] G. Li, P. Li, C. Zhang, Y. Yu, H. Liu, S. Zhang, X. Jia, X. Yang, Z. Xue, S. Ryu, Inhomogeneous toughening of carbon fiber/epoxy composite using electrospun polysulfone nanofibrous membranes by in situ phase separation, Composites Science and Technology, Volume 68, Issues 3–4, March 2008, Pages 987-994.

[28] K. Magniez, C. De Lavigne, B.L. Fox, The effects of molecular weight and polymorphism on the fracture and thermo-mechanical properties of a carbon-fiber composite modified by electrospun poly (vinylidene fluoride) membranes, Polymer, Volume 51, Issue 12, 28 May 2010, Pages 2585-2596.

[29] S.T. Chiu, Y.Y. Liou, Y.C. Chang, C.L. Ong, Low velocity impact behaviour of prestressed composite laminates, Materials Chemistry and Physics, Volume 47, Issues 2–3, February 1997, Pages 268-272.

[30] M.D. Robb, W.S. Arnold, I.H. Marshall, The damage tolerance of GRP laminates under biaxial prestress, Composite Structures, Volume 32, Issues 1–4, 1995, Pages 141-149.

[31] B. Whittingham, I.H. Marshall, T. Mitrevski, R. Jones, The response of composite structures with pre-stress subject to low velocity impact damage, Composite Structures, Volume 66, Issues 1–4, October–December 2004, Pages 685-698.

[32] T. Mitrevski, I.H. Marshall, R.S. Thomson, R. Jones, Low-velocity impacts on preloaded GFRP specimens with various impactor shapes, Composite Structures, Volume 76, Issue 3, November 2006, Pages 209-217.

[33] G. Minak, S. Abrate, D. Ghelli, R. Panciroli, A. Zucchelli, Low-velocity impact on carbon/epoxy tubes subjected to torque – Experimental results, analytical models and FEM analysis, Composite Structures, Volume 92, Issue 3, February 2010, Pages 623-632.

[34] S.M.R. Khalili, M. Soroush, A. Davar, O. Rahmani, Finite element modeling of low-velocity impact on laminated composite plates and cylindrical shells, Composite Structures, Volume 93, Issue 5, April 2011, Pages 1363-1375.

[35] D. Zheng, W. K. Binienda, Analysis of Impact Response of Composite Laminates under Prestress, Journal of Aerospace Engineering, Volume 21, Issue 4, October 2008, Pages 197-205.

[36] D. Ghelli, G. Minak, Numerical analysis of the effect of membrane preloads on the low-speed impact response of composite laminates, Mechanics of Composite Materials, Volume 46, Issue 3, 2010, Pages 299–316.

[37] S. Heimbs, S. Heller, P. Middendorf, F. Hähnel, J. Weiße, Low velocity impact on CFRP plates with compressive preload: Test and modeling, International Journal of Impact Engineering, Volume 36, Issues 10–11, October–November 2009, Pages 1182-1193.

[38] L.S. Kistler, Experimental investigation of the impact response of cylindrically curved laminated composite panels. In: AIAA/ASME/ASCE/AHS/ASC structures, structural dynamics, and materials conference, 35th, Hilton Head, SC, April 18– 20, 1994. Technical Papers, Pt. 4 (A94-23876 06-39). Washington, DC: American Institute of Aeronautics and Astronautics; 1994. pp. 2292–97.

[39] L.S. Kistler, A. M. Waas, On the response of curved laminated panels subjected to transverse impact loads. International Journal of Solids and Structure, Volume 36, 1999, Pages 1311–27.

[40] L.S. Kistler, A.M. Waas, On the response of curved laminated panels subjected to transverse impact loads, International Journal of Solids and Structures, Volume 36, Issue 9, 1 March 1999, Pages 1311-1327.

[41] Y.N. Kim, K.H. Im, I.Y. Yang, Characterization of impact damages and responses in CFRP composite shells, Material Science Forum, Volume 465–466, 2004, Pages 252–347.

[42] D.R. Ambur, Jr. H. Starnes, Effect of curvature on the impact damage characteristics and residual strength of composite plates. In: 39th AIAA/ASME/ASCHE/AHS/ASC structures, structural dynamics, and materials conference, AIAA Paper No. 98–1881; 1998.

[43] P.J. Schulz, D. Liu, Effects of camber height and boundary condition on energy absorption of arched composite laminates, Composites Science and Technology, Volume 69, Issue 6, May 2009, Pages 718-724.

[44] G.J. Short, F.J. Guild, M.J. Pavier, Post-impact compressive strength of curved GFRP laminates, Composites Part A: Applied Science and Manufacturing, Volume 33, Issue 11, November 2002, Pages 1487-1495.

[45] Z. Leylek, M. L. Scott, S. Georgiadis, R.S. Thomson, Computer modeling of impact on curved fiber composite panels, Composite Structures, Volume 47, Issues 1–4, December 1999, Pages 789-796.

[46] N.O. Yokoyama, M.V. Donadon, S.F.M. de Almeida, A numerical study on the impact resistance of composite shells using an energy based failure model, Composite Structures, Volume 93, Issue 1, December 2010, Pages 142-152.

[47] K.S. Krishnamurthy, P. Mahajan, R.K. Mittal, A parametric study of the impact response and damage of laminated cylindrical composite shells, Composites Science and Technology, Volume 61, Issue 12, September 2001, Pages 1655-1669.

[48] S. Ganapathy, K.P. Rao, Failure analysis of laminated composite cylindrical/spherical shell panels subjected to low-velocity impact, Computers & Structures, Volume 68, Issue 6, September 1998, Pages 627-641.

[49] G.P. Zhao, C.D. Cho, Damage initiation and propagation in composite shells subjected to impact, Composite Structures, Volume 78, Issue 1, March 2007, Pages 91-100.

[50] S.C. Her, Y.C. Liang, The finite element analysis of composite laminates and shell structures subjected to low velocity impact, Composite Structures, Volume 66, Issues 1–4, October–December 2004, Pages 277-285.

[51] S.L. Toh, S.W. Gong, V.P.W. Shim, Transient stresses generated by low velocity impact on orthotropic laminated cylindrical shells, Composite Structures, Volume 31, Issue 3, 1995, Pages 213-228.

[52] S.J. Kim, N.S. Goo, T.W Kim, The effect of curvature on the dynamic response and impact-induced damage in composite laminates, Composites Science and Technology, Volume 57, Issue 7, 1997, Pages 763-773.

[53] S. Ganapathy, K.P. Rao, Interlaminar stresses in laminated composite plates, cylindrical/spherical shell panels damaged by low-velocity impact, Composite Structures, Volume 38, Issues 1–4, May–August 1997, Pages 157-168.

[54] S.W. Gong, V.P.W. Shim, S.L. Toh, Impact response of laminated shells with orthogonal curvatures, Composites Engineering, Volume 5, Issue 3, 1995, Pages 257-275.

[55] R. Vaziri, X. Quan, M.D. Olson, Impact analysis of laminated composite plates and shells by super finite elements, International Journal of Impact Engineering, Volume 18, Issues 7–8, October–December 1996, Pages 765-782.

[56] U.K.Vaidya, B. Thattaiparthasarthy, E. Anderson, S. Pillay, Effect of panel curvature and pre-stress on the low velocity and ballistic impact response of navy relevant composites, 26th Annual Technical Conference of the American Society for Composites 2011 and the 2nd Joint US-Canada Conference on Composites 3 , pp. 2037-2044.

[57] X. Zhang, G.A.O. Davies, D. Hitchings, Impact damage with compressive preload and post-impact compression of carbon composite plates, International Journal of Impact Engineering, Volume 22, Issue 5, May 1999, Pages 485-509.

[58] I. Herszberg, T. Weller, Impact damage resistance of buckled carbon/epoxy panels, Composite Structures, Volume 73, Issue 2, May 2006, Pages 130-137.

[59] A.F. Johnson, M. Holzapfel, Influence of delamination on impact damage in composite structures, Composites Science and Technology, Volume 66, Issue 6, May 2006, Pages 807-815.

[60] A.K. Bledzki, A. Kessler, R. Rikards, A. Chate, Determination of elastic constants of glass/epoxy unidirectional laminates by the vibration testing of plates, Composite Science and Technology, Volume 59, Issue 13, 1999, Pages, 2015-2024.

[61] Kaw AK. Mechanics of Composite Materials. CRC Press Taylor & Francis Group, 2006.

[62] G.J. Short, F.J. Guild, M.J. Pavier, Delaminations in flat and curved composite laminates subjected to compressive load, Composite Structures, Volume 58, Issue 2, 2002, Pages 249-258.

[63] G. Zhou. The use of experimentally-determined impact force as a damage measure in impact damage resistance and tolerance of composite structures, Composite Structures, Volume 42, Issue 4, 1998, Pages 375-82.

[64] G.A. Schoeppner, S, Abrate, Delamination threshold loads for low velocity impact on composite laminates, Composite Part A: Applied Science and Manufacturing, Volume 31, Issue 9, 2000, Pages 903-915.

[65] G. Minak, D, Ghelli. Influence of diameter and boundary conditions on low velocity impact response of CFRP circular laminated plates, Composite Part B-Engineering, Volume 39, Issue 6, 2008, Pages 962-972.

[66] D. Ghelli, G. Minak, Low velocity impact and compression after impact tests on thin carbon/epoxy laminates, Composite Part B-Engineering, Volume 42, Issue 7, 2011, Pages 2067-2079.

[67] C.T. Sun, S. Chattopadhyay, Dynamic response of anisotropic laminated plates under initial stress to impact of a mass. Journal of Applied Mechanics, Volume 42, 1975, 693-698.

[68] K.S. Krishnamurthy, P. Mahajan, R.K. Mittal, Impact response and damage in laminated composite cylindrical shells. Composite Structures, Volume 59, Issue 1, 2003, Pages 15-36.

[69] S. Sridharan. Delamination behaviour of composites. CRC Press.

[70] M. Hojo, S. Matsuda, M. Tanaka, S. Ochiai, A. Murakami, Mode I delamination fatigue properties of interlayer-toughened CF/epoxy laminates, Composite Science and Technology, Volume 66, Issue 5, 2006, Pages 665-675.

[71] T. Yang, C.H. Wang, J. Zhang, S. He, A.P. Mouritz, Toughening and self-healing of epoxy matrix laminates using mendable polymer stitching, Composite Science and Technology, Volume 72, Issue 12, 2012, Pages 1396-1401.

[72] E. Fuoss, P.V. Straznicky, C. Poon, Effects of stacking sequence on the impact resistance in composite laminates-Part 1: parametric study. Composite Structures, Volume 41, Issue 1, 1998, Pages 67-77.

[73] W.E. Howard, T. Gossard, R.M. Jones, M.J. Robert, Reinforcement of composite laminate free edges with U-shaped caps, AIAA Paper 1986.

[74] I.K. Partridge, D.D.R. Cartie, Delamination resistant laminates by Z-Fiber pinning: Part I manufacture and fracture performance, Composites A-Applied Science and Manufacturing, Volume 36, Issue 1, 2005, Pages 55-64.

[75] G. Tang, Y. Yan, X. Chen, J. Zhang, B. Xu, Z. Feng, Dynamic damage and fracture mechanism of three-dimensional braided carbon fiber-epoxy resin composites, Materials & Design, Volume 22, Issue 1, 2001, Pages 21-5.

[76] G. Bohong, F.K. Chang, Energy absorption features of 3-D braided rectangular composite under different strain rates compressive loading, Aerospace Science and Technology, Volume 11, Issues 7–8, November–December 2007, Pages 535-545.

[77] Y.A. Dzenis, D.H. Reneker, United States patent 6265333: delamination resistant composites prepared by small diameter fiber reinforcement at ply, interfaces; 2001.

[78] P. K. Baumgarten, Electrostatic spinning of acrylic microfibers, Journal of Colloid and Interface Science, Volume 36, Issue 1, May 1971, Pages 71-79.

[79] L. Larrondo, R. Manley, Electrostatic fiber spinning from polymer melts. II. Examination of the flow field in an electrically driven jet , Journal of Polymer Science: Polymer Physics Edition, Volume 19, Issue 6, June 1981, pages 921–932.

[80] L. Larrondo, R. Manley, Electrostatic fiber spinning from polymer melts. III. Electrostatic deformation of a pendant drop of polymer melt, Journal of Polymer Science: Polymer Physics Edition Volume 19, Issue 6, June 1981, pages 933–940.

[81] A. Formhals, US patent 1975504: Process and apparatus for preparing artificial threads; 1934.

[82] A. Formhals, US patent 2160962: Method and apparatus for spinning (OCR), 1939.

[83] K.H. Lee, H.Y. Kim, H.J. Bang, Y.H. Jung, S.G. Lee , The change of bead morphology formed on electrospun polystyrene fibers, Polymer, Volume 44, Issue 14, June 2003, Pages 4029-4034.

[84] J.M. Deitzel, J. Kleinmeyer, D. Harris, N.C. Beck Tan, The effect of processing variables on the morphology of electrospun nanofibers and textiles, Polymer, Volume 42, Issue 1, 2001, Pages 261–272.

[85] H. Fong, I. Chun, D.H. Reneker, Beaded nanofibers formed during electrospinning, Polymer, Volume 40, Issue 16, 1999, Pages 4585-4592.

[86] Q. Yang, Z. Li, Y. Hong, Y. Zhao, S. Qiu, C. Wang, Y. Wei, Influence of solvents on the formation of ultrathin uniform poly(vinyl pyrrolidone) nanofibers with electrospinning. Journal of Polymer Science, Part B: Polymer Physics, Volume 42, Issue 20, 2004, Pages 3721–3726.

[87] D.H. Reneker, I. Chun, Nanometre diameter fibres of polymer, produced by electrospinning, Journal of Nanotechnology, Volume 7, Issue 3, 1996, Pages 216–223.

[88] C. Zhang, X. Yuan, L. Wu, Y. Han, J. Sheng , Study on morphology of electrospun poly(vinyl alcohol) mats, European Polymer Journal, Volume 41, Issue 3, 2005, 423-432.

[89] X. Yuan, Y. Zhang, C. Dong, J. Sheng, Morphology of ultrafine polysulfone fibers prepared by electrospinning, Polymer International, Volume 53, Issue 11, 2004, Pages 1704–1710.

[90] C.J. Buchko, L.C. Chen, Y. Shen, D.C. Martin, Processing and microstructural characterization of porous biocompatible protein polymer thin films, Polymer, Volume 40, Issue 26, 1999, Pages 7397-7407.

[91] M.M. Demir, I. Yilgor, E. Yilgor, B. Erman , Electrospinning of polyurethane fibers, Polymer, Volume 43, Issue 1, 2002, 3303–3309.

[92] C. Mituppatham, M. Nithitanakul, P. Supaphol, Ultrafine electrospun polyamide-6 fibers: Effect of solution conditions on morphology and average fiber diameter. Macromolecular Chemistry and Physics, Volume 205, Issue 17, 2004, 2327-2338.

[93] Y. Dzenis, D.H. Reneker. US patent 6265333: Delamination Resistant Composites Prepared by Small Diameter Fiber Reinforcement at Ply Interfaces; 2001.

[94] P. Akangah, S. Lingaiah, K. Shivakumar, Effect of Nylon-66 nano-fiber interleaving on impact damage resistance of epoxy/carbon fiber composite laminates, Composite Structures, Volume 92, Issue 6, May 2010, Pages 1432-1439.

[95] N.G. Yun, Y.G. Won, S.C. Kim, Toughening of epoxy composite by dispersing polysulfone particle to form morphology spectrum, Polymer Bulletin, Volume 52, 2004, Pages 365–72.

[96] N.G. Yun, Y. G. Won, S. C. Kim, Toughening of carbon fiber/epoxy composite by inserting polysulfone film to form morphology spectrum, Polymer, Volume 45, Issue 20, 16 September 2004, Pages 6953-6958.

[97] S. Matsuda, M. Hojo, S. Ochiai, A. Murakami, H. Akimoto, M. Ando, Effect of ionomer thickness on mode I interlaminar fracture toughness for ionomer toughened CFRP, Composites Part A: Applied Science and Manufacturing, Volume 30, Issue 11, November 1999, Pages 1311-1319.

[98] S.N. Yadav, V. Kumar, S. K. Verma, Fracture toughness behavior of carbon fiber epoxy composite with Kevlar reinforced interleave, Materials Science and Engineering: B, Volume 132, Issues 1–2, 25 July 2006, Pages 108-112.

[99] W.Y.W. Doris, L. Lin, P.T. McGrail, T. Peijs, P. J. Hogg, Improved fracture toughness of carbon fiber/epoxy composite laminates using dissolvable thermoplastic fibers, Composites Part A: Applied Science and Manufacturing, Volume 41, Issue 6, June 2010, Pages 759-767.

[100] M.S. Sohn, X.Z. Hu, J.K. Kim, L. Walker, Impact damage characterization of carbon fiber/epoxy composites with multi-layer reinforcement, Composites Part B: Engineering, Volume 31, Issue 8, 2000, Pages 681-691.

[101] A. Duarte, I. Herszberg, R. Paton, Impact resistance and tolerance of interleaved tape laminates, Composite Structures, Volume 47, Issues 1–4, December 1999, Pages 753-758.

[102] X.S. Yi, X.F. An, Effect of interleaf sequence on impact damage and residual strength in a graphite/epoxy laminate, Journal of materials science, Volume 39, 2004, Pages 3253- 3255.

[103] W.H. Lu, F.S. Liao, A.C. Su, P.W. Kao, T.J. Hsu, Effect of interleaving on the impact response of a unidirectional carbon/epoxy composite, Composites, Volume 26, 1995, Pages 215-222.

[104] I. Martinez, M.D. Martin, A. Eceiza, P. Oyanguren, I. Mondragon, Phase separation in polysulfone-modified epoxy mixtures. Relationships between curing conditions, morphology and ultimate behavior, Polymer, Volume 41, Issue 3, February 2000, Pages 1027-1035.

[105] X. Xie, H. Yang, Phase structure control of epoxy/polysulfone blends - effects of molecular weight of epoxy resins, Materials & Design, Volume 22, Issue 1, February 2001, Pages 7-9.

[106] R.J. Varley, J.H. Hodgkin, D.G. Hawthorne, G.P. Simon, D. McCulloch, Toughening of a trifunctional epoxy system Part III. Kinetic and morphological study of the thermoplastic modified cure process, Polymer, Volume 41, Issue 9, April 2000, Pages 3425-3436.

[107] A.C. Garg, Y.W. Mai, Failure prediction in toughened epoxy resins, Composites Science and Technology, Volume 31, Issue 3, 1988, Pages 225-242.

[108] G. Li, P. Li, C. Zhang, Y. Yu, H. Liu, S. Zhang, X. Jia, X. Yang, Z. Xue, S. Ryu, Inhomogeneous toughening of carbon fiber/epoxy composite using electrospun polysulfone nanofibrous membranes by in situ phase separation, Composites Science and Technology, Volume 68, Issues 3-4, March 2008, Pages 987-994.

[109] J. Zhang, T. Yang, T. Lin, C. H. Wang, Phase morphology of nanofibre interlayers: Critical factor for toughening carbon/epoxy composites, Composites Science and Technology, Volume 72, Issue 2, 18 January 2012, Pages 256-262.

[110] R. Palazzetti, A. Zucchelli, I. Trendafilova, The self-reinforcing effect of Nylon 6,6 nano-fibres on CFRP laminates subjected to low velocity impact, Composite Structures, Volume 106, December 2013, Pages 661-671.

[111] R. Palazzetti, A. Zucchelli, C. Gualandi, M.L. Focarete, L. Donati, G. Minak, S. Ramakrishna, Influence of electrospun Nylon 6,6 nanofibrous mats on the interlaminar properties of Gr–epoxy composite laminates, Composite Structures, Volume 94, Issue 2, January 2012, Pages 571-579.

[112] R. Palazzetti, X.T. Yan, A. Zucchelli, Influence of geometrical features of electrospun Nylon 6,6 interleave on the CFRP laminates mechanical properties, Polymer Composites, Volume 35, Issue 1, January 2014, pages 137–150.

[113] F. Moroni, R. Palazzetti, A. Zucchelli, A. Pirondi, A numerical investigation on the interlaminar strength of nanomodified composite interfaces, Composites Part B: Engineering, Volume 55, December 2013, Pages 635-641.

[114] P. Akangah, S. Lingaiah, K. Shivakumar, Effect of Nylon-66 nano-fiber interleaving on impact damage resistance of epoxy/carbon fiber composite laminates, Composite Structures, Volume 92, Issue 6, May 2010, Pages 1432-1439.

[115] J. Zhang, T. Lin, X. Wang, Electrospun nanofiber toughened carbon/epoxy composites: Effects of polyetherketone cardo (PEK-C) nanofiber diameter and interlayer thickness, Composites Science and Technology, Volume 70, Issue 11, 15 October 2010, Pages 1660-1666.

[116] L. Van Der Schueren, B. De Schoenmaker, O.I. Kalaoglu, K. De Clerck, An alternative solvent system for the steady state electrospinning of polycaprolactone, European Polymer Journal, Volume 47, Issue 6, June 2011, Pages 1256-1263.

[117] ASTM D5528, Standard test method for mode-I interlaminar fracture toughness of unidirectional fiber-reinforced polymer matrix composites. Annual book of ASTM standards; 2007.

[118] Protocol No 2 for interlaminar fracture toughness testing of composites: mode II. European Structural Integrity Society; 1993.

[119] J.L. Chen, F.C. Chang, Temperature-dependent phase behavior in poly(ϵ-caprolactone)–epoxy blends, Polymer, Volume 42, Issue 5, March 2001, Pages 2193-2199.

[120] Y. Ni, S. Zheng, Influence of intramolecular specific interactions on phase behavior of epoxy resin and poly(ε-caprolactone) blends cured with aromatic amines, Polymer, Volume 46, Issue 15, 11 July 2005, Pages 5828-583.

Acknowledgment

There are many friends, colleagues and family that I would like to thank for their continued support and guidance during my graduate studies.

First and foremost, I would like to express my sincere appreciation to my supervisor, Prof. Giangiacomo Minak, for his guidance, advice and support of this research over the past few years. He provided me all equipments I needed for this research and also supported me in different conferences and short courses which were very useful for my research. I also thank Prof. Andrea Zucchelli for all his supports and specially for his patient. He was really a good friend for me during these years and tried to solve many of my problems.

I also would like to thank my friends: Roberto, Ricardo, Tommaso, Juri, Luca, and Marco for their support during my works in electrospinning laboratory and my tests.

Last but not least, I dedicate this work to my family. First my wife who was under a big pressure in a foreign country, but bore it to support me. I really appreciate her patient and supports. Without encouragement of my father and mother, Ahmad and Fariba, I could not be in this level, I really thank them. Finally I want to appreciate my uncle, AhmadAli who was the first that encourage me to continue my studies in this PhD program.

Hamed Saghafi

17/03/2014, Bologna